

AD A111047

AFWAL-TR-81-1086

12

LEVEL II



RADIATION EFFECTS IN PIGTAILED GaAs AND GaAlAs LEDs

C.E. Barnes

Sandia National Laboratories
Albuquerque, New Mexico 87185

DTIC
S
B

June 1981

Final Report for period 12 February 1979 through 30 September 1980

Approved for public release; distribution unlimited.

DTIC FILE COPY

AVIONICS LABORATORY

AIR FORCE WRIGHT AERONAUTICAL LABORATORIES

AIR FORCE SYSTEMS COMMAND

WRIGHT PATTERSON AIR FORCE BASE, OHIO 45433

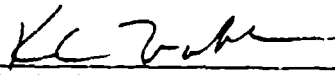
915-100


NOTICE

When Government drawings, specifications, or other data are used for any purpose other than in connection with a definitely related Government Procurement operation, the United States Government thereby incurs no responsibility nor any obligation whatsoever; and the fact that the government may have formulated, furnished, or in any way supplied the said drawings, specifications, or other data, is not to be regarded by implication or otherwise as in any manner licensing the holder or any other person or corporation, or conveying any rights or permission to manufacture use, or sell any patented invention that may in any way be related thereto.


This report has been reviewed by the Office of Public Affairs (ASD/PA) and is releasable to the National Technical Information Service (NTIS). At NTIS, it will be available to the general public, including foreign nations.

This technical report has been reviewed and is approved for publication.


K. C. TRUMBLE
Project Engineer
Information Transfer Group
Information Processing Technology
Branch
System Avionics Division


DONALD L. MOON
Chief, Information Processing
Technology Branch
System Avionics Division
Avionics Laboratory

FOR THE COMMANDER


FRANK A. SCARPINO, Acting Chief
System Avionics Division
Avionics Laboratory

"If your address has changed, if you wish to be removed from our mailing list, or if the addressee is no longer employed by your organization please notify AFWAL/AAAT-3, W-PAFB, OH 45433 to help us maintain a current mailing list".

Copies of this report should not be returned unless return is required by security considerations, contractual obligations, or notice on a specific document.

UNCLASSIFIED

SECURITY CLASSIFICATION OF THIS PAGE (When Data Entered)

REPORT DOCUMENTATION PAGE		READ INSTRUCTIONS BEFORE COMPLETING FORM
1. REPORT NUMBER AFWAL-TR-81-1086	2. GOVT ACCESSION NO. AD-A111047	3. RECIPIENT'S CATALOG NUMBER
4. TITLE (and Subtitle) Radiation Effects in Pigtails GaAs and GaAlAs LEDs		5. TYPE OF REPORT & PERIOD COVERED Final 12 Feb. 1979-30 Sept. 1980
		6. PERFORMING ORG. REPORT NUMBER SAND81-0929
7. AUTHOR(s) C. E. Barnes		8. CONTRACT OR GRANT NUMBER(s) WAL02543, WAL92431P, 77-27; Contract DE-AC04-76-DP00789
9. PERFORMING ORGANIZATION NAME AND ADDRESS Sandia National Laboratories Albuquerque, New Mexico 87185		10. PROGRAM ELEMENT, PROJECT, TASK AREA & WORK UNIT NUMBERS ILIR 9213
11. CONTROLLING OFFICE NAME AND ADDRESS Avionics Laboratory (AFWAL/AAAT-3) Air Force Wright Aeronautical Laboratories (AFSC) Wright Patterson Air Force Base, Ohio 45433		12. REPORT DATE June 1981
		13. NUMBER OF PAGES 105
14. MONITORING AGENCY NAME & ADDRESS (if different from Controlling Office)		15. SECURITY CLASS. (of this report) Unclassified
		15a. DECLASSIFICATION/DOWNGRADING SCHEDULE
16. DISTRIBUTION STATEMENT (of this Report) Approved for public release; distribution unlimited		
17. DISTRIBUTION STATEMENT (of the abstract entered in Block 20, if different from Report)		
18. SUPPLEMENTARY NOTES		
19. KEY WORDS (Continue on reverse side if necessary and identify by block number) Radiation Effects, LEDs, Optical Fibers, Neutron Irradiation, Pulsed X-ray, Degradation, Gallium Arsenide, Gallium Aluminum Arsenide.		
20. ABSTRACT (Continue on reverse side if necessary and identify by block number) Permanent and transient radiation effects have been studied in Plessey pig- tailed, high radiance GaAs and GaAlAs LEDs using neutron, gamma ray and X-ray sources. The radiation-induced source of degradation in these devices was determined by also examining both bare, unpigtailed LEDs and separate samples of the Corning fibers used as pigtails. No transient effects were observed in the unpigtailed LEDs during either pulsed neutron or X-ray exposure. In contrast, the Corning doped silica fibers exhibited strong transient attenuation following pulsed X-ray bombardment. Permanent neutron damage in these pigtailed		

DD FORM 1 JAN 73 1473

EDITION OF 1 NOV 65 IS OBSOLETE

UNCLASSIFIED

SECURITY CLASSIFICATION OF THIS PAGE (When Data Entered)

UNCLASSIFIED

SECURITY CLASSIFICATION OF THIS PAGE(When Data Entered)

LEDs consisted essentially of light output degradation in the LED itself. While this effect was significant, it is important to note that these LEDs have exceptionally good neutron tolerance in that their average light output degrades by only a factor of 1.7 at fluences near 1×10^{14} n/cm². Permanent gamma ray effects due to a Cs-60 irradiation of 1 megarad were restricted to a small increase in attenuation in the fiber. The two primary radiation effects were then transient attenuation in the fiber pigtail and permanent neutron-induced degradation of the LED.

UNCLASSIFIED

SECURITY CLASSIFICATION OF THIS PAGE(When Data Entered)

FOREWORD

This report describes an investigation performed under Contract No. DE-AC04-76-DP00789 of radiation effects in pigtailed GaAs and GaAlAs LEDs. These devices were developed by the Plessey Company of England to satisfy Air Force requirements for fiber optic applications. The radiation effects studies of these LEDs were carried out at Sandia National Laboratories (SNL) in Albuquerque, New Mexico. The principal investigator was C. E. Barnes who was assisted by L. Hansen and G. Lyons. The author would also like to acknowledge helpful discussions with J. J. Wiczer and R. Chaffin. We are also indebted to R. Goodfellow and R. Davis of the Plessey Company for information and advice concerning the LEDs. Lastly, we wish to thank the operating staffs of the SPR, GIF, REBA and HERMES II facilities at SNL for their cooperation and assistance.

The period in which this work was done was from February 1979 to September 1980 with submission of this report in June 1981.

The Air Force Program Monitor was Ken Trumble AFWAL/APAT-3.

Accepted for filing
INDEXED
SERIALIZED
JUN 1967
FBI - NEW YORK

✓

NY
DISTRICT OF COLUMBIA
RECEIVED
JUN 19 1967
FBI - NEW YORK

A

TABLE OF CONTENTS

SECTION		PAGE
I	INTRODUCTION	1
II	BACKGROUND	1
	1. Light Emitting Diodes	1
	2. Fibers	7
III	EXPERIMENTAL PROCEDURES	11
IV	EXPERIMENTAL RESULTS	21
	1. Permanent Neutron Damage Effects on LED Spectra	21
	2. Permanent Neutron Degradation of Total LED Light Output and Current-Voltage	38
	3. Neutron Damage of LEDs at Different Temperatures	55
	4. Transient Neutron-Induced Effects in LEDs	55
	5. Permanent Gamma Ray Damage in LEDs	67
	6. Permanent Gamma Ray Attenuation in Fibers	67
	7. Transient Attenuation in Corning Fibers	67
V	DISCUSSION	79
	1. Neutron Damage in the LEDs	79
	2. Transient Fiber Attenuation and Pigtailed LED Output	91
VI	CONCLUSIONS AND RECOMMENDATIONS	101
VII	REFERENCES	105

LIST OF ILLUSTRATIONS

<u>FIGURE NO.</u>		<u>PAGE</u>
1	Schematic of Fiber Response to an X-Ray Pulse	8
2	Example of Transient Fiber Attenuation	9
3	Structure of Plessey (PL) Etched-Well LEDs	13
4	Overall Structure of Packaged LEDs	14
	Stripping of Corning Fiber	16
6	Experimental Set-up for Transient Attenuation Measurements	20
7	Irradiation 76K Spectra from GaAs	22
8	Pre-Irradiation 300K Spectra from GaAs	23
9	Pre-Irradiation 300K Spectra from GaAlAs	24
10	Pre-Irradiation 76K Spectra from GaAlAs	25
11	Degradation of 76K Spectra from GaAs	27
12	Degradation of 300K Spectra from GaAs	28
13	Degradation of 300K Spectra from Lensed GaAs	29
14	Degradation of 76K Spectra from GaAlAs	30
15	Degradation of 300K Spectra from GaAlAs	31
16	Degradation of 300K Spectra from Pigtailed GaAlAs	32
17	Pre-Irradiation 300K Spectra from PL and Texas Instruments (TI) GaAs	34
18	Pre-Irradiation 300K Spectra from PL GaAs and GaAlAs	35
19	Pre-Irradiation 300K Spectra from PL GaAlAs	37
20	Current-Voltage Characteristics at 300K of PL and TI GaAs	39
21	Current-Voltage Curves at 300K of PL GaAs LEDs	40
22	Current-Voltage Curves at 300K of PL and TI GaAlAs	42
23	Light Intensity-Voltage Curves at 300K of PL and TI GaAs	43

<u>FIGURE NO.</u>		<u>PAGE</u>
24	Light Intensity-Voltage Curves at 300K of PL GaAs LEDs	45
25	Comparison of Output Degradation in PL GaAs and GaAlAs LEDs	46
26	Light Intensity-Voltage Curves for PL and TI GaAlAs	47
27	Light Intensity-Current Density Curves for PL and TI GaAs	49
28	Light Intensity-Current Curves for PL GaAs LEDs	50
29	Light Intensity-Current Density Curves for PL and TI GaAlAs	51
30	Light Intensity-Current Curves for PL GaAlAs LEDs	52
31	Light Intensity-Current Curves for Final PL GaAlAs LEDs	54
32	Current-Voltage Curves at Different Temperatures for PL GaAs	56
33	Light Intensity-Voltage Curves at Different Temperatures for PL GaAs	57
34	Light Intensity-Current Curves at Different Temperatures for PL GaAs	58
35	Current-Voltage Curves at Different Temperatures for PL GaAlAs	59
36	Light Intensity-Voltage Curves at Different Temperatures for PL GaAlAs	60
37	Light Intensity-Current Curves at Different Temperatures for PL GaAlAs	61
38	Response of PL GaAs LED to a Neutron Pulse	63
39	Response of LEDs to Neutron Pulses	65
40	Response of PL GaAlAs LEDs to Neutron Pulses	66
41	Co-60 Irradiation of PL GaAs and GaAlAs LEDs	68
42	Peak Transient Attenuation at 300K in the Corning Fiber	70
43	Normalized Attenuation in the Corning Fiber	71
44	Peak Transient Attenuation at Different Doses in the Corning SDF Fiber	73
45	Peak Transient Attenuation at Different Temperatures in the SDF Fiber	74

<u>FIGURE NO.</u>		<u>PAGE</u>
46	Recovery of Transient Attenuation at Different Temperatures	75
47	Recovery of Normalized Transient Attenuation	77
48	Recovery of Normalized Transient Attenuation for Different Dose Rates	78
49	Degradation of Light Intensity from PL and TI LEDs	80
50	Degradation of Efficiency at Different Currents	82
51	Degradation of Light Output for TI and PL GaAlAs	83
52	Degradation of Light Output for a Variety of LEDs	84
53	Analysis of Degradation in PL GaAs LEDs	88
54	Analysis of Degradation in PL GaAlAs LEDs	89
55	Recovery of Normalized Attenuation in a Variety of Fibers	92
56	Recovery of Attenuation in Corning Fibers	93
57	LED Power Output after X-Ray Irradiation of Pigtail	97
58	Degraded LED Output after X-Ray Irradiation of Pigtail	98
59	Degraded LED Output after X-Ray Irradiation of Pigtail	99
60	Room Temperature Power Output After X-Ray and Neutron Irradiation	100

LIST OF TABLES

<u>TABLE NO.</u>	<u>PAGE</u>
1 Characteristics of Plessey LEDs	12
2 Lifetime - Damage Constant Products for LEDs	90

SECTION I

INTRODUCTION

For fiber optic data links which must function in a radiation environment, the selection of the optoelectronic components making up the link must be done judiciously because of the variation in radiation sensitivity of these devices. If the effect of radiation on one component, for example the fiber, is particularly strong, this sensitivity can dictate the choice of operating wavelength and the other components of the transmission system. Consequently, the system designer must have access to information concerning the behavior of all the optoelectronic components in the radiation environment in which the link will be used. In this report we will describe the results of a radiation effects study of fiber pigtailed, high radiance GaAs and GaAlAs LEDs contemplated for use by the Air Force Wright Aeronautical Laboratories (Avionics Laboratory) and possibly other Air Force organizations. In particular, it will be shown that the two primary radiation damage effects are transient attenuation in the fiber pigtails and permanent neutron-induced degradation of the LEDs. Also, for the specific LEDs studied herein the GaAlAs LED is the preferred choice over the GaAs emitter.

SECTION II

BACKGROUND

1. Light Emitting Diodes

LEDs fabricated from GaAs and GaAs-related ternary compounds have been the subject of several radiation effects studies.¹⁻⁶ A wide variety of LEDs have been studied in the past at Sandia National Laboratories, and this work is summarized in reference 1. Polimadei, Epstein and coworkers examined radiation effects in both $\text{Ga}_{1-x}\text{Al}_x\text{As}$ and $\text{GaAs}_{1-x}\text{P}_x$ LEDs. Variations with x were found

in the radiation-induced degradation of light output for both types of LEDs. Both the gamma and neutron damage constants for $\text{Ga}_{1-x}\text{Al}_x\text{As}$ decreased with increasing Al content.² For neutron irradiated $\text{GaAs}_{1-x}\text{P}_x$, minimum degradation rates were found at intermediate values of x by Epstein, et al.³ In contrast, an earlier study by Epstein, et al.⁴ revealed about the same degradation rates in gamma irradiated GaP and $\text{GaAs}_{0.1}\text{P}_{0.9}$ LEDs. However, in later work⁵ on $\text{Ga}_{1-x}\text{Al}_x\text{As}$ and $\text{GaAs}_{1-x}\text{P}_x$ LEDs exposed to gamma irradiation, it was found that the damage constant decreased with increasing Al or P content. Epstein and coworkers have suggested that ternary compounds are intrinsically less radiation sensitive than binary materials. That is, the addition of Al to GaAs results in an LED which degrades less when exposed to radiation. Recent work in our laboratory on a set of $\text{Ga}_{1-x}\text{Al}_x\text{As}$ LEDs with varying Al content from Texas Instruments indicates that other parameters are more important. For example, variations in growth method, doping levels, and dopant types can result in GaAlAs LEDs which are more sensitive to irradiation than GaAs devices in which some attention has been given to radiation hardening. As will be shown, the LEDs examined in this study fortunately exhibit some of the characteristics which result in good radiation hardness.

The common view of the physical mechanism which causes radiation-induced degradation of the light output from LEDs is that nonradiative recombination centers are introduced which compete with radiative centers for excess carriers resulting in a decrease in minority carrier lifetime. The total initial lifetime can be written,

$$\frac{1}{\tau_0} = \frac{1}{\tau_{0R}} + \frac{1}{\tau_{0NR}} \quad , \quad \text{sec}^{-1} \quad (1)$$

where τ_0 is the total pre-irradiation minority carrier lifetime, and τ_{OR} and τ_{ONR} are the lifetimes associated with radiative and nonradiative processes, respectively. It is the decrease in τ_{ONR} which is usually responsible for the reduction in τ , although there are examples such as SiC where the reduction in lifetime is due to decreases in τ_{OR} (increased light output). However, here we will assume that the degradation takes place through a reduction in non-radiative lifetime. The lifetimes are usually written,

$$\frac{1}{\tau_{OR}} = \sigma_R v_{th} N_R \text{ and } \frac{1}{\tau_{ONR}} = \sigma_{NR} v_{th} N_{NR} \quad , \text{ sec}^{-1} \quad (2)$$

where σ_R and σ_{NR} are carrier capture cross-sections associated with radiative and nonradiative centers, respectively. N_R and N_{NR} are the concentrations of radiative and nonradiative centers, respectively. Finally, v_{th} is the minority carrier thermal velocity. Following irradiation the total minority carrier lifetime is written,

$$\frac{1}{\tau} = \frac{1}{\tau_{OR}} + \frac{1}{\tau_{ONR}} + \sigma_{NRI} v_{th} N_{NRI} \quad , \text{ sec}^{-1} \quad (3)$$

or

$$\frac{1}{\tau} = \frac{1}{\tau_0} + \sigma_{NRI} v_{th} N_{NRI} \quad , \text{ sec}^{-1} \quad (4)$$

Here τ is the total, post-irradiation lifetime and the subscript NRI refers to radiation-induced, nonradiative centers. The usual method is to define

the concentration of radiation-induced, nonradiative centers by,

$$N_{NRI} \equiv C_I \phi, \text{ cm}^{-3} \quad (5)$$

where ϕ is the radiation fluence, or dose, and C_I is a constant whose magnitude involves the probability of generation of a particular defect by a unit radiation fluence. The damage constant K is then defined by,

$$K \equiv \sigma_{NRI} v_{th} C_I, \text{ cm}^2/\text{sec} \quad (6)$$

and the phenomenological equation which is used to describe LED radiation damage is given by

$$\frac{1}{\tau} = \frac{1}{\tau_0} + K\phi, \text{ sec}^{-1} \quad (7)$$

or

$$\frac{\tau_0}{\tau} = 1 + \tau_0 K\phi. \quad (8)$$

It should be noted that K , given by the definition (6), is likely to be a superposition of σ_{NRI} and C_I for several types of radiation-induced defects. Clearly, the detailed physics governing the interaction of radiation with the semiconductor material is hidden in the damage constant K , and a complete understanding of the physical mechanisms must come from more basic measurements. However, for prediction of device degradation, the phenomenological approach is useful, keeping in mind certain rules and limitations which are discussed below. Therefore, the quantity of interest in this investigation is the value of the initial lifetime-damage constant product, $\tau_0 K$.

The measurable quantities in an experiment are the total light output and current as a function of forward bias. In order to determine a meaningful damage constant, the current controlling mechanisms in the operating region of the device must be known. For example, using the linearly graded junction approximation, and for an LED whose light output is due to a radiative current which is diffusion controlled, the relationship between light output, L , and minority carrier lifetime is given by,⁶

$$L = C\tau e^{qV/kT}, \text{ arbitrary units} \quad (9)$$

where C is a constant containing parameters which do not depend on τ or T .

Then, rearranging Eq. (8) and substituting from Eq. (9), we have, at constant voltage,

$$\frac{\tau_0}{\tau} = \frac{L_0}{L} + 1 + \tau_0 K\phi, \quad (10)$$

where L_0 and L are the pre-irradiation and post-irradiation light outputs.

Analysis of device degradation at constant current is useful since it is essentially efficiency degradation, and also because LEDs are usually operated at constant current. The external efficiency is proportional to the radiative current, or light output L , divided by the total current. To obtain an equation similar to Eq. (10) but for constant current, Eq. (9) must be expressed in terms of J , the total current density. For a total current dominated by diffusion,

$$J = (C_1/\sqrt{\tau}) e^{qV/kT} \quad \text{A/cm}^2 \quad (11)$$

Solving for $e^{qV/kT}$ and substituting into Eq. (9) gives

$$L = C_2 \tau^{3/2} J, \text{ arbitrary units} \quad (12)$$

where C_1 and C_2 are constants. Equation (8) then becomes, at constant current,

$$\frac{\tau_o}{\tau} = \left(\frac{L_o}{L} \right)^{2/3} = 1 + \tau_o K \phi. \quad (13)$$

For a total current dominated by space charge recombination (SCR),

$$J = (C_3/\tau) e^{qV/2kT}. \text{ A/cm}^2 \quad (14)$$

Proceeding the same way, at constant current, Eq. (8) becomes

$$\frac{\tau_o}{\tau} = \left(\frac{L_o}{L} \right)^{1/3} = 1 + \tau_o K \phi. \quad (15)$$

Since significant degradation occurs when the value of $\tau_o K \phi$ becomes comparable to unity, it is the value of the $\tau_o K$ product which is of interest.

Differences in degradation rates between constant voltage operation (Eq. 10) and constant current operation (Eq. 13) can generally be ascribed to neutron-induced excess currents.¹ When such non-radiative currents are significant, the constant current degradation rate is larger than the constant voltage degradation rate. Since the neutron-added currents are usually due to SCR,¹ they have their greatest impact at low voltages. At large voltages and current densities, the total current is dominated by a diffusion mechanism and the radiation-induced currents are insignificant. It follows that one can expect that high radiance LEDs, which operate at very high current densities because of their small junction areas, will exhibit minimal neutron-induced excess currents.

2. Fibers

Radiation effects in optical fibers have been studied extensively in recent years.^{7,8,9} Although ionizing radiation induces significant luminescence in fibers this is not a serious problem for most potential applications because the temporal behavior of the luminescence coincides with that of the radiation. In contrast, the attenuation induced in a fiber can last for several orders of magnitude in time after exposure to a short burst of ionizing radiation. These effects are shown schematically in Fig. 1 for a 50ns wide radiation pulse. During the pulse the light signal exceeds the quiescent DC level from the light source due to the induced luminescence. Following the radiation burst, the combination of luminescence and attenuation produces a negative peak in the light signal, I_p , which is used in defining the peak transient attenuation, α_p :

$$\alpha_p = \frac{10}{\ell \text{ (m)}} \log \left(\frac{I_o}{I_p} \right), \text{ dB/m} \quad (16)$$

where ℓ is the exposed fiber length and I_o is the pre-pulse light signal. The attenuation recovers over a long period of time often resulting in a residual "permanent" (present after 24 hrs.) attenuation effect. The recovery kinetics of the attenuation are usually complex and often involve the superposition of different recovery mechanisms. The intensity and duration of the attenuation can depend on a variety of parameters including fiber characteristics, wavelength, and temperature.

Three examples of peak transient attenuation in relatively radiation hard fibers are shown in Fig. 2 as a function of wavelength. These curves clearly illustrate the severity of the transient attenuation problem when compared with the curve for intrinsic plus permanent attenuation induced in a typical low loss silica

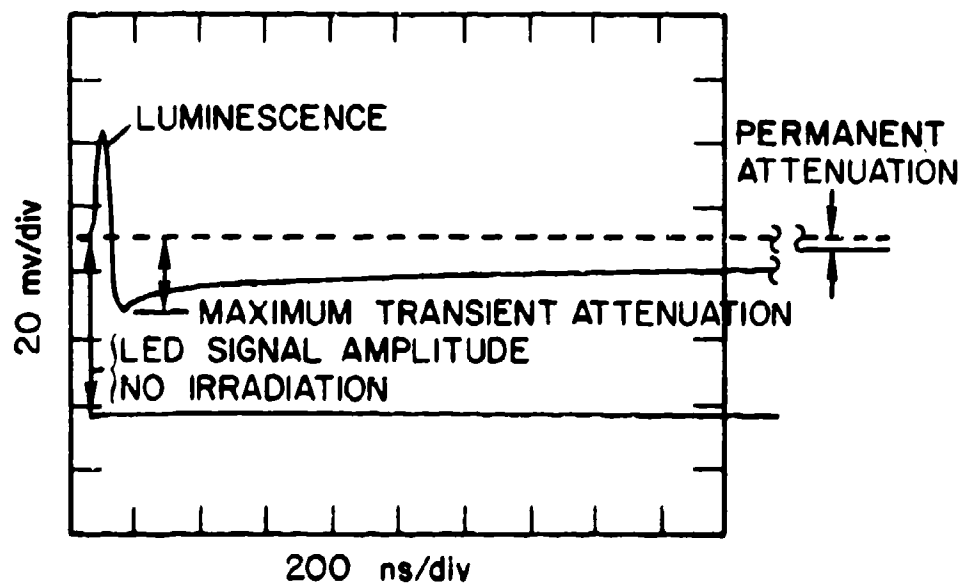


Figure 1. Oscilloscope trace of the typical response of an optical filter to bombardment by a narrow x-ray pulse. Note that while the X-ray generated luminescence follows the pulse, the transient attenuation can last for several orders of magnitude in time after the pulse. [from D. L. Mattern, I. M. Watkins, C. D. Skoog, J. R. Brandon and E. Barsis, IEEE Trans. Nucl. Sci. NS-21, No. 6, 81 (1974).]

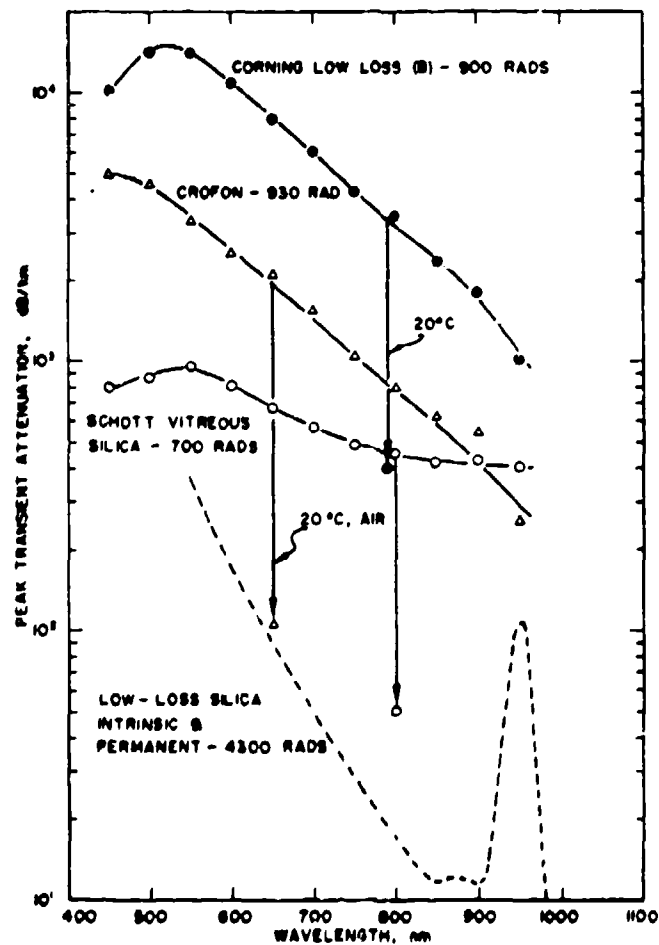


Figure 2. Peak transient attenuation spectra of three "radiation-hard" fibers following irradiation to the doses shown. The vertical arrows indicate the expected decrease in attenuation after a recovery time of 1 msec for the Corning fiber at 20°C, the Crofon fiber at 20°C in air, and the Schott fiber at temperatures above -54°C. Also shown for comparison is the total attenuation, intrinsic plus that induced by 4300 Rads of Co-60, for a typical silica fiber. [Peak transient attenuation data taken from C. D. Shoog, Sandia Tech. Report SAND76-0056 (Nov. 1976)].

fiber by 4300 rads of Co-60 gamma rays. Note that for the similar Schott fiber, α_p is much greater than the permanent attenuation after the smaller dose of only 700 rads (X-ray). In addition, α_p is particularly strong in the Corning fiber which has a doped silica core as opposed to the pure vitreous silica core in the Schott fiber. For both glass fibers α_p decreases with increasing wavelength for $\lambda > 550$ nm. Previous work^{7,8,9} has shown that the rate of recovery after the ionizing pulse is independent of wavelength so that the spectral shape in Fig. 2 is maintained at later times. As an example of the expected recovery of transient attenuation, the vertical arrows in Fig. 2 indicate the reduction in attenuation after 1 msec. As implied by the 20°C specification, recovery in the Corning fiber is temperature dependent with the recovery being slower at lower temperatures. In contrast, for temperatures greater than -54°C the recovery kinetics in the Schott fiber are independent of temperature.⁹ Mattern, et al⁷ and Skoog⁹ found that the kinetics of attenuation recovery in glass fibers are also generally independent of radiation dose, dose rate, and type of radiation.

The peak transient attenuation curve for the plastic Crofon fiber in Fig. 2 is similar to that for the glass fibers. However, unlike glass fibers the intrinsic attenuation in plastic core fibers often increases with increasing wavelength above 600 nm. Since this dependence is opposite to that for the transient attenuation, the resulting total net attenuation following a radiation pulse will have a minimum whose wavelength location may be time dependent. In addition to this complication, the recovery kinetics can depend on the ambient temperature and atmosphere, the recovery proceeding more slowly in oxygen free environments (vacuum, N₂).^{7,9}

SECTION III

EXPERIMENTAL PROCEDURES

All of the LEDs examined in this study were fabricated at Plessey Research Labs, Caswell, England. The devices were supplied in three groups as shown in Table 1 which lists each LED and its characteristics. All of the devices are high radiance, double heterostructure etched well LEDs with either GaAs or Ga_{0.95}Al_{0.05}As active regions grown by liquid phase epitaxy. The structures of the LEDs are similar to that shown in Fig. 3 with the exception of the variations given in Table 1. The complete pigtailed LED is shown in Fig. 4. From the point of view of radiation damage, three components of the LED are of interest:

(1) the LED chip itself, (2) the silica-titania lens, and (3) the optical fiber making up the pigtail. Although pigtailed devices were included in the first group, no data were obtained on them for two reasons. First, the mechanical integrity of these early pigtailed LEDs was such that the pigtails became easily detached. Second, attempts were made to mount these devices on Al blocks for reproducible low temperature testing. However, considerable breakage occurred and these efforts were given up. As a consequence only data on "bare" (unlensed, unpigtailed) LEDs were obtained from the first group of devices.

As indicated in Table 1, the second set of LEDs (CXL003, CXL004, CXL009, CXL013) contained GaAs and GaAlAs lensed devices with and without fiber pigtails. Therefore, comparisons of results taken on these devices and those in the first group allowed us to assess the relative radiation sensitivity of the three major LED components. The purpose of the final and third set of 12 LEDs was to determine the variation in radiation sensitivity within a group of devices that were all essentially the same. This was contrasted

TABLE 1
Characteristics of Flessey high radiance LEDs examined in this study.

<u>LED Number</u>	<u>Active Region Material</u>	<u>Doping Level</u>	<u>Lensed?</u>	<u>Pigtailed?</u>	<u>Isolation Technique</u>
D2503AP-46 and 47	GaAs	Low ($\approx 5 \times 10^{17} \text{ cm}^{-3}$)	Yes	Corning 1025	Oxide
D2503AP-49 and 50	GaAs	Low ($\approx 5 \times 10^{17} \text{ cm}^{-3}$)	No	No	Oxide
P65B-1 and 3	GaAlAs	$3 \times 10^{18} \text{ cm}^{-3}$	Yes	Corning 1025	Oxide
P65B-12 and 13	GaAlAs	$3 \times 10^{18} \text{ cm}^{-3}$	No	No	Oxide
<hr/>					
CXL003	GaAs	Low ($\approx 5 \times 10^{17} \text{ cm}^{-3}$)	Yes	Corning 1025	proton
CXL004	GaAs	Low ($\approx 5 \times 10^{17} \text{ cm}^{-3}$)	Yes	No	proton
CXL009	GaAlAs	$2 \times 10^{18} \text{ cm}^{-3}$	Yes	Corning 1025	proton
CXL013	GaAlAs	$2 \times 10^{18} \text{ cm}^{-3}$	Yes	No	proton
<hr/>					
C45 (P124AP, P135AP, P142AP)	GaAlAs	$4.5 \times 10^{18} \text{ cm}^{-3}$	Yes	Corning SDF	proton
-12 LEDs in					
Total					

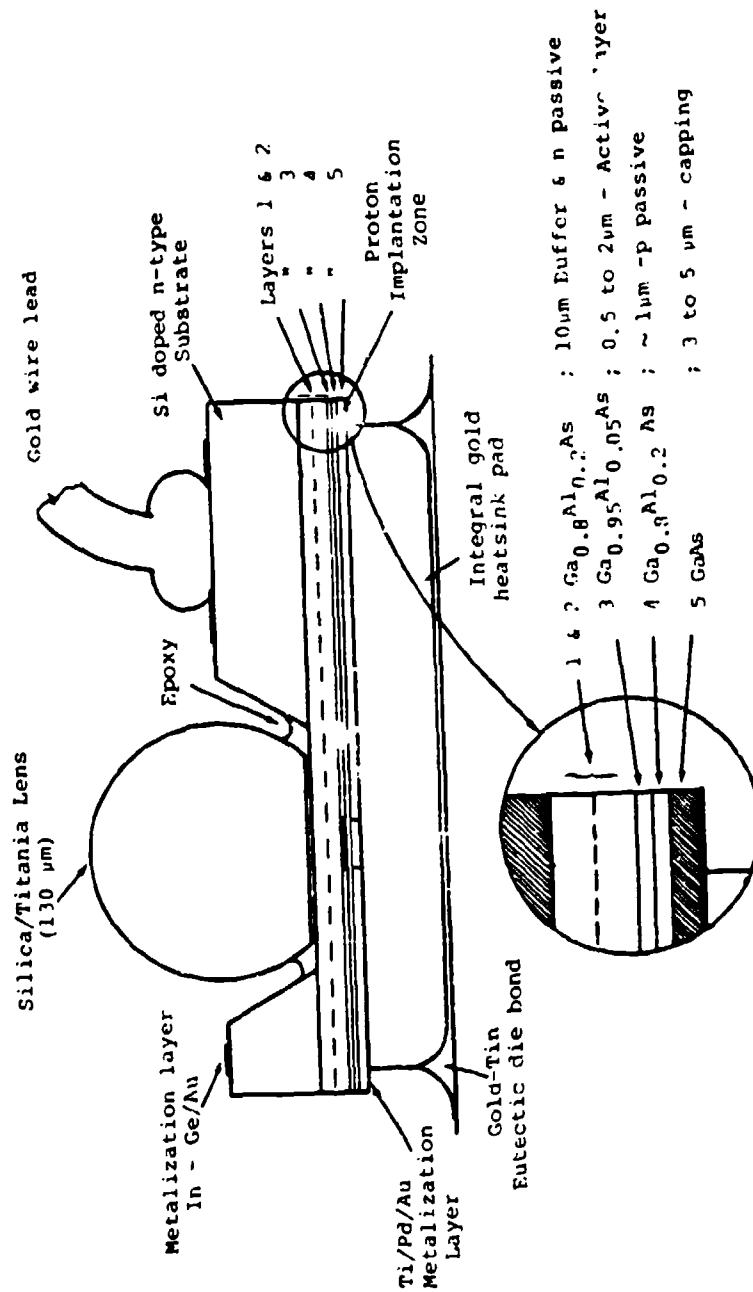


Figure 3. General structure of the Plessey high radiance, etched well LED including the silica-titanium lens. As indicated in Table 1, variations in this structure occur among the LEDs examined in this study. For some LEDs, the active region is GaAs. Oxide isolation was used rather than proton bombardment for some LEDs. [Courtesy of R. Davis, Plessey Central Research Labs.]

LENS COUPLED LED

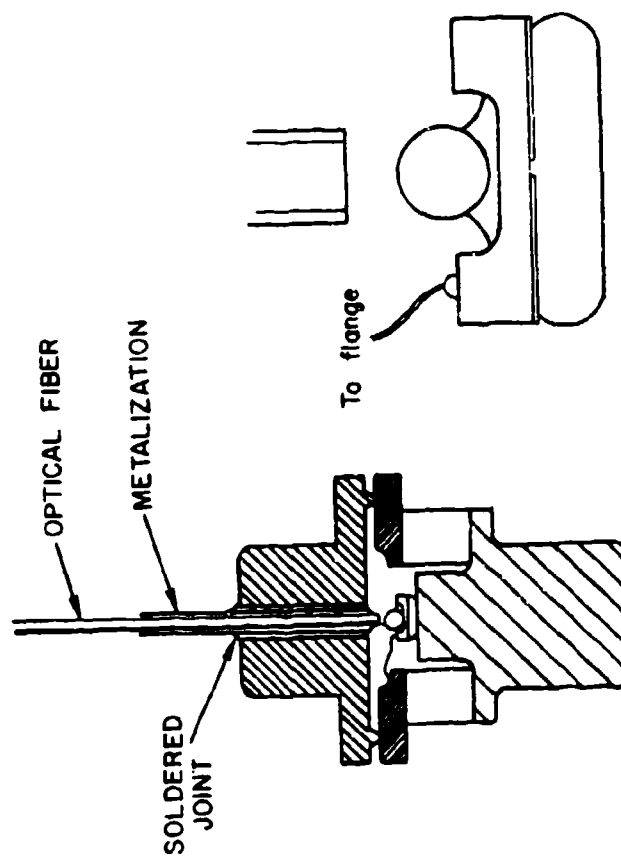


Figure 4. Overall structure of the pigtailed Passsey high radiance LED. Recall that some of the LEDs examined in this study had neither pigtail nor lens while others had a lens but no pigtail. Note that the geometry of this LED is slightly different from that in Fig. 3.

same. This was contrasted with the first two sets of devices in which there were never more than two tested LEDs which were the same. It is our understanding that this last set of LEDs represents the final design for the intended application.

In addition to the various LEDs supplied for this study, separate pieces of Corning fiber were also provided. Two different fibers were examined in the course of this work. The earlier fiber was a Corning step index 1025 silica fiber with a core diameter of $90\mu\text{m}$ and $\text{N.A.} = .16$. More recently we have studied the fiber now used as a pigtail for the most recent set of 12 LEDs. This is a step index Corning (SDF), designated BP356, with core diameter of $100\mu\text{m}$ and an N.A. of 0.3.

When studying light attenuation in short lengths of fiber as appropriate for pigtails, one must take care that cladding modes are not present in the light emitted from the fiber. This is because in most applications these modes are lost so that inclusion of them in the detected signal will result in an erroneous estimate of the radiation-induced attenuation if the cladding modes are affected differently by irradiation. If the fiber being tested is not long enough to cause damping of the cladding modes, an oil of appropriate index of refraction placed on the cladding along about an inch of fiber will allow these modes to escape from the fiber. This type of mode stripping was used in our experiments when necessary. Checking for cladding modes was accomplished by either passing visible light through the fiber to be tested, or for a pigtail, by viewing the LED output from the pigtail through an infrared microscope. An example of such a check is shown in the two photographs in Fig. 5 taken end-on of the light exiting from a short length of the Corning step index



a) No mode stripping oil.



b) With mode stripping oil.

Figure 5. An example of the stripping of cladding modes from a short length of the Corning 1025 step index fiber. These micro photographs are of green light emitted from the end of the fiber with and without a few drops of high index oil spread along approximately 1 in. of the cladding. In the upper picture, note the outer ring of light due to mode propagation within the cladding.

1025 fiber. Note the outer ring of light emitted from the fiber prior to using high index mode stripping oil. An additional easy check was to use a portable IR viewer to look for light leakage on the portion of fiber on which the oil was placed.

In the course of testing the LEDs several radiation facilities at Sandia National Labs were used. In each case the measurement technique varied somewhat so that we will discuss the radiation source and the measurement methods together for each radiation source. The central part of our studies concerned the determination of permanent neutron damage effects on the LED characteristics. The LED parameters of interest were total current, total light output, and electroluminescence spectrum as a function of forward bias voltage prior to and following successive neutron irradiations at room temperature in the Sandia Pulsed Reactor (SPR) facility. This reactor is a bare, unmoderated reactor which has a near-fission neutron spectrum with an average energy of approximately 1 MeV. The reactor can be operated steady state or in the pulsed mode for which the neutron pulse is approximately 45 μ sec wide. The neutron fluence, ϕ , for neutron energies greater than 10 KeV was measured by sulfur dosimetry using the appropriate boron-shielded plutonium-to-sulfur ratio for the SPR.

For LEDs without pigtails measurements were performed at both room temperature and liquid nitrogen temperature (76K). The LEDs were reproducibly mounted in a cryostat whose window looked directly into a cooled S-1 response photomultiplier for total output measurements, or into the entrance slit of a 1 meter Perkin Elmer grating monochromator for spectral measurements. The photomultiplier signal was phase sensitively detected and processed by a HP9825A calculator system which controlled the measurement system.

In the case of the pigtailed LEDs measurements were made only at room temperature. The end of the fiber was mounted in the slot of a 3 inch long 1/4" diameter cylinder. The bottom of the slot was approximately the same diameter as the fiber cladding diameter so that the fiber did not move appreciably within the cylinder. The cylinder could then be reproducibly mounted in an x-y translator at the same distance from the face of the S-1 photomultiplier or the monochromator slit after each neutron irradiation.

Measurements of LED output during and immediately following a neutron pulse from the SPR were also conducted. After selecting the appropriate distance for the desired fluence, a fiber was set up in front of the LED to accept the light output. All but about 1 inch of the fiber was shielded with lead to eliminate attenuation and luminescence due to the prompt gamma rays accompanying the neutron pulse (approximately 1.6×10^5 rads = total reactor output per pulse). The amount of gamma radiation absorbed by the fiber is considered to be negligible. Approximately 30 meters of fiber was required to transfer the light output from the reactor room to an adjoining instrument building where the signal was detected by a Si APD and displayed on an oscilloscope. Problems were encountered because of the sensitivity of the APD to gamma rays and electrical noise even as far away as the instrument building. However, measurements with additional detector shielding revealed that pulses observed during the neutron burst were due to these sources and not to effects occurring in the LED or shielded fiber.

The Sandia Gamma Irradiation Facility (GIF), a Co-60 source with a maximum strength of approximately 10 megarads/hr, was employed for studying permanent gamma induced damage in both LEDs and fibers. LED irradiation and measurement were carried out in the same manner as for neutron irradiation. That is, the LED was reproducibly mounted in the cryostat and measured prior to irradiation, taken

out to the GIF for exposure, and then returned to the laboratory for post-irradiation measurement. In Contrast, Co-60 induced fiber attenuation was measured with the fiber in place within the GIF cell. The LED and detector were mounted outside the cell, the fiber was aligned in front of each and this setup was not disturbed until after post-irradiation measurements were made. The irradiation of the fiber was accomplished by running the fiber into the cell through serpentine access holes and back out again. This arrangement allowed pre- and post-irradiation measurements to be made without the problem of LED/detector-fiber alignment reproducibility.

Transient ionization effects in the Corning fibers were studied using two pulsed electron beam machines in the X-ray mode: the Relativistic Electron Beam Accelerator (REBA) and the High-Energy Radiation Megavolt Electron Source II (HERMES II). It was necessary to use HERMES II, the larger of the two machines, in order to exceed dose rates of 1×10^{11} rads/sec. However, most of the work was done on REBA which generates an X-ray pulse approximately 50 nsec wide using an average electron energy of about 2.5 MeV. The experimental set-up for the later temperature dependent measurements on the Corning SDF fiber is shown in Fig. 6. A fiber length sufficient to produce significant attenuation was wound in roughly a 3 inch diameter circle onto a brass block which could be cooled with cold N₂ gas. The fiber was held down with a flexible plastic plate in order to avoid stressing the fiber during cooling or heating. The light source for the fiber was one of the recently obtained pigtailed GaAlAs LEDs. The pigtail was fused to the test fiber whose other end was butted up against a 200 μ m dia. core PCS carrier fiber which transferred the signal into an instrument van. An RCA temperature compensated Si avalanche photodiode with integral pre-amplifier was used as a detector. The signal was monitored with transient digitizers and oscilloscopes covering sweep times of 100 nsec to 0.1 sec. Dosimetry (TLD 400's) was used on each shot in order to monitor the dose received by the fiber.

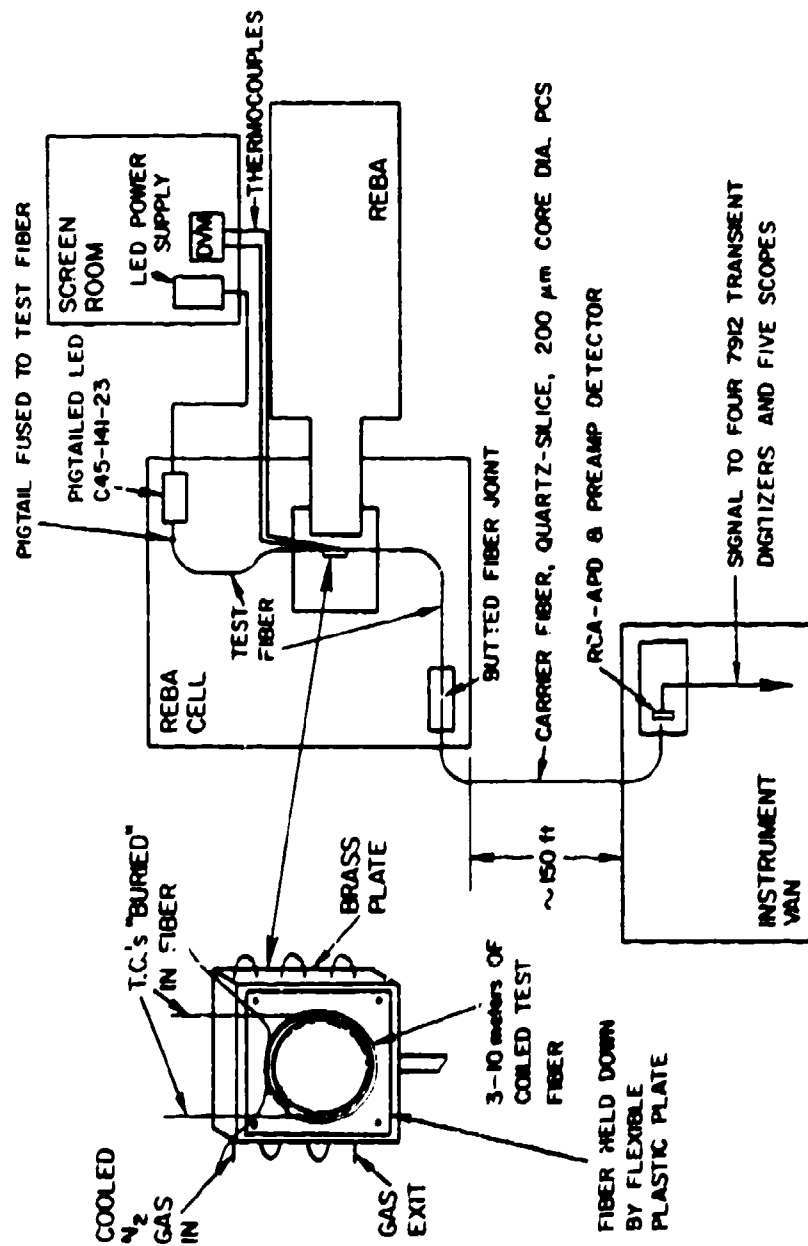


Figure 6. Experimental layout for X-ray induced transient attenuation measurements of the Corning SF fiber as a function of temperature and dose using the Relativistic Electron Beam Accelerator (REBA) facility at Sandia National Labs. The REBA emits a 50 ns wide X-ray pulse with an average energy of about 2.5 MeV. Beam turn-around time is approximately 15 min.

SECTION IV

EXPERIMENTAL RESULTS

1. Permanent Neutron Damage Effects on LED Spectra

In this section we present the results of measurements of electroluminescence spectra at 76K and 300K before and after successive neutron irradiations of LEDs from the three groups shown in Table 1.

The dependence of the emission spectrum on LED current prior to any irradiation is shown in Fig. 7 at 76K and Fig. 8 at 300K for the bare GaAs LED, D2503AP-50. At 76K, Fig. 3 illustrates the typical "shifting-peak" spectra often observed for GaAs LEDs at low temperatures.¹ The shift of the peak to shorter wavelength as the current is increased from 9.0 μ A to 24mA is due to recombination of excess carriers between their respective Fermi levels, the separation of which is proportional to applied voltage. Therefore, as the voltage is increased the peak energy increases. In contrast, Fig. 8 shows that at 300K no peak shift is observed over the range 30 μ A to 75mA. As indicated in Fig. 9, this is also true for the bare GaAlAs LEDs at room temperature. However, as shown in Figs. 9 and 10, multiple peaks are usually observed for the GaAlAs LEDs at 300K and 76K. As in the case of GaAs, peak shifts as a function of current are also observed for GaAlAs at 76K. Note that the high energy, near-edge peak has a stronger shift than the longer wavelength impurity emission.

These results are not merely device physics details; rather they are relevant to fiber optic data link applications because the behavior of the fiber in a radiation environment is dependent on wavelength.^{7,8,9} For example, the occurrence of shifting peak spectra at operating temperatures could cause problems if the LED emission shifts to wavelengths where fiber attenuation is increased when the LED current is changed.

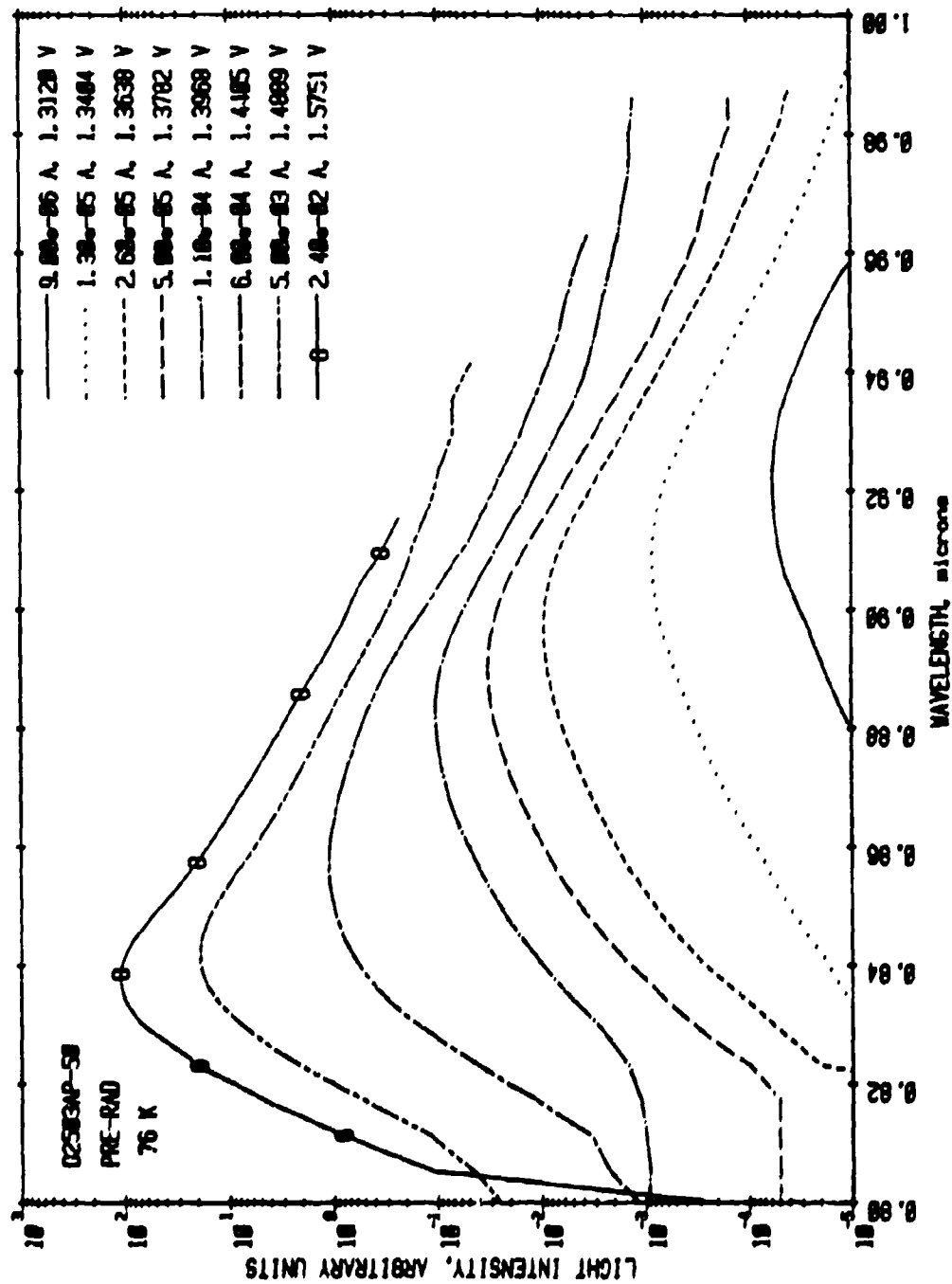


Figure 7. Pre-irradiation electroluminescence spectra at liquid nitrogen (76 K) from a bare (no lens or pigtail) Plessey GaAs LED as a function of LED current. Note the peak shifts rapidly with increasing voltage.

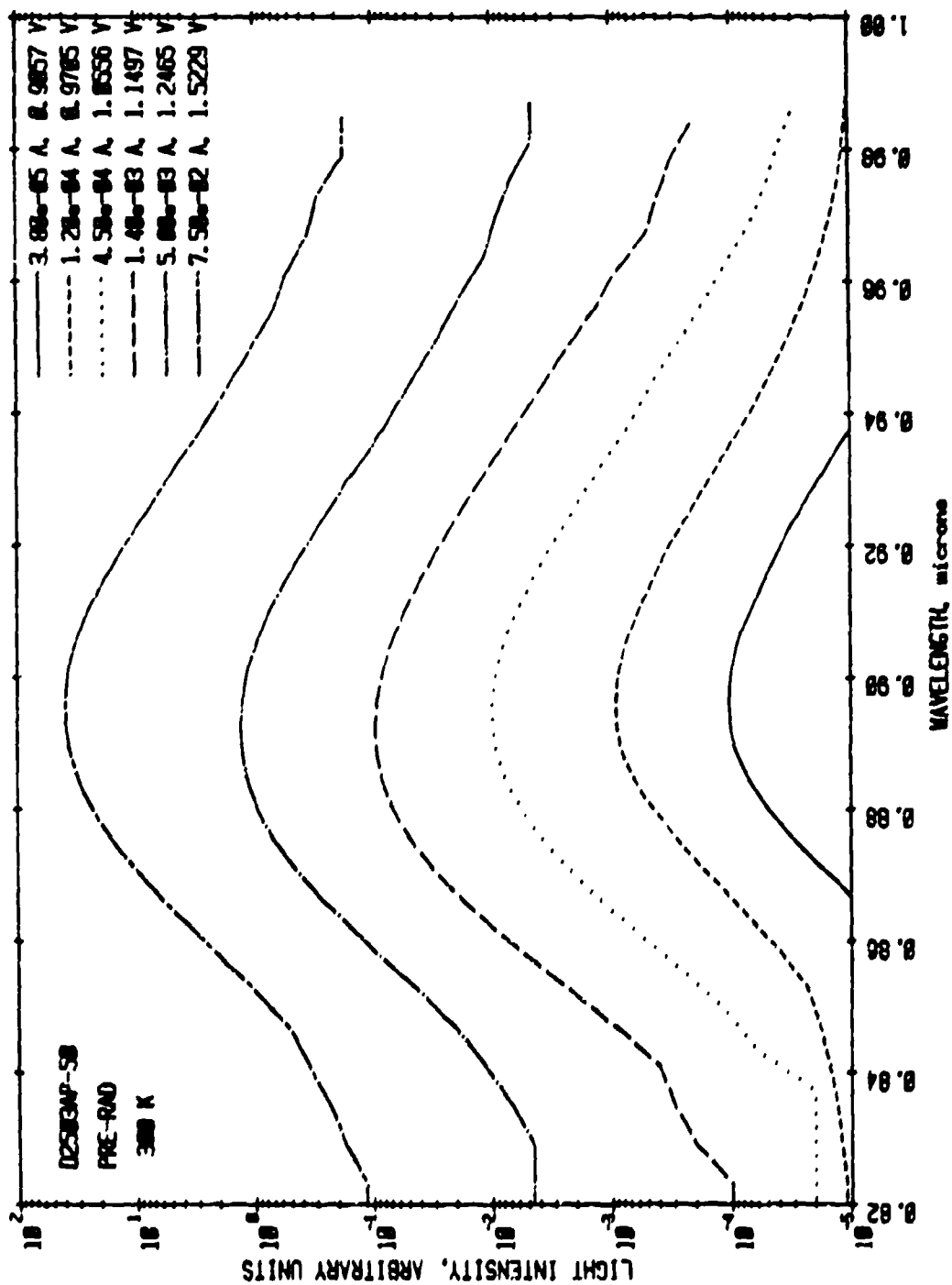


Figure 8. Pre-irradiation room temperature electroluminescence spectra from a bare (no lens or pigtail) Plessey GaAs LED as a function of LED current. In contrast with the 76K spectra, there is no peak shift.

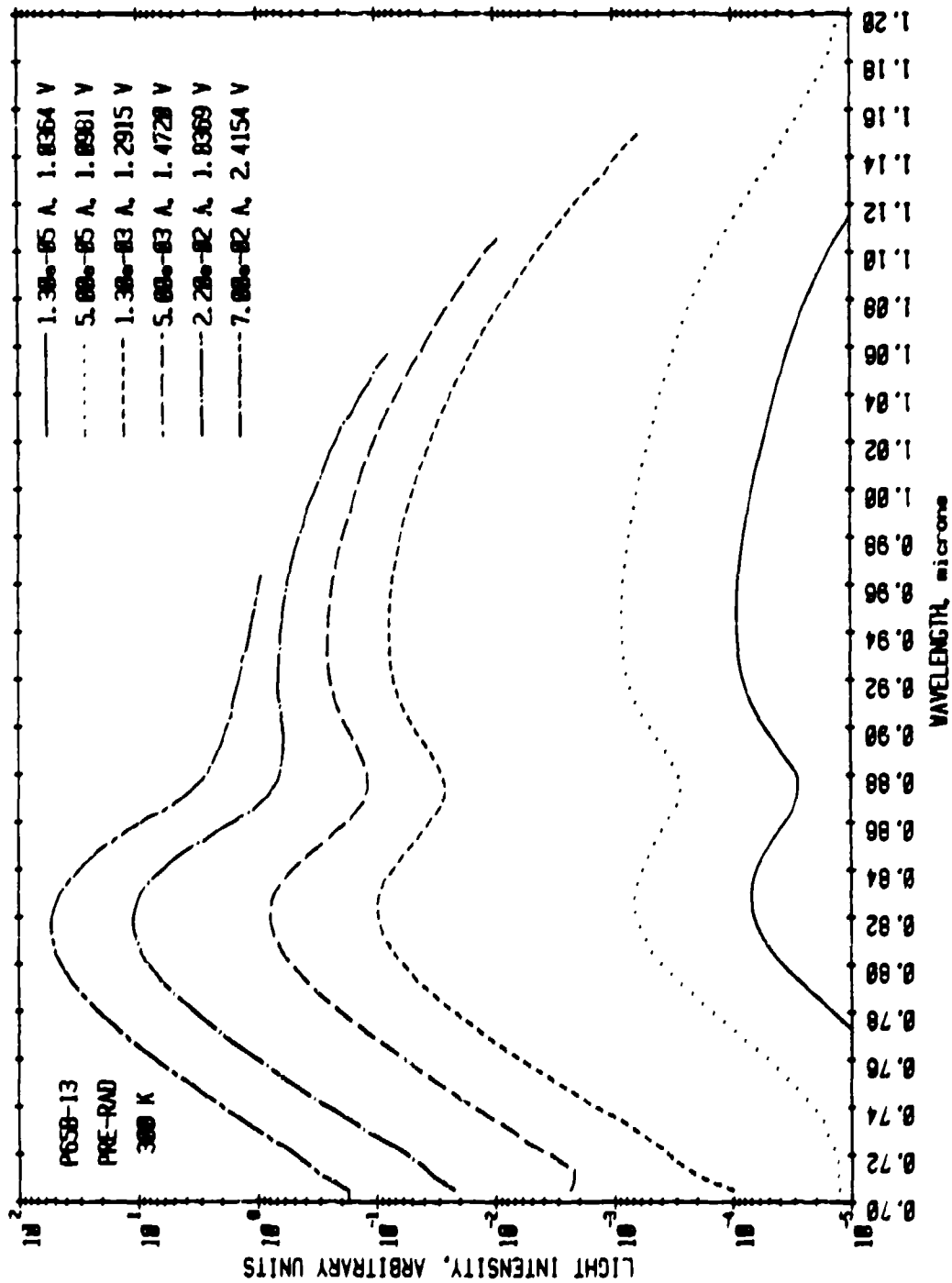


Figure 2. Pre-irradiation room temperature electroluminescence spectra from a bare (no lens or pigtail) Plessey Ga_{0.9}Al_{0.1}As LED as a function of LED current. Note that the long wavelength band is dominant at low currents.

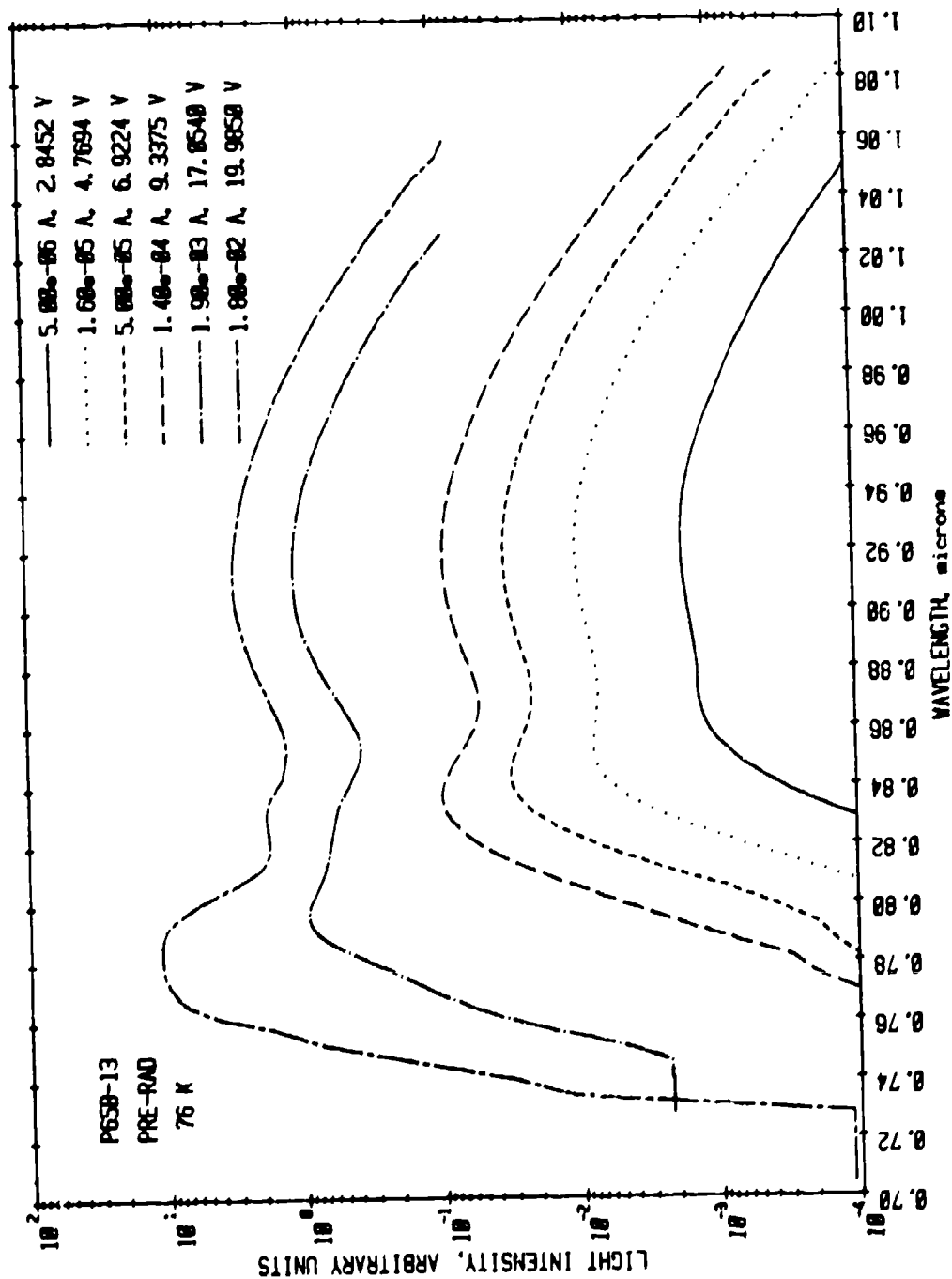


Figure 17. Pre-irradiation 76 μ electroluminescence spectra from a large (no lens or pigtail) Plessey Ga_{0.95}In_{0.05}As LED as a function of LED current. In contrast with the long wavelength emission, the near-edge band shifts rapidly with voltage.

Figures 11, 12 and 13 show the neutron-induced reduction in spectral output at 76K and 300K, respectively, for the GaAs LEDs at a constant current of 5.0mA. Note that for D2503AP-50, the reduction in output is much greater at 300K than at 76K for fluences varying from $6.6 \times 10^{12} \text{ n/cm}^2$ to $5.1 \times 10^{14} \text{ n/cm}^2$. This difference necessitates the use of a log scale for the 300K data in Fig. 12. At both temperatures there is no significant neutron-induced change in spectral shape or peak wavelength except for large fluences at 76K. This is also true of the room temperature data for the later lensed GaAs LED, CXL004-81, shown in Fig. 13. This independence of peak energy is important for reasons outlined in the previous paragraph. Comparison of Figs. 12 and 13 indicates that the bare and lensed GaAs LEDs have about the same degradation rate. This rate is also characteristic of the CXL003 GaAs LEDs which are both lensed and pigtailed. Consequently, from the point of view of spectral degradation, the lens and pigtail have no significant effect on neutron-induced degradation.

Neutron-induced spectral degradation in the GaAlAs LEDs is illustrated in Figs. 14-16. A comparison of Figs. 14 and 15 for P65B-13, the bare LED, indicates that as in the case of GaAs the spectral output of GaAlAs is less sensitive to neutron degradation at 76K. At this temperature and in the mA range, the longer wavelength impurity emission is prominent. Note that the degradation rate of this band is approximately the same as that for the near-edge emission at $0.80 \mu\text{m}$. In contrast, the temperature spectra at 5.0mA shown in Fig. 15 indicate that the near edge emission band is more sensitive to degradation than the impurity emission. At lower currents, however where the long wavelength band is more intense than the edge emission, the degradation rates are about equal.

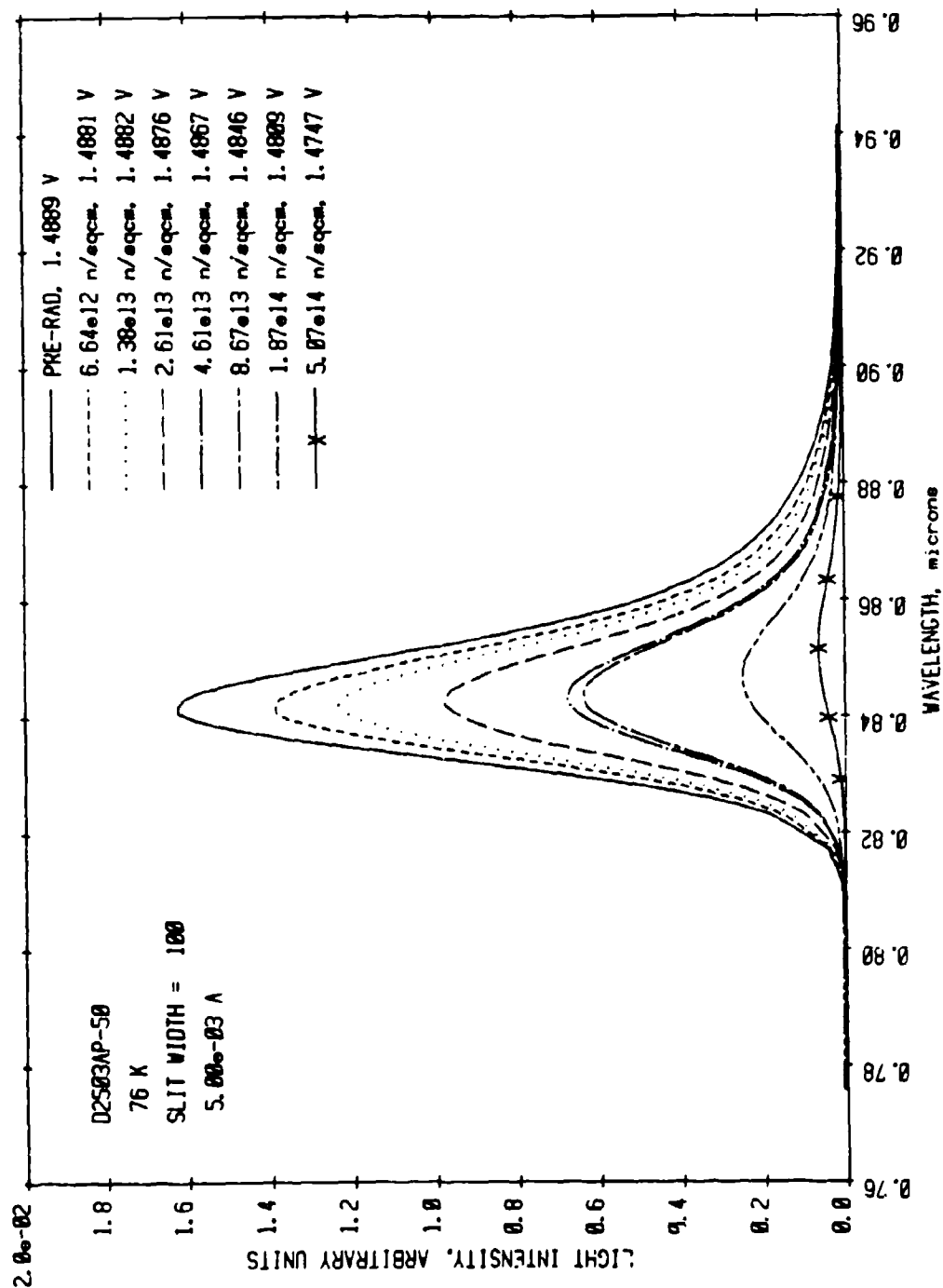


Figure 11. Neutron-induced degradation of the 76K electroluminescence spectra from a bare (no lens or pigtail) Plessey GaAs LED at a constant current of 5.0 mA. Note that except for large fluences, there is no irradiation induced shift in the peak wavelength.

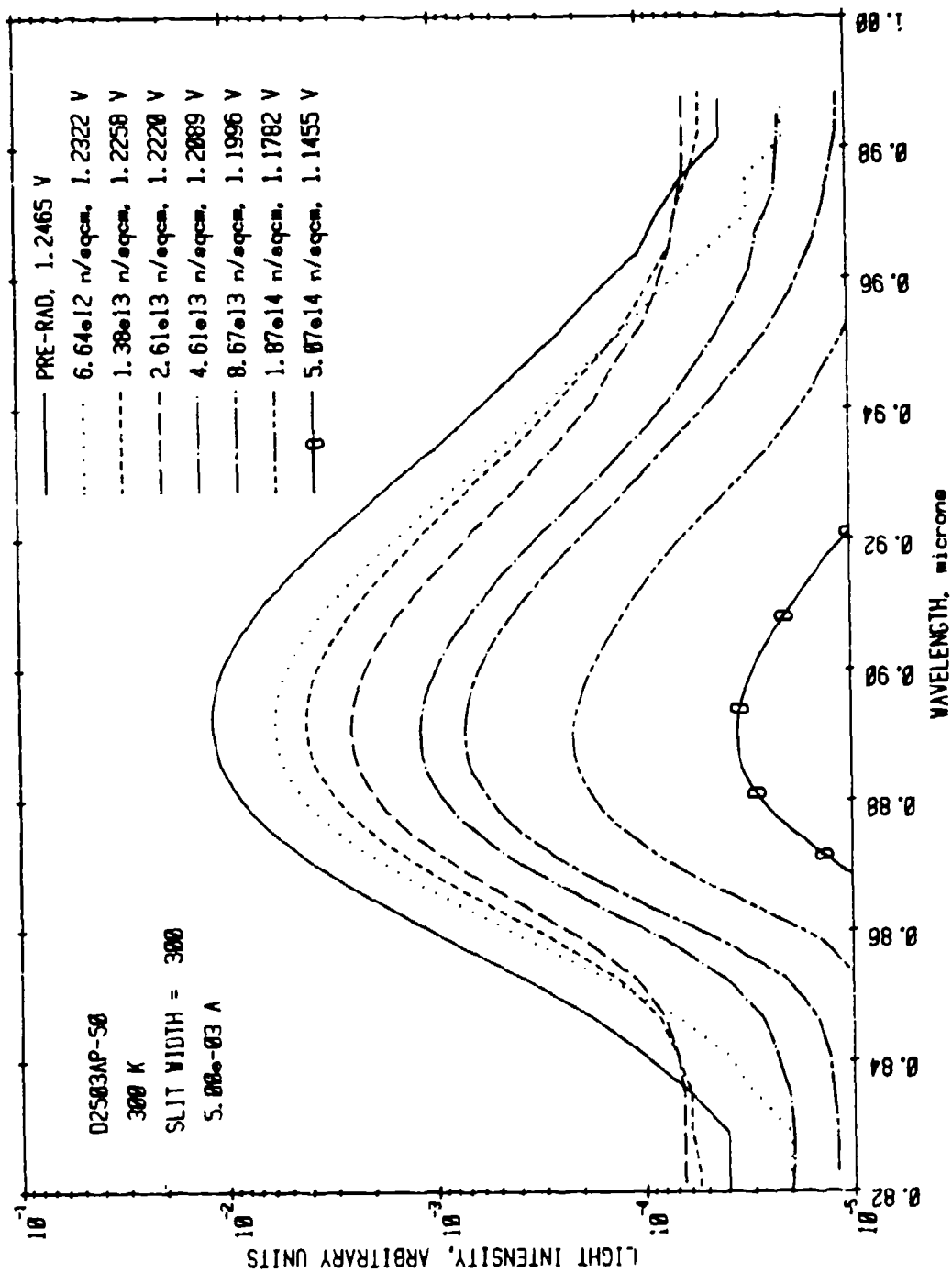


Figure 12. Neutron-induced degradation of the 3000 K electroluminescence spectra from a bare (no lens or pigtail) Plessey GaAs LED at a constant current of 5.0 mA. Note the lack of any neutron-induced peak shift.

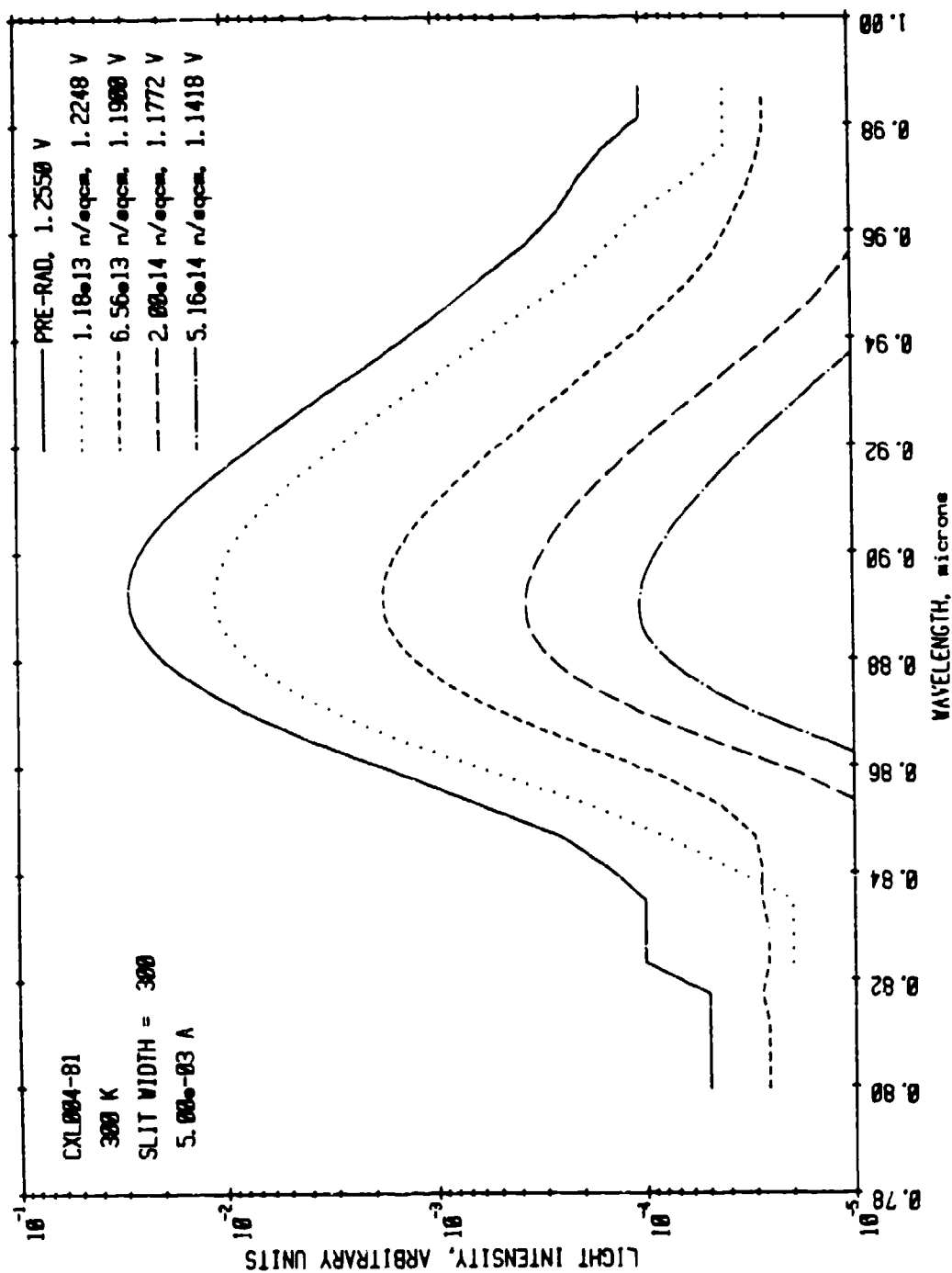


Figure 13. Neutron-induced degradation of the room temperature electroluminescence spectra from a lensed but unpoled Plessey GaAs LED at a constant current of 5.0 mA. The rate of degradation is about the same as for the bare LED in Fig. 12.

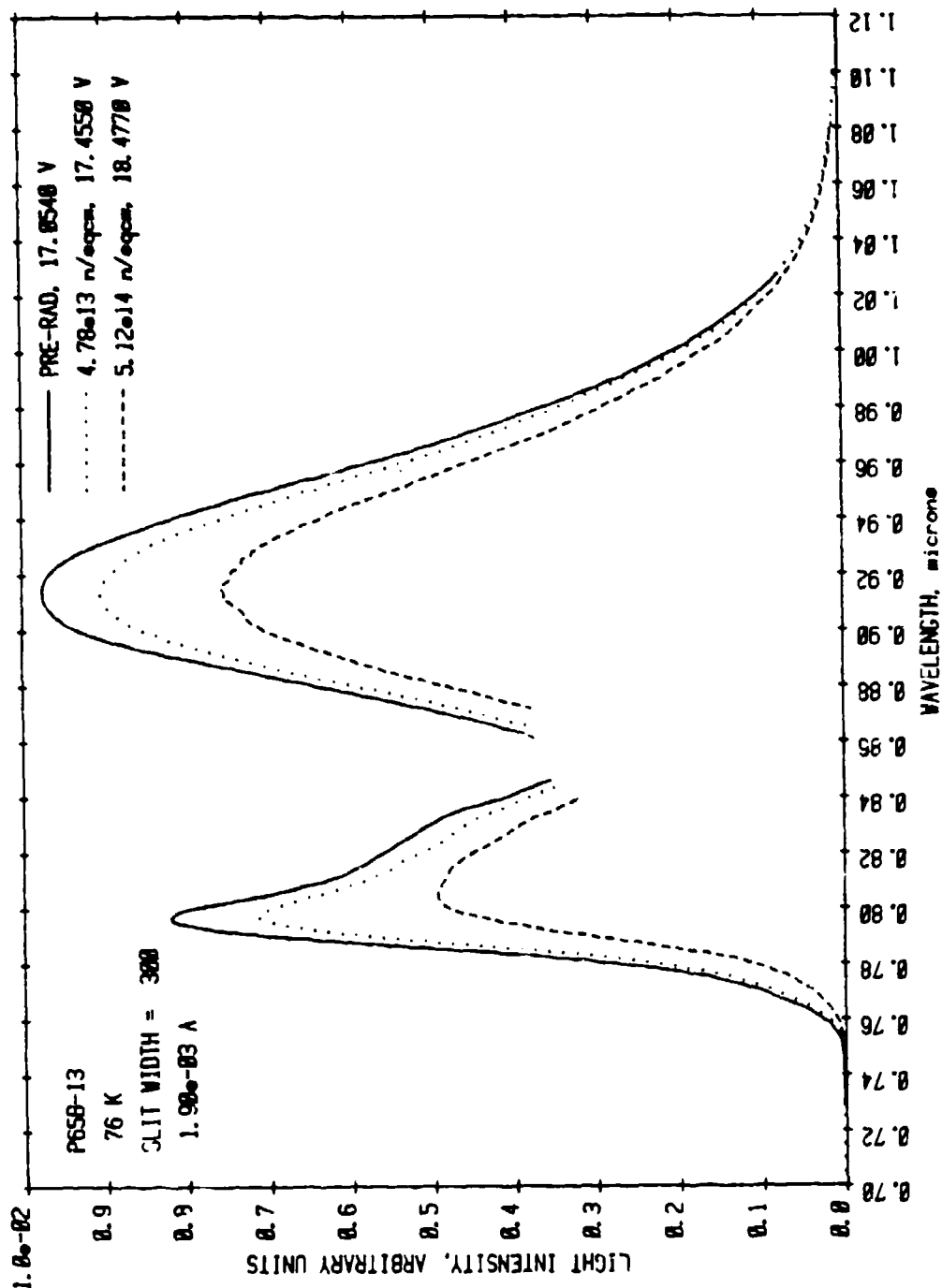


Figure 14. Neutron-induced degradation of the 76K electroluminescence spectra from a bare Plessey GaAs LED at a constant current of 1.9 mA. Note that both bands degrade at about the same rate.

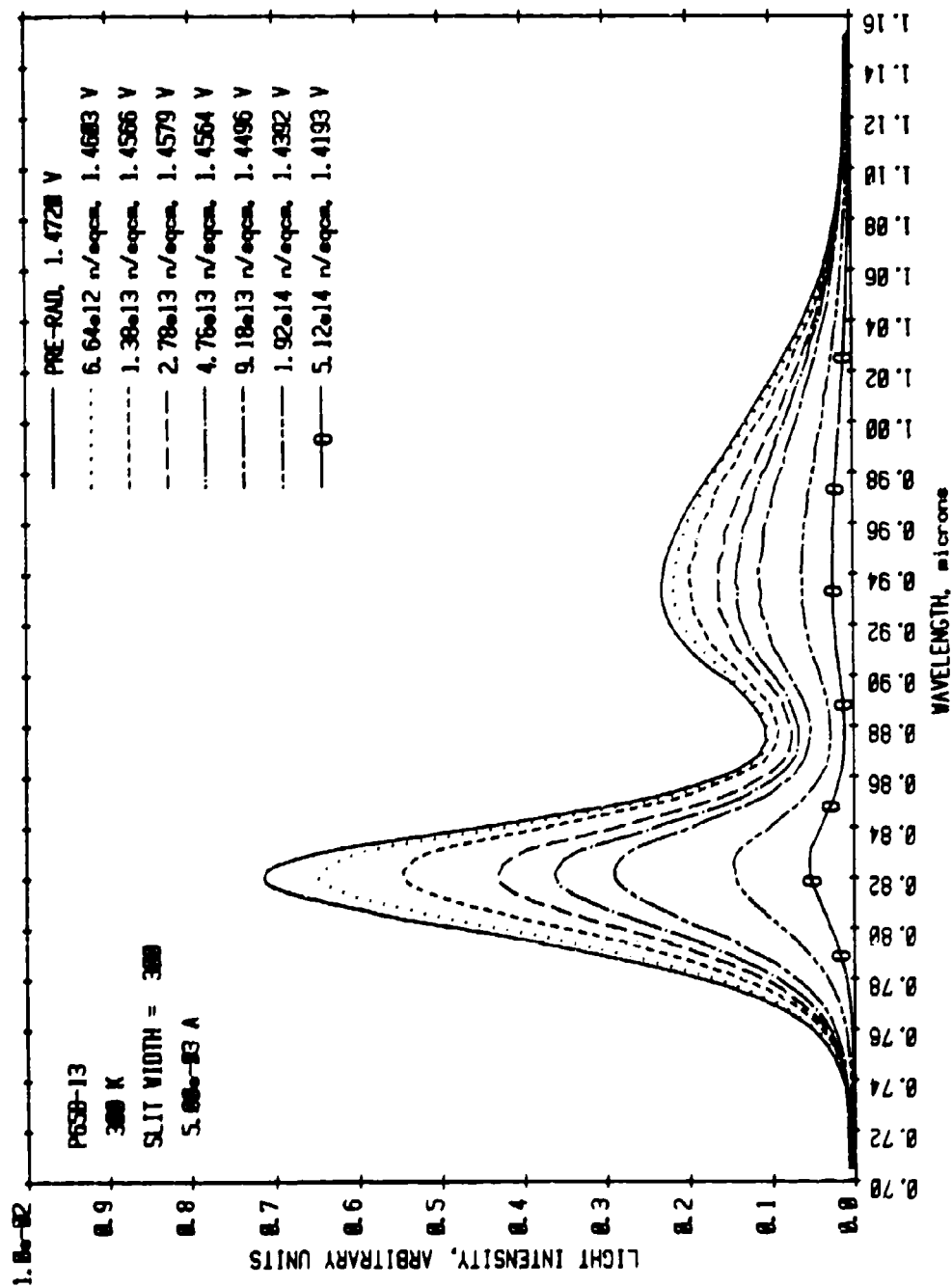


Figure 15. Neutron-induced degradation of the room temperature electroluminescence spectra from a bare (no lens or pigtail) Plessey GaAs LED at a constant current of 5.0 mA. The near edge band is somewhat more sensitive than the long wavelength emission. Neither band shifts with fluence.

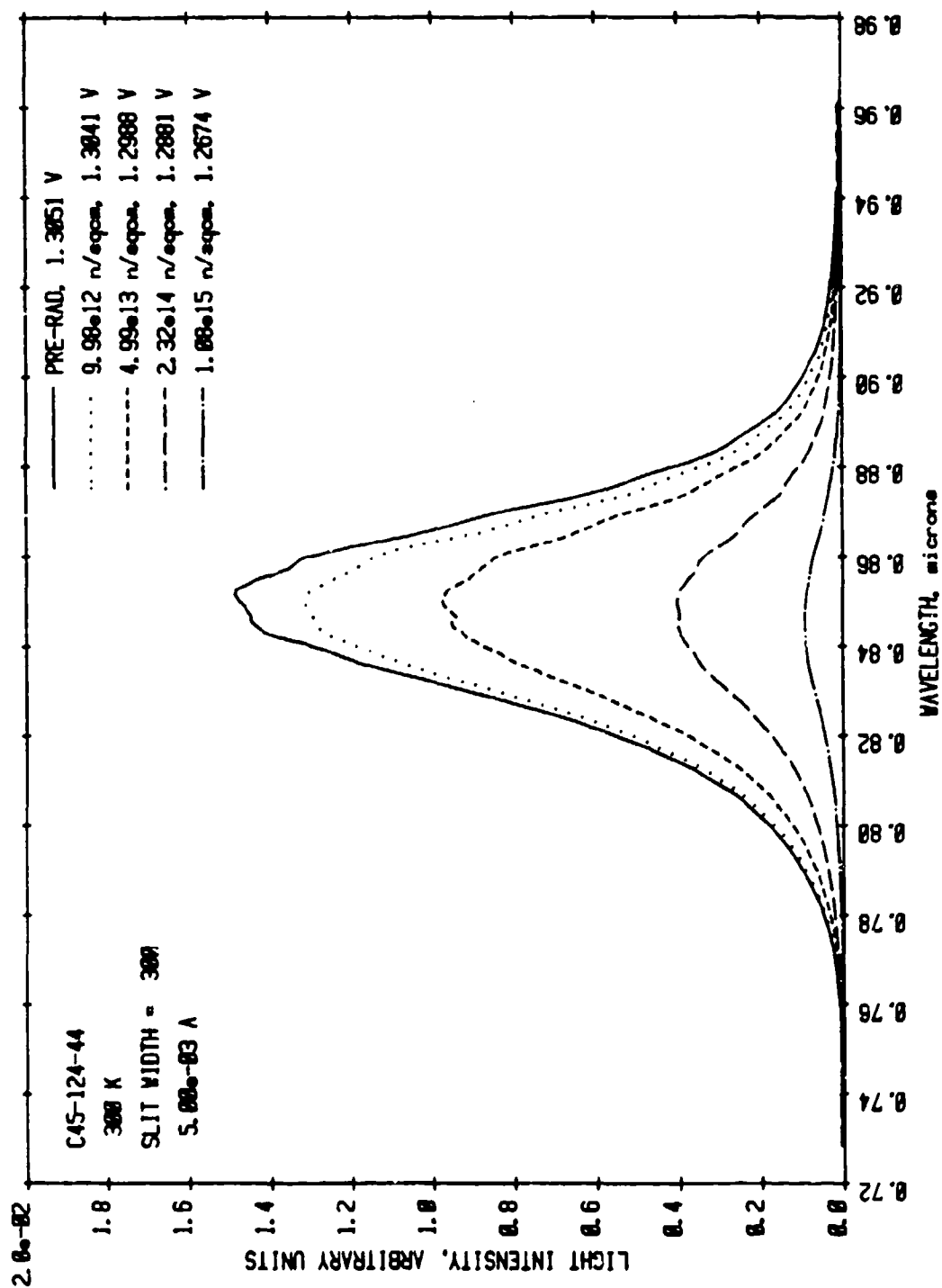


Figure 16. Neutron-induced degradation of the room temperature electroluminescence spectra from a pigtailed Plessey GaAs LED at a constant current of 5.0 mA. Note the absence of the long wavelength band found in earlier LEDs, and the lack of any peak shift with fluence.

An example of spectral degradation of one of the pigtailed LEDs from the most recent group is shown in Fig. 16. Note that the long wavelength emission band exhibited by the first group of LEDs is not present in these later devices. As for all the other LEDs at 300K, neutron irradiation does not result in a peak shift of the emission band. The degradation rate shown in Fig. 16 is approximately the same as that for the bare LED in Fig. 15, again suggesting that the lens and pigtail do not play a role in the LED degradation.

The next three figures, Figs. 17-19, illustrate a series of spectral comparisons between various LED types. Returning attention to GaAs, Fig. 17 shows a comparison between the Plessey bare LED, D2503AP-50, and a similar LED selected from a group of devices manufactured for our radiation effects studies by Texas Instruments (TI). While both are GaAs LEDs, the structures are significantly different in that the TI device, SLH-1-2, is a planar emitter with a buried junction structure. These 300K spectra have been normalized to the same peak value. The junction area of SLH-1-2 is about 100x greater than that for D2503AP-50. Therefore, the currents indicated result in approximately the same current density. Note that the spectral shapes are quite similar except that the D2503AP-50 LED has a peak location at a slightly longer wavelength.

Four normalized spectra are shown in Fig. 18 at 300K and a LED current of 5.0mA. All the LEDs are Plessey devices, three are GaAs, while P65B-13 is a bare GaAlAs LED. The structure of the three GaAs LEDs is as follows: D2503AP-50 is bare, CXL004-81 has no fiber pigtail but does have a lens, and CXL003-82 has both pigtail and lens. The spectra for the two unpigtailed LEDs are identical while the fibered LED spectrum has the same shape but is shifted to shorter

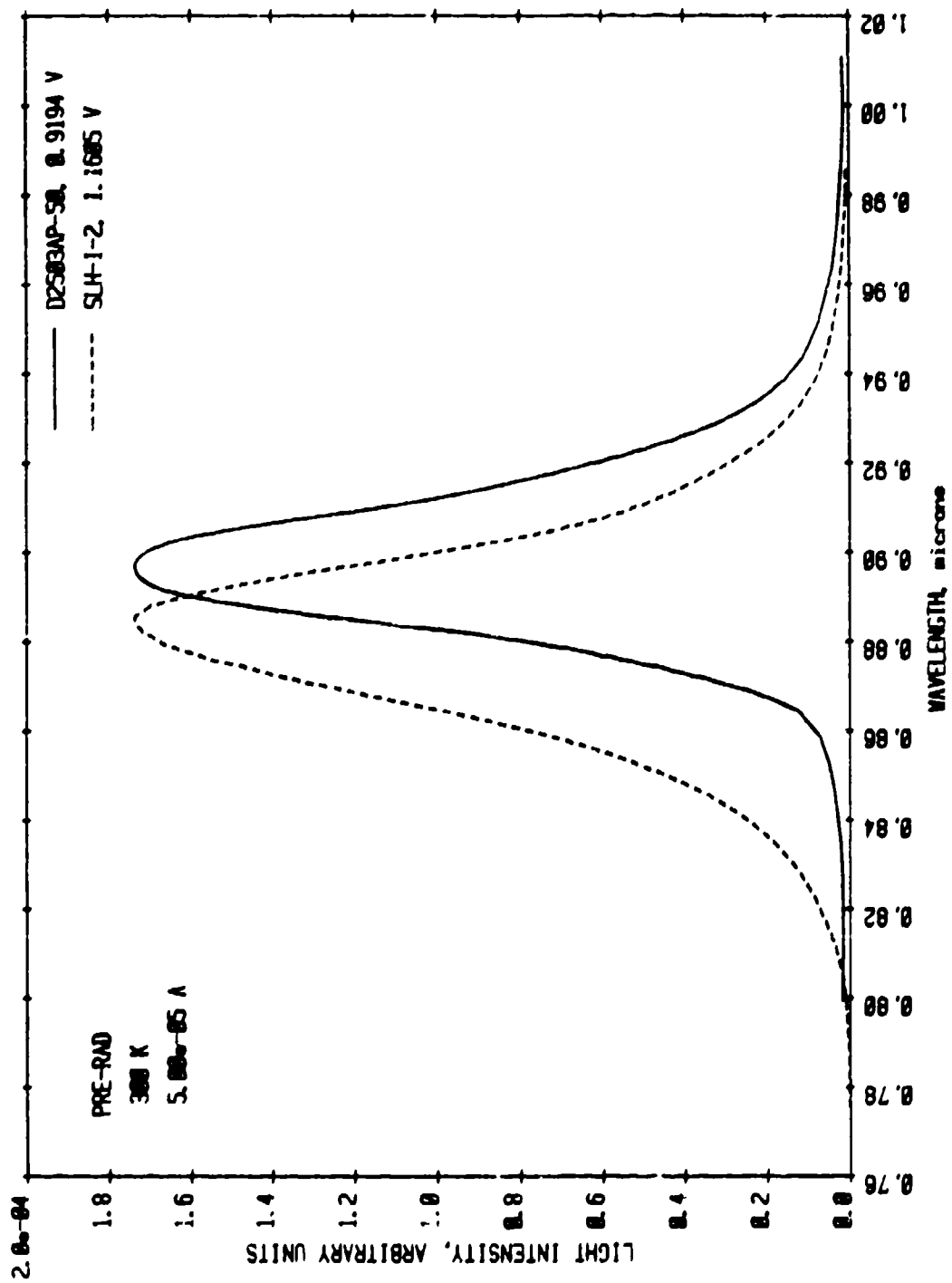


Figure 17. Pre-irradiation room temperature electroluminescence spectra at 50 μ A from a bare Plessey GaAs LED (DZ583AP) and a planar TI GaAs LED (SLH-1-2). The spectra have been normalized to the same peak height.

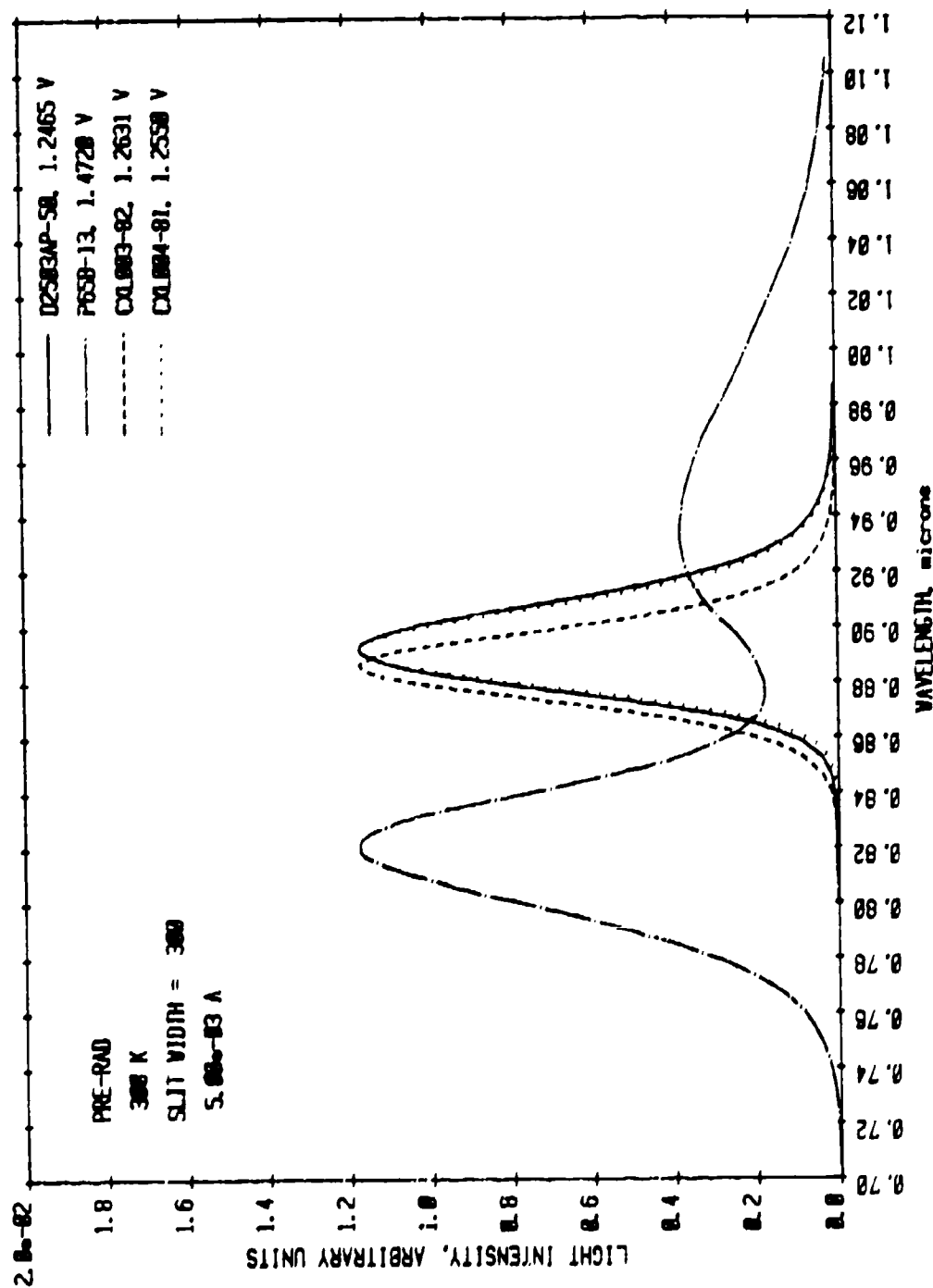


Figure 18. Pre-irradiation room temperature electroluminescence spectra at 5.0 mA from a bare Plessey GaAlAs LED (P658) and three Plessey GaAs LEDs: bare (D2583AP), lensed (CXL004), and lensed and pigtailed (CXL003). Peak heights have been normalized to the same value.

wavelengths. This result indicates that the lens has no effect on the spectrum, but the Corning fiber pigtail, because of its absorption and coupling characteristics, may be responsible for small changes in the LED output spectrum.

The GaAlAs (P65B-13) spectrum is quite different from any of the GaAs LEDs. The shorter wavelength band is of course due to the increased energy gap of the GaAlAs which allows the edge emission to occur at higher energies than in GaAs. These GaAlAs devices also possess a longer wavelength impurity emission band centered at about $0.93\mu\text{m}$ which is not present in the GaAs devices. As shown in Fig. 19, this band also does not occur in later GaAlAs devices supplied by Plessey. The CXL009-93 and C45-124-44 samples have a fiber and lens, while CXL013-18 has only a lens. Apparently these later LEDs are lacking the impurity or defect responsible for the long wavelength band. The introduction of this impurity band may be due to material variations or to the fact that proton bombardment isolation was used for CXL009, CXL013, and C45-124-44 while oxide isolation was used for P65B. The slight difference in peak location between CXL009 and CXL013 is in the opposite direction compared to GaAs (Fig. 18) for fibered versus unfibered LEDs. This result suggests that these shifts are due to effects other than the fiber or that the fiber attenuation is a minimum near $0.84\mu\text{m}$; that is for GaAs there is increased fiber absorption above $0.89\mu\text{m}$ so that pigtailling causes a shift to shorter wavelength, while for GaAlAs the attenuation increases with decreasing wavelength below about $0.84\mu\text{m}$ causing an opposite shift. At any rate, these shifts are relatively small even in comparison to the apparent doping level shift between C45-124-44 (doping level increased to increase speed) and CXL009, CXL013, P65B($2-3 \times 10^{18}\text{Ga/cm}^3$).

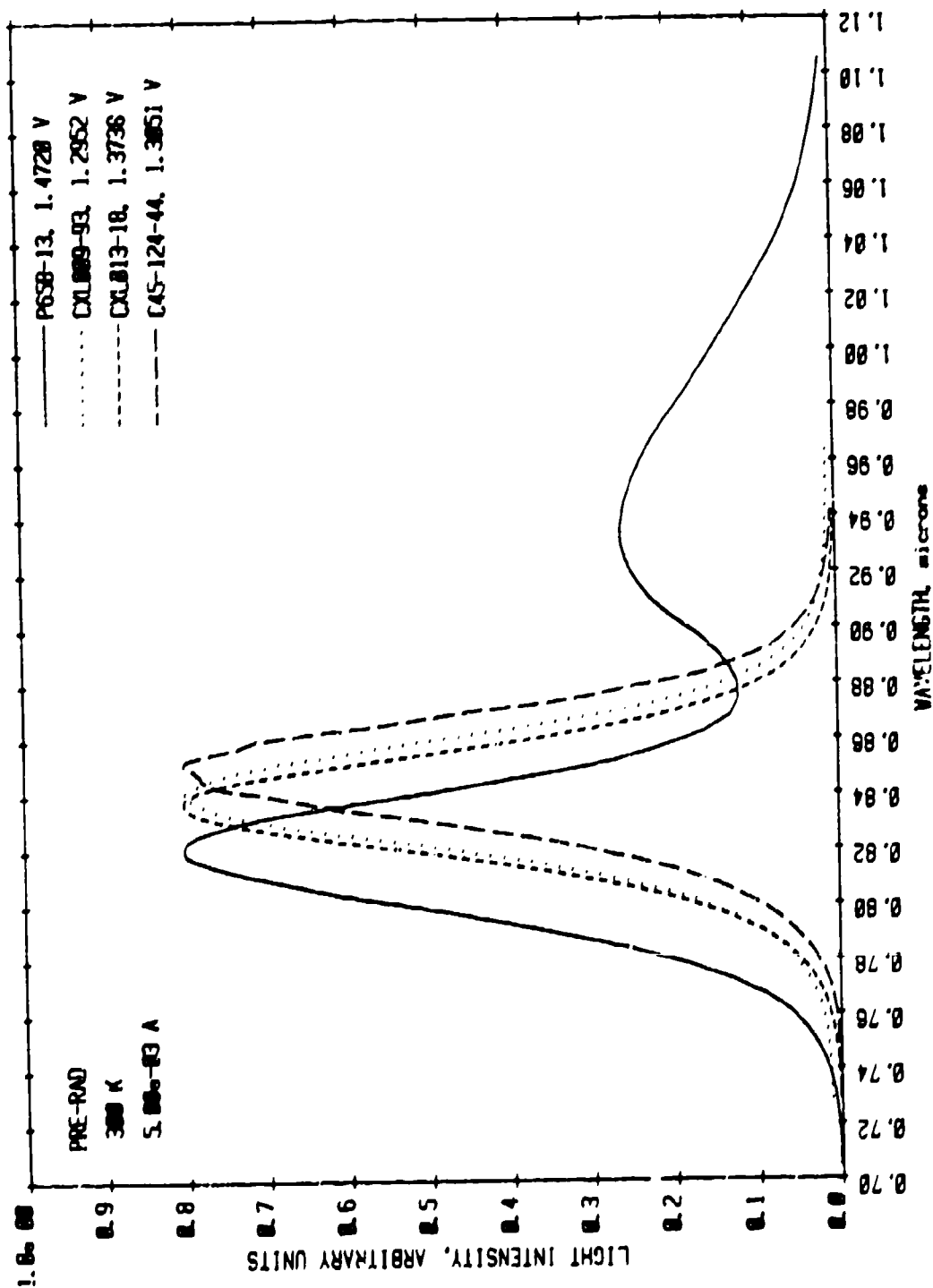


Figure 19. Pre-irradiation room temperature electroluminescence spectra at 5.0 mA from Plessey high radiance GaAs LEDs: bare (P658), lensed (CX1009 and CX1013), and pigtailed (CX5-124-44). Peak wavelengths have been normalized to the same value. Note the absence of the long wavelength emission in the later devices.

2. Permanent Neutron Degradation of Total LED Light Output and Current-Voltage

In this section we present a series of figures depicting total light output versus voltage and current and also the current-voltage characteristics as a function of neutron fluence. Comparisons will also be made between the various LEDs supplied by Plessey (PL) and also with the planar LEDs manufactured by Texas Instruments (TI).

The results presented thus far indicate that the high radiance Plessey GaAs and GaAlAs LEDs are quite insensitive to neutron irradiation. One of the primary reasons for this is that these devices operate at very high current densities in a range where the neutron-induced excess current is very small. This result is demonstrated in Fig. 20 where the current density, J , -voltage characteristic of the Plessey GaAs LED D2503AP-50 is compared with that of the TI planar GaAs LED, SLH-1-2, before and after about $5 \times 10^{14} \text{ n/cm}^2$. These data extend to the maximum allowable operating current density, J_m , for both LEDs. At lower current densities both LEDs show significant neutron-added excess current after $5 \times 10^{14} \text{ n/cm}^2$. Since this current does not cause light emission it causes a decrease in light output at constant total current. Note that at about 1.2V, the voltage corresponding to J_m for SLH-1-2, the neutron-added current is about the same for both LEDs. From another point of view, at $J = 100 \text{ A/cm}^2$ the decrease in the voltage necessary to maintain this value for J is actually greater for the Plessey LED, D2503AP. However, above a voltage of about 1.4V ($J > 4 \times 10^3 \text{ A/cm}^2$) there is no neutron induced current for the high radiance LED, D2503AP. Since this upper current range corresponds to typical operating levels, this component of neutron degradation does not contribute to reduced output at constant current for practical applications.

The lack of neutron-induced excess current at high currents in the various Plessey GaAs LEDs examined in this study is illustrated in Fig. 21. The devices

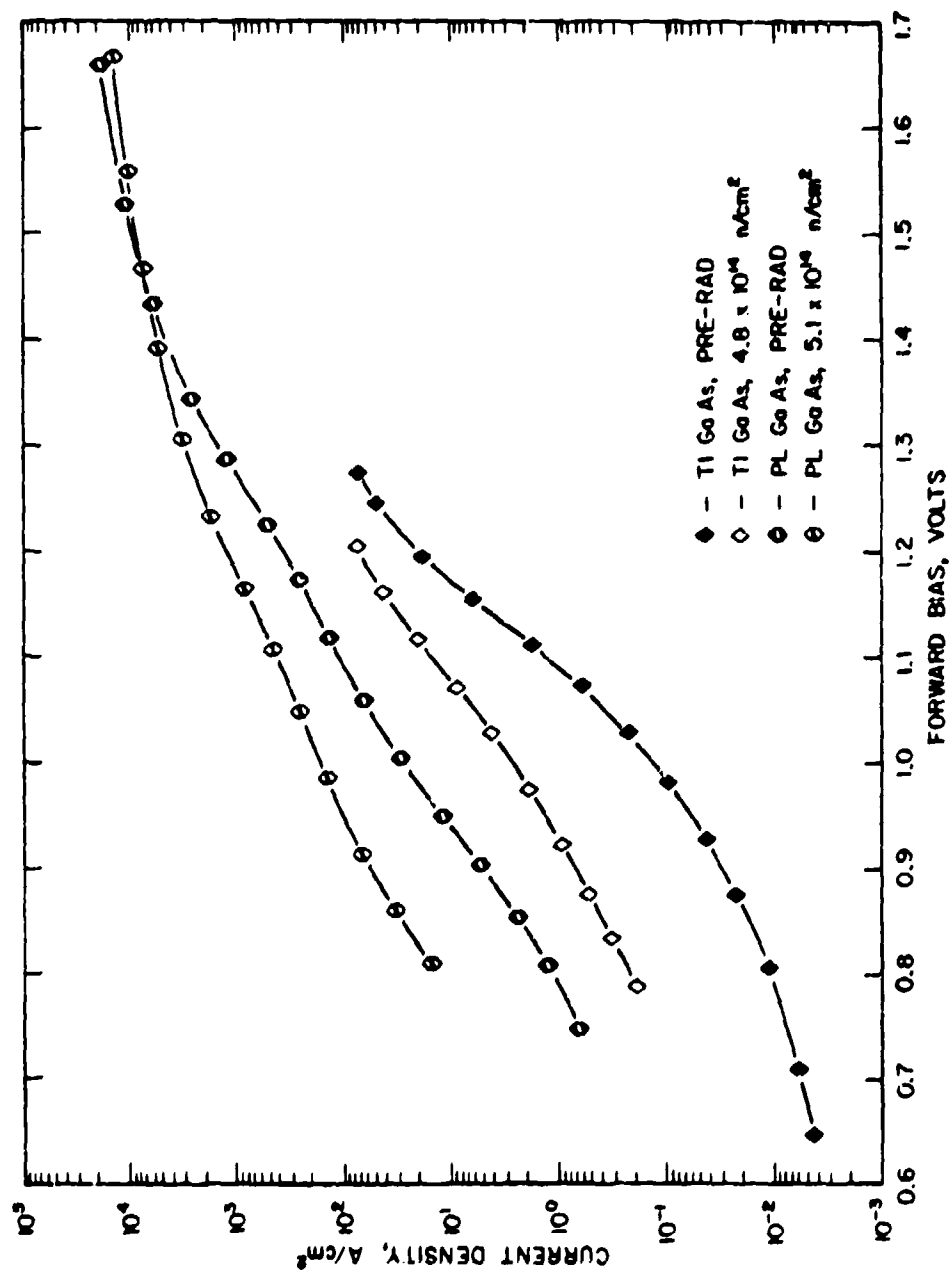


Figure 20. Current density versus forward bias at room temperature prior to and following irradiations of about 5×10^{14} n/cm² for a bare, high-radiance Plessey GaAs LED (D2503AP) and a planar TI GaAs LED (SLH-1-2). Note the lack of neutron-induced excess current at large current densities.

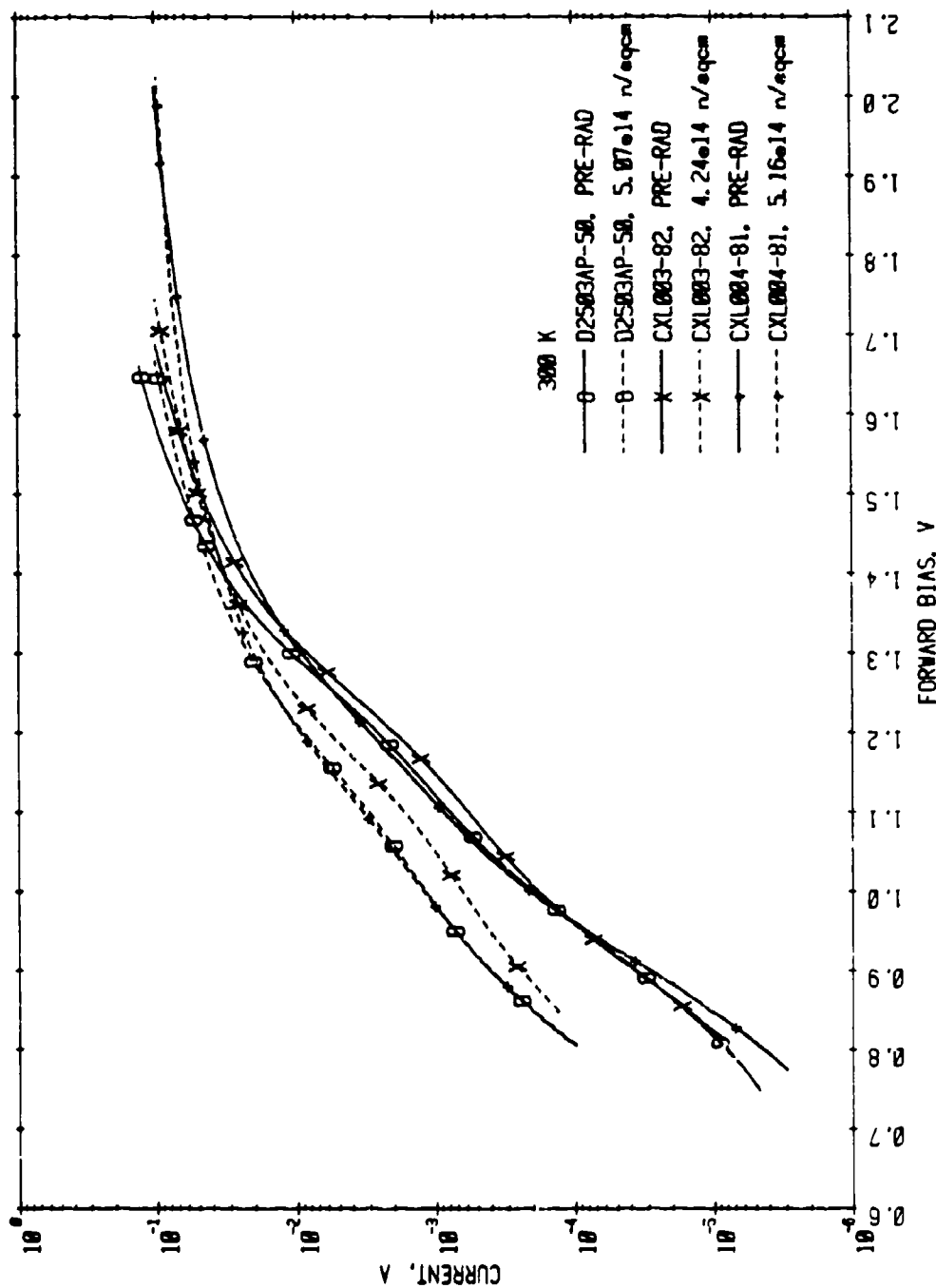


Figure 21. A comparison of current-voltage curves before and after irradiation to approximately 5×10^{14} n/cm² of three types of Plessey GaAs LEDs: bare (D2503AP), lensed (CXL004), and pigtailed (CXL003). In all three cases, the neutron-induced excess current is minimal at large currents.

included in this figure are: the bare LED, D2503AP-50; the lensed but unfibered LED, CXL004-81; and the lensed and fibered LED, CXI.003-82. Figure 21 shows that the neutron-added current is generally similar for the three devices. At low voltages there is significant additional current, but in the high voltage range there is no neutron-induced excess current. We conclude therefore, that as one might expect, the lens and fiber do not influence the neutron-induced excess current in the LED whether bare or completely packaged. Similar comparisons and conclusions can be drawn for the GaAlAs LEDs. For example the comparison shown in Fig. 22 of the bare Plessey device with a similar GaAlAs planar LED from TI again illustrates the lack of neutron-induced currents at high currents. Indeed, from the similarity in the shape of the curves at low voltages, one suspects that if the TI device could be operated at higher current densities it would show a similar characteristic.

In addition to neutron-added current, a major component of neutron-induced light output degradation is the reduction in minority carrier lifetime due to the introduction of recombination centers in the neutral p-region where radiative recombination occurs. These neutron induced centers compete for excess carriers resulting in reduced light output at constant voltage. Since the neutron added current can be accommodated at constant voltage, this mode of degradation is not observed when the voltage is held constant. Therefore, comparisons of light output degradation revealed in plots of total light intensity, L , versus voltage provide information about the degradation due to competitive nonradiative recombination at neutron induced centers in the neutral region. Such data are shown in Fig. 23 for the bare Plessey GaAs LED, D2503AP-50 and the planar TI device, SLH-1-2. Over the entire voltage range, L decreases more rapidly with neutron fluence, ϕ , at constant voltage for D2503AP-50

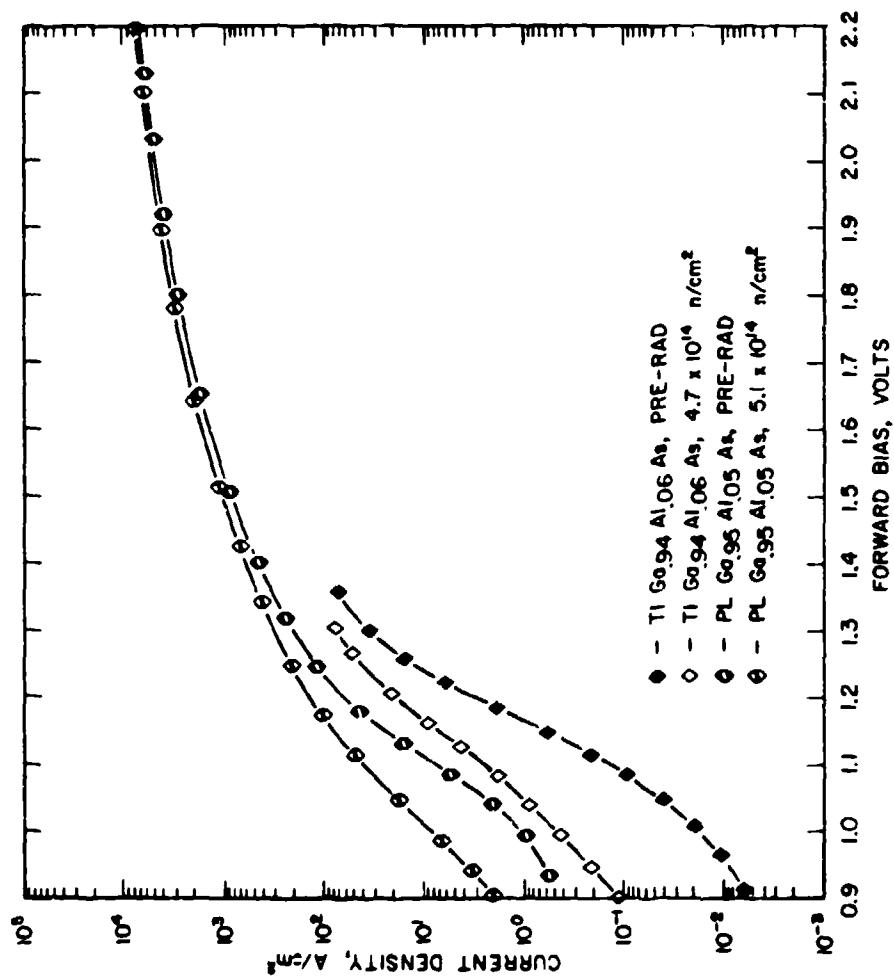


Figure 22. Pre- and post-irradiation room temperature current density - voltage curves for a bare, high radiance Plessey GaAs LED (P65R) and a planar TI GaAs LED (S411-5-51). Note the lack of excess current at large current densities.

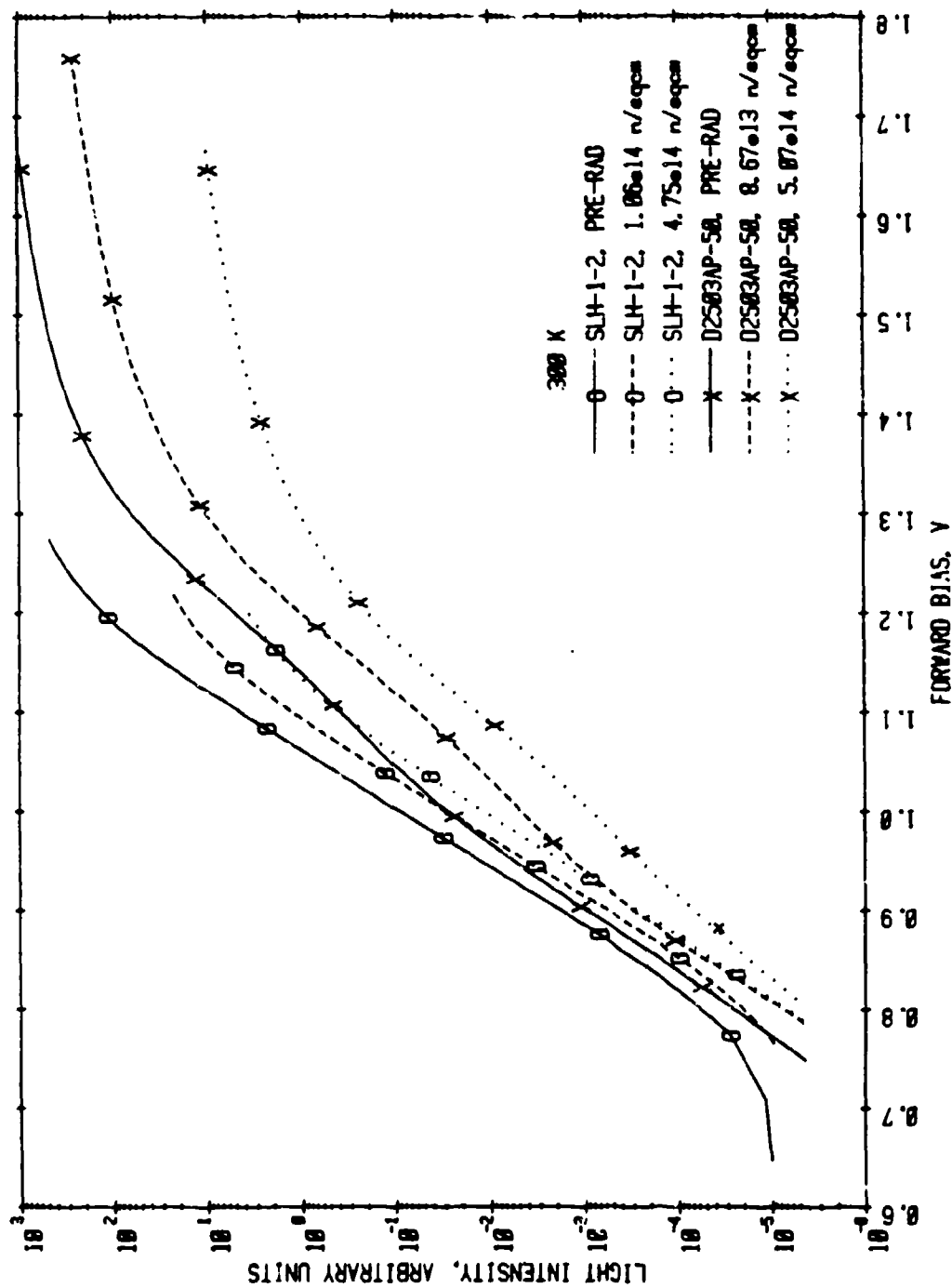


Figure 23. A comparison of the degradation of room temperature total light intensity - voltage characteristics for a pure, high resistance Plessey GaAs LED (D2503AP) and a planar TI GaAs LED (SLH-1-2). Note that over most of the voltage range, the Plessey device is more sensitive to irradiation.

than for SLH-1-2. Recall that the neutron induced excess current was stronger for SLH-1-2 than for D2503AP-50 at their respective maximum operating currents. consequently, the extent of the two modes of degradation differ markedly in these two devices.

A comparison of light intensity-voltage characteristic prior to and following an irradiation of approximately $5 \times 10^{14} \text{ n/cm}^2$ for the three types of GaAs LEDs studied is given in Fig. 24. These data and additional results on LEDs from these groups indicate that neither the lens nor the pigtail affect the light output degradation rates as a function of voltage. In Fig. 24 at lower voltages there is some variation in the reduction of L, but note that at larger voltages this decrease is about the same for the three LEDs.

Turning attention to the GaAlAs LEDs, Figs. 25 and 26 illustrate comparisons of the L-V characteristic for P65B-13, the bare GaAlAs LED, with the bare GaAs LED and a TI planar GaAlAs LED, respectively. Note that P65B-13 experiences less degradation over the entire voltage range than either of these other LEDs. As in the case of the GaAs LEDs, similar data for fibered and lensed LEDs and for lensed-only LEDs show that neither the fiber or lens play a role in the degradation of the L-V characteristic.

Thus far we have presented results illustrating two modes of neutron-induced degradation of LEDs: (1) excess non-radiative current, and (2) light output reduction due to competing recombination at non-radiative centers in the neutral region. As indicated in the Background section, when light output is measured as a function of LED current, one observes the combined effect of both these types of degradation. Consequently, the light output reduction at constant current is greater than that at constant voltage. The next four

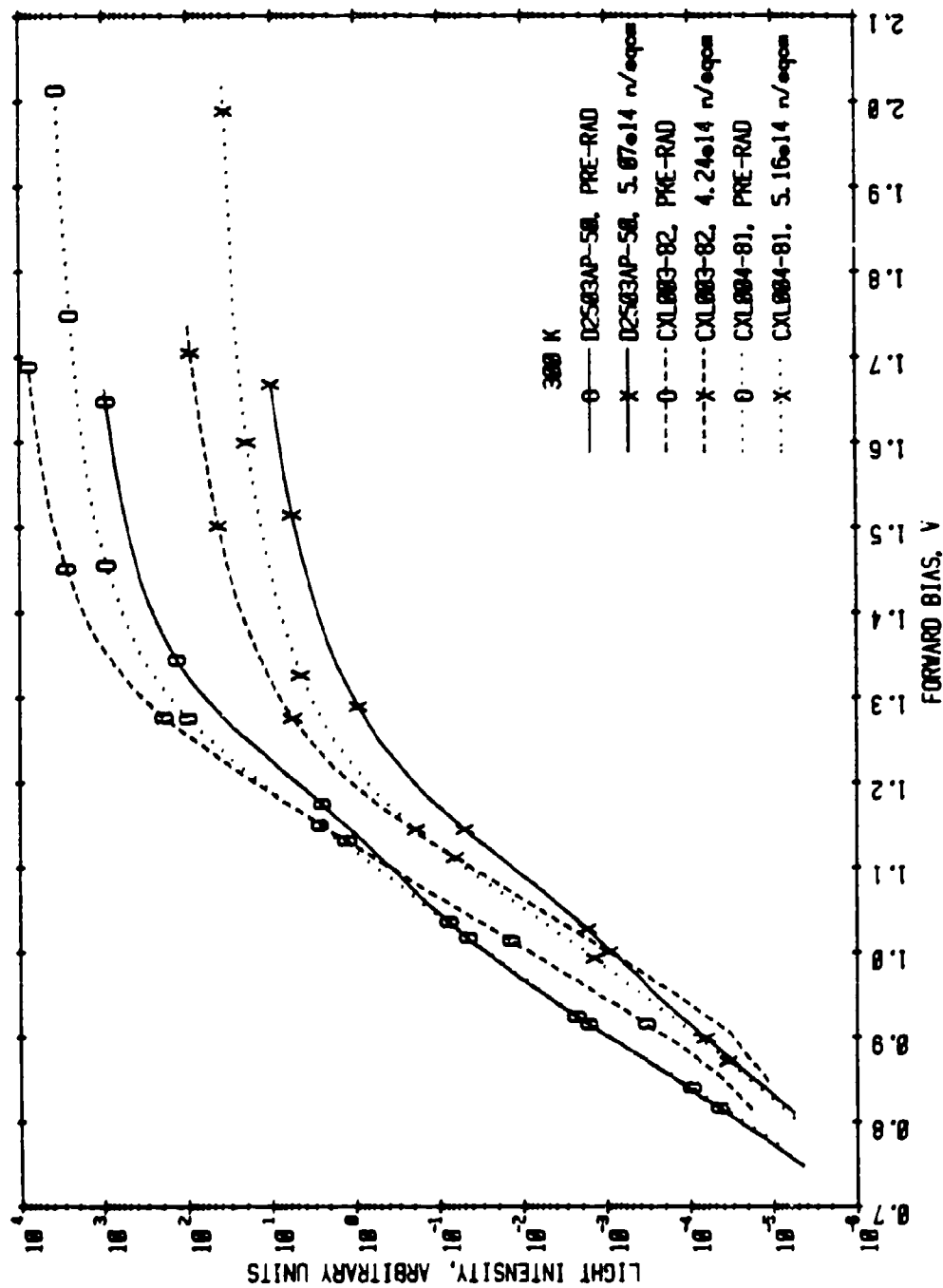


Figure 24. A comparison of the degradation of room temperature total light intensity-voltage curves for three types of Plessey high radiant GaAs LEDs: bare (D2503AP), lensed (CXL004), and lensed and pigtailed (CXL003). Degradation is approximately the same in all three LEDs.

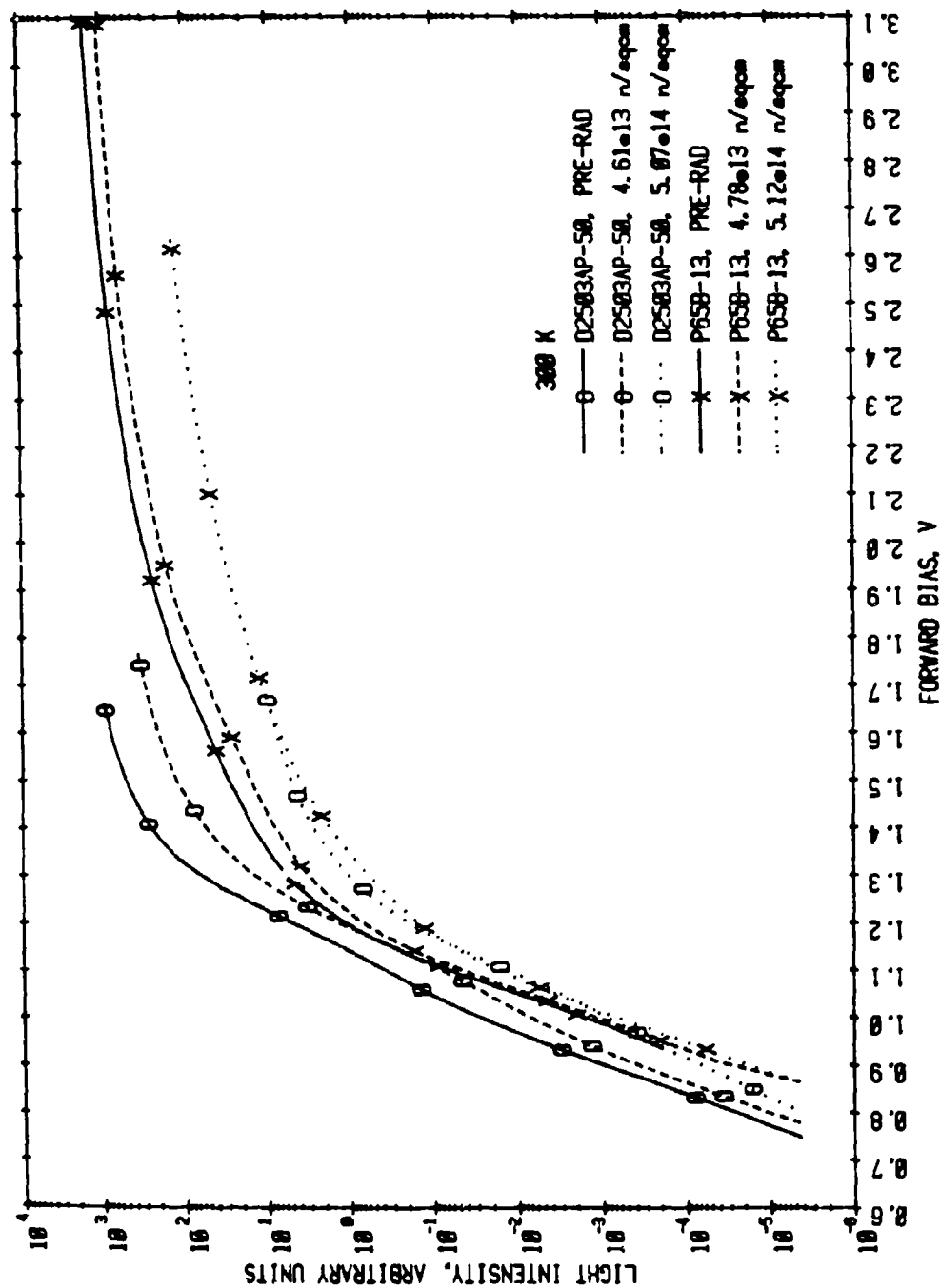


Figure 25. Degradation of room temperature light output as a function of voltage for a bare Plessey GaAs LED (D2503AP) and a bare Plessey GaAs LED (P65B) Over the entire voltage range, the GaAs device is less sensitive to neutron irradiation.

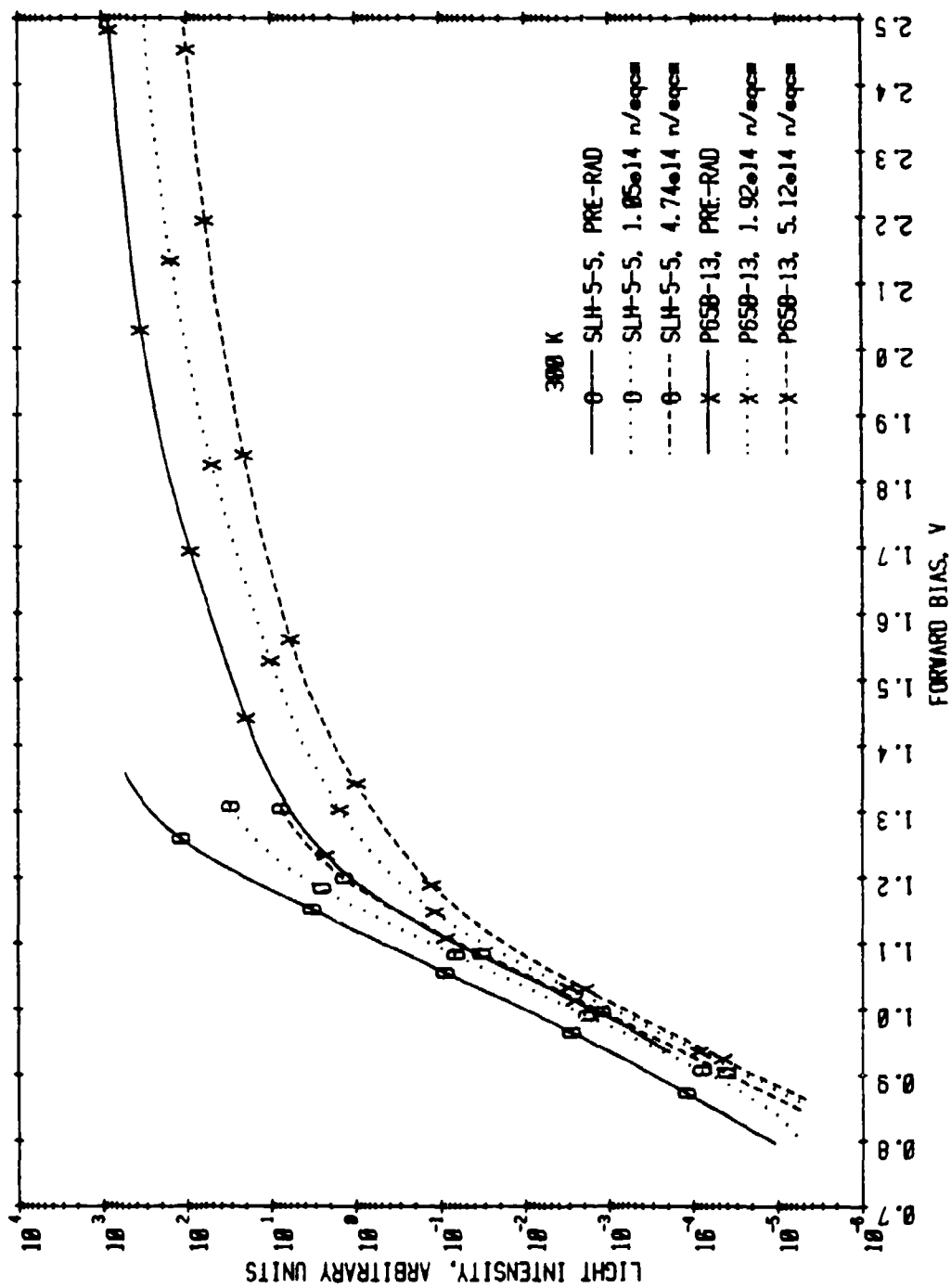


Figure 26. A comparison of neutron-induced degradation of total room temperature light output as a function of voltage in a bare Plessey GaAlAs LED (P659) and a planar TI GaAlAs LED (SLH-5-5). Note that the Plessey device degrades less than the TI LED.

figures, Figs. 27-30, illustrate these combined effects. In Fig. 27, L is plotted versus current density for the bare Plessey GaAs LED, D2503AP-50, and the TI planar GaAs LED, SLH-1-2. Recall that SLH-1-2 exhibited greater neutron-induced current but less light output degradation at constant voltage. Therefore, for constant current operation one expects the net effect to be approximately the same degradation rate in the two devices. The two groups of curves in Fig. 27 have about the same shape and separation with fluence indicating that this is the case.

The data in Fig. 28 illustrate that the three types of Plessey GaAs LEDs, that is bare, lensed, and fibered and lensed, have approximately the same constant current degradation rate over the range of current investigated. This is to be expected since the J - V data indicated that the lens and fiber did not affect the LED degradation rate. This conclusion is supported by additional data on other Plessey GaAs LEDs. In the case of the GaAlAs LEDs, both the excess current and the degradation of L at constant voltage were less for the Plessey device, P65B-13, than for the equivalent TI planar LED, SLH-5-5. Consequently, we can expect that for constant current operation the Plessey GaAlAs LEDs will possess a significant range over which they are insensitive to irradiation relative to the TI devices. This is borne out by the light intensity-current density curves for P65B-13 and SLH-5-5 in Fig. 29. Note that over the entire range of J , P65B-13 degrades less with fluence (the maximum ϕ for P65B-13 is $> \phi_{\max}$ for SLH-5-5) than SLH-5-5. The degradation rate is also significantly smaller than for the GaAs LEDs.

A comparison of bare, lensed, and fiber plus lensed GaAlAs LEDs is given in Fig. 30 for light intensity versus current prior to and following $5 \times 10^{14} \text{ n/cm}^2$. There is some variation in light intensity degradation at

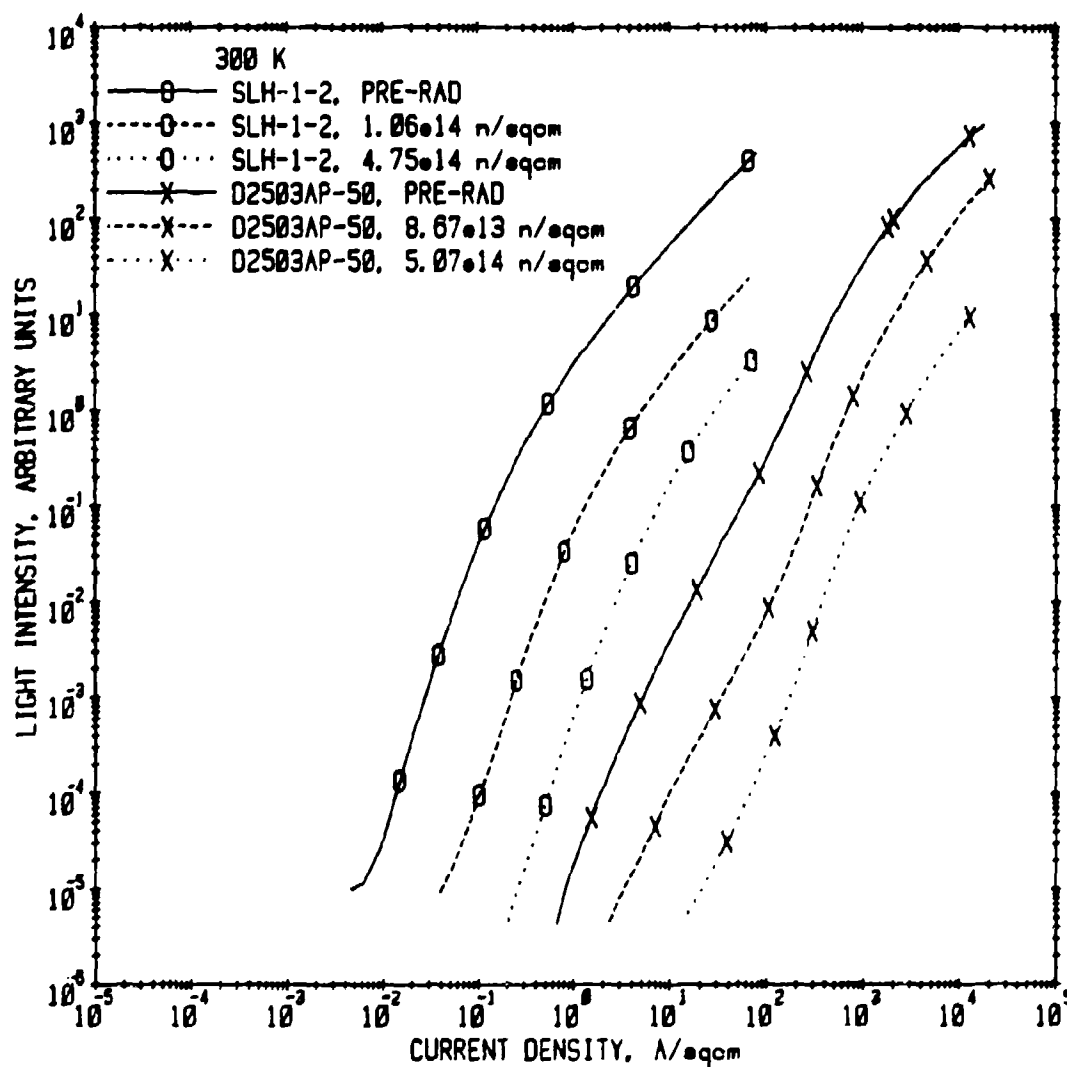


Figure 27. Neutron-induced degradation of room temperature total light intensity as a function of current density in a bare Plessey, high radiance GaAs LED (D2503AP) and a planar TI GaAs LED (SLH-1-2). The degradation rates are roughly the same in the two devices.

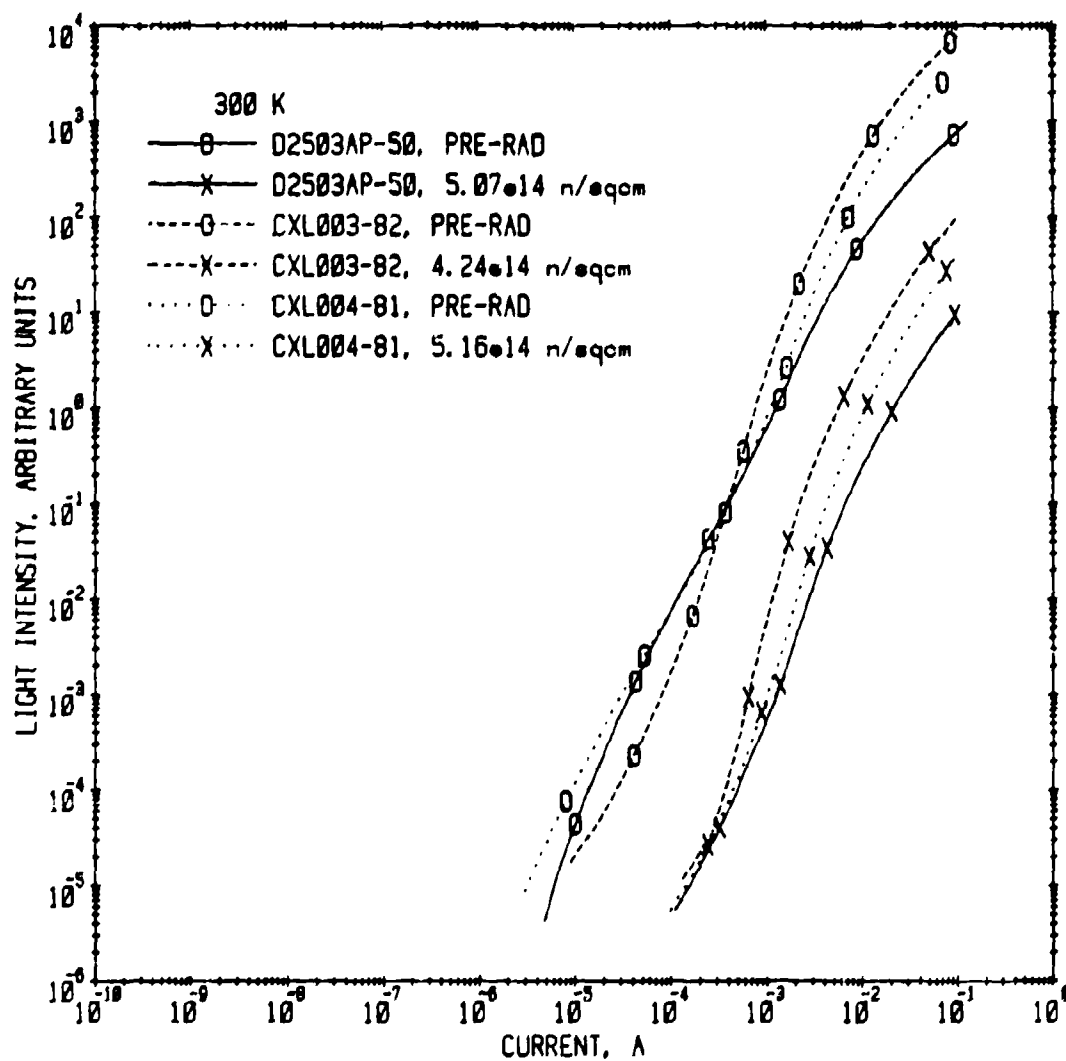


Figure 28. A comparison of neutron-induced degradation of total light intensity-current characteristics in three Plessey high radiance GaAs LEDs: bare (D2503AP), lensed (CXL004), and lensed and pigtailed (CXL003). The degradation rates are the same in the three LEDs.

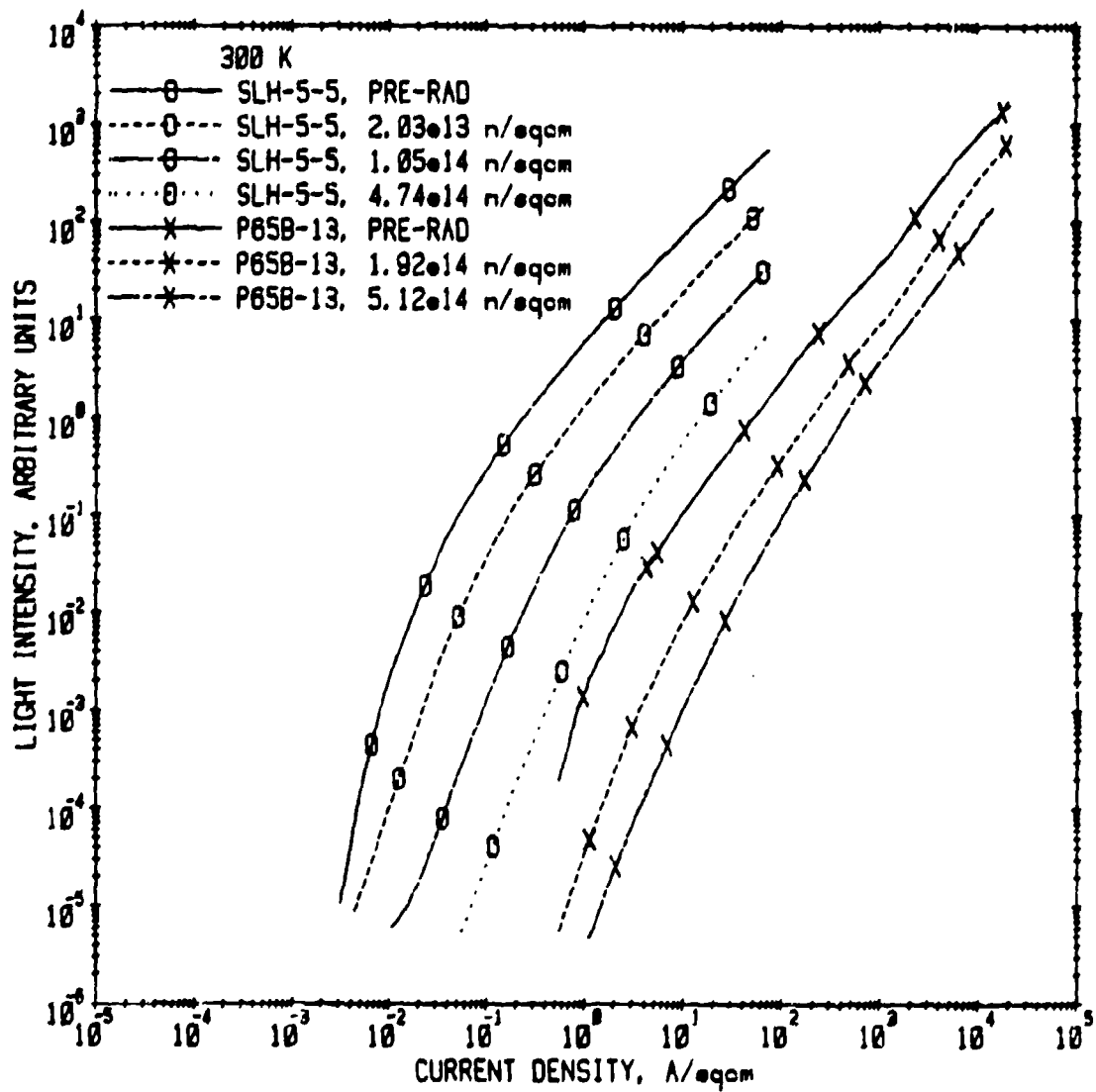


Figure 29. Neutron-induced reduction in total light output as a function of current density for two GeAlAs LEDs: SLH-5 is a planar TI device, and P65B is a high radiance Plessey LED. Note that the Plessey device degrades significantly less than the TI LED.

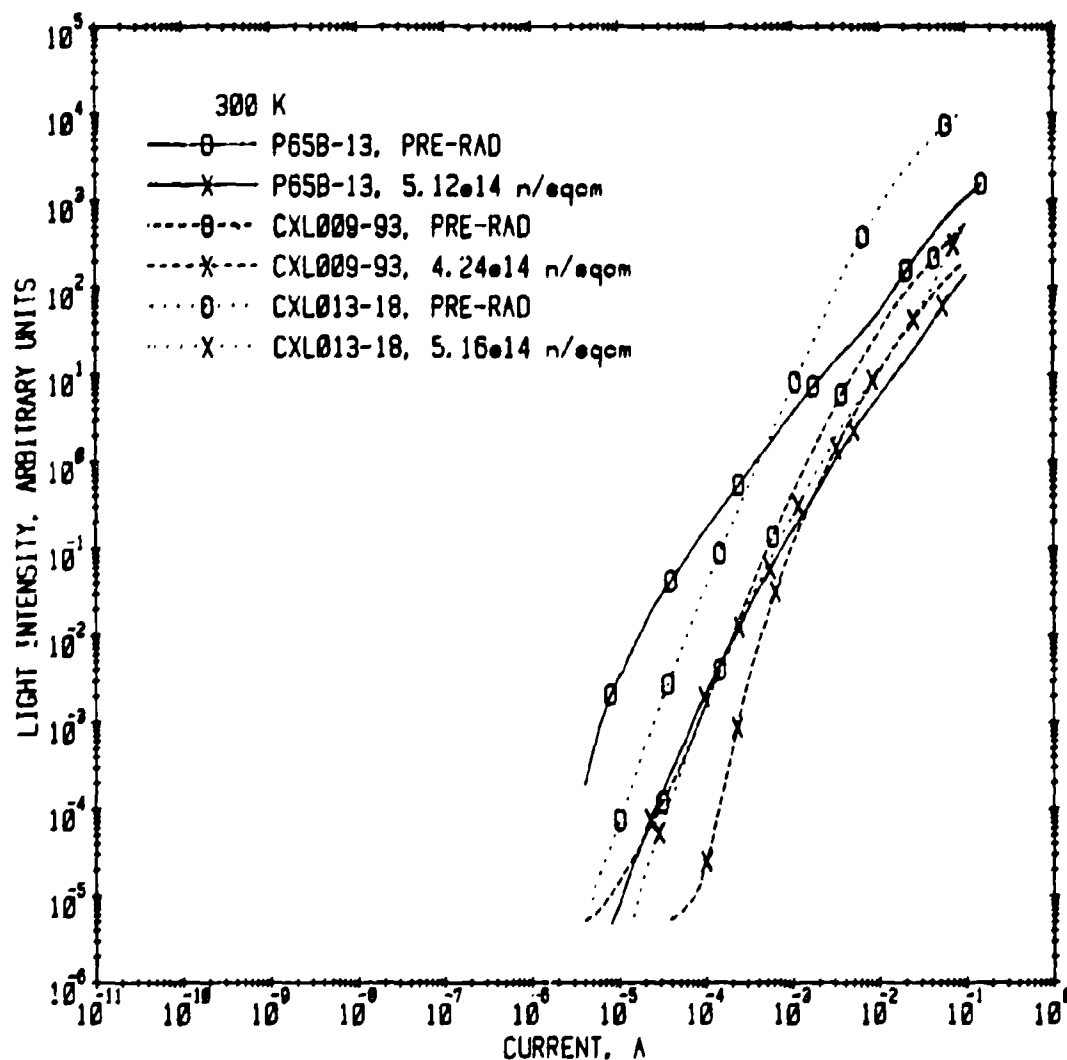


Figure 30. A comparison of neutron-induced degradation of the total light intensity-current characteristic of three types of Plessey GaAlAs LEDs: bare (P65B), lensed (CXL013), and lensed and pigtailed (CXL009). Note that the fluence for CXL009-93 is significantly less than for the other two LEDs.

constant current depending on the current one selects. This is attributed to material-induced variations in pre-irradiation lifetime rather than any effect of the lens or fiber. Other LEDs examined in this manner do not reveal any trend that can be associated with the lens or fiber. In addition, one should note that the lower fluence for CXL009-93 is partially responsible for the smaller degradation relative to the other two LEDs. In spite of the differing degradation rates, one can say that for all three LEDs the degradation is less than that for the GaAs LEDs for similar fluences. As in the case of GaAs, there is no evidence that the presence of the lens or the fiber pigtail, or both, affects the response of the LED to neutron irradiation.

The comparisons presented thus far between the various Plessey GaAlAs LEDs have primarily concerned devices from the first two groups supplied to us. As indicated in Table 1, the third group consisted of 12 similar LEDs (C45). The purpose of testing LEDs from this set was to investigate the variations in radiation response within a similar group of devices. Nine of the twelve LEDs were carried through a series of 8 irradiations to a maximum cumulative fluence of $1.1 \times 10^{15} \text{ n/cm}^2$. Light output degradation as a function of current is shown for these devices in Fig. 31. Except for $1.1 \times 10^{14} \text{ n/cm}^2$ and $5.5 \times 10^{14} \text{ n/cm}^2$, intermediate irradiations have been omitted for clarity. The symbols represent average values for the nine LEDs, while the bars represent maximum and minimum values within the set for a given fluence and current. Note that for both pre- and post-irradiation curves, there is a greater multiplicative (note the log scale) variation in output within the group at lower currents. As irradiation proceeds, the length of the bars increases indicating a variation in radiation sensitivity. However, at larger currents this change is not particularly significant. It is also important to note that on a linear scale the variation

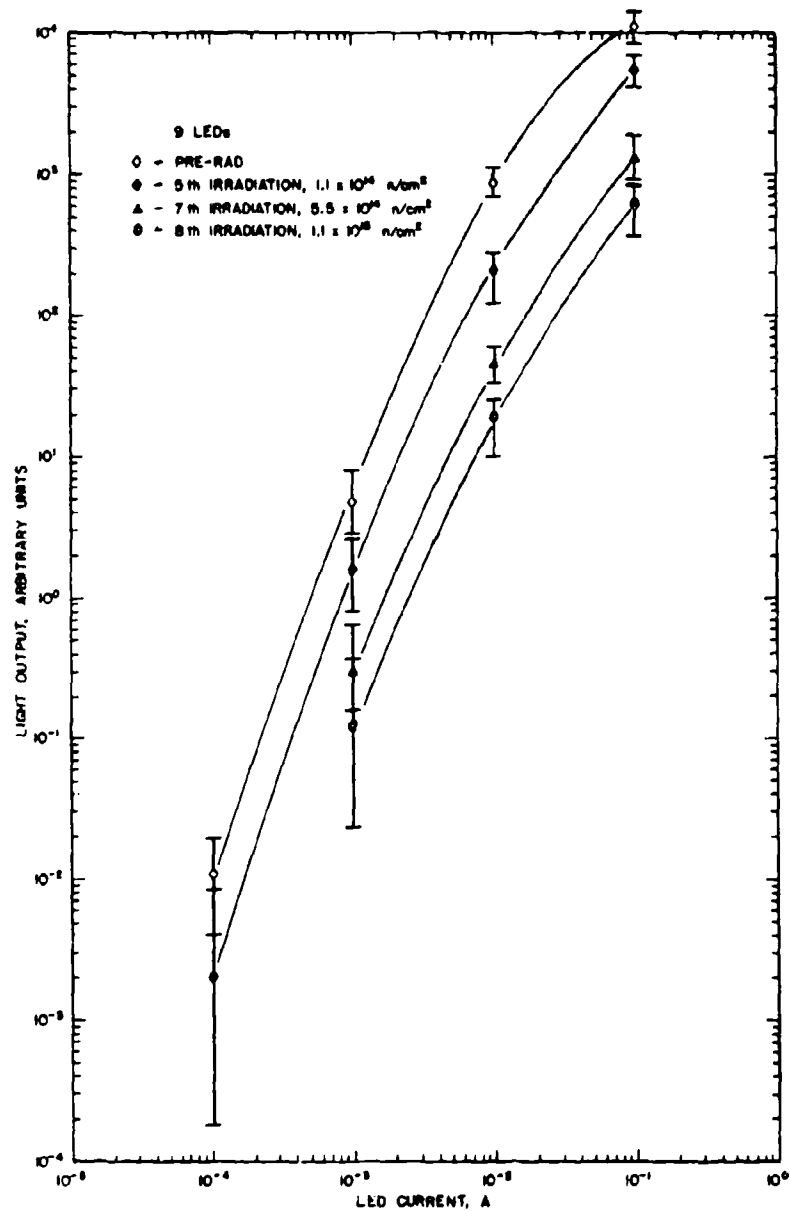


Figure 31. Neutron-induced degradation of total light output as a function of LED current for the most recent group of nine pigtailed GaAlAs Plessey high radiance LEDs. Symbols represent average values for the nine devices while the bars represent maximum and minimum values within the group for each measurement.

in light output after a given fluence is small relative to pre-irradiation light output values. Most important of all, however, is the fact that these LEDs exhibit excellent radiation hardness at large currents. At 100mA the decrease in average output after $5.5 \times 10^{14} \text{ n/cm}^2$ is only a factor of 8.

3. Neutron Damage of LEDs at Different Temperatures

The effect of measurement temperature on the sensitivity to neutron irradiation is shown in Figs. 32-34 for the bare Plessey GaAs LED. The changes in current-voltage characteristics at 220K, 300K and 360K after the maximum fluence of $5.1 \times 10^{14} \text{ n/cm}^2$ are shown in Fig. 32. Note that neither the magnitude of the neutron-added current or its variation with bias depend significantly on temperature. Figures 33 and 34 indicate that the neutron-induced decrease in light output at constant voltage (Fig. 33) or current (Fig. 34) is also relatively temperature independent. Close examination reveals that there is less degradation at lower temperatures but this is not a significant effect.

The effect of GaAlAs LED temperature on the sensitivity to neutron damage is shown in Figs. 35-37. Unlike GaAs (Figs. 32-34), there is a small but clearly discernible temperature effect. Both the neutron-induced excess current (low voltages in Fig. 35) and the light intensity degradation (Figs. 36, 37) are greater at higher temperatures. This dependence was also observed in other GaAlAs LEDs; however, the temperature effect is not large enough to be of significant practical concern, especially when compared to the temperature dependence^{7,8,9} of the recovery of Corning fibers after an ionization pulse.

4. Transient Neutron-Induced Effects in LEDs

The output of a variety of LEDs was measured during and after a neutron pulse from the SPR II reactor. These measurements were performed on three different occasions with some of the earlier experiments being repeated because of noise

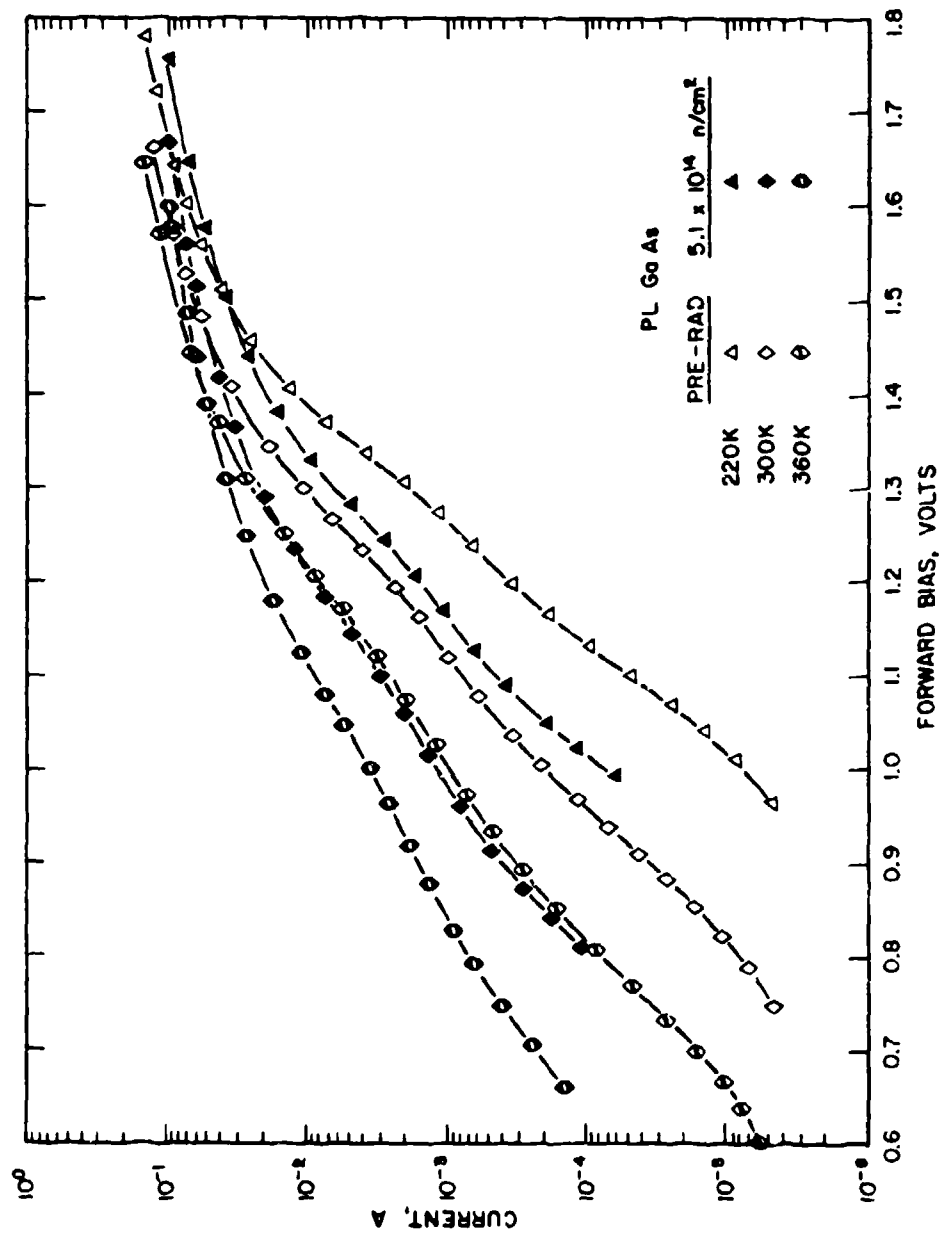


Figure 32. Change in current-voltage characteristic at three temperatures caused by a neutron irradiation of $5.1 \times 10^{14} \text{ n/cm}^2$ of a bare Plessey GaAs LED (02503AP). Relative changes caused by irradiation are independent of temperature.

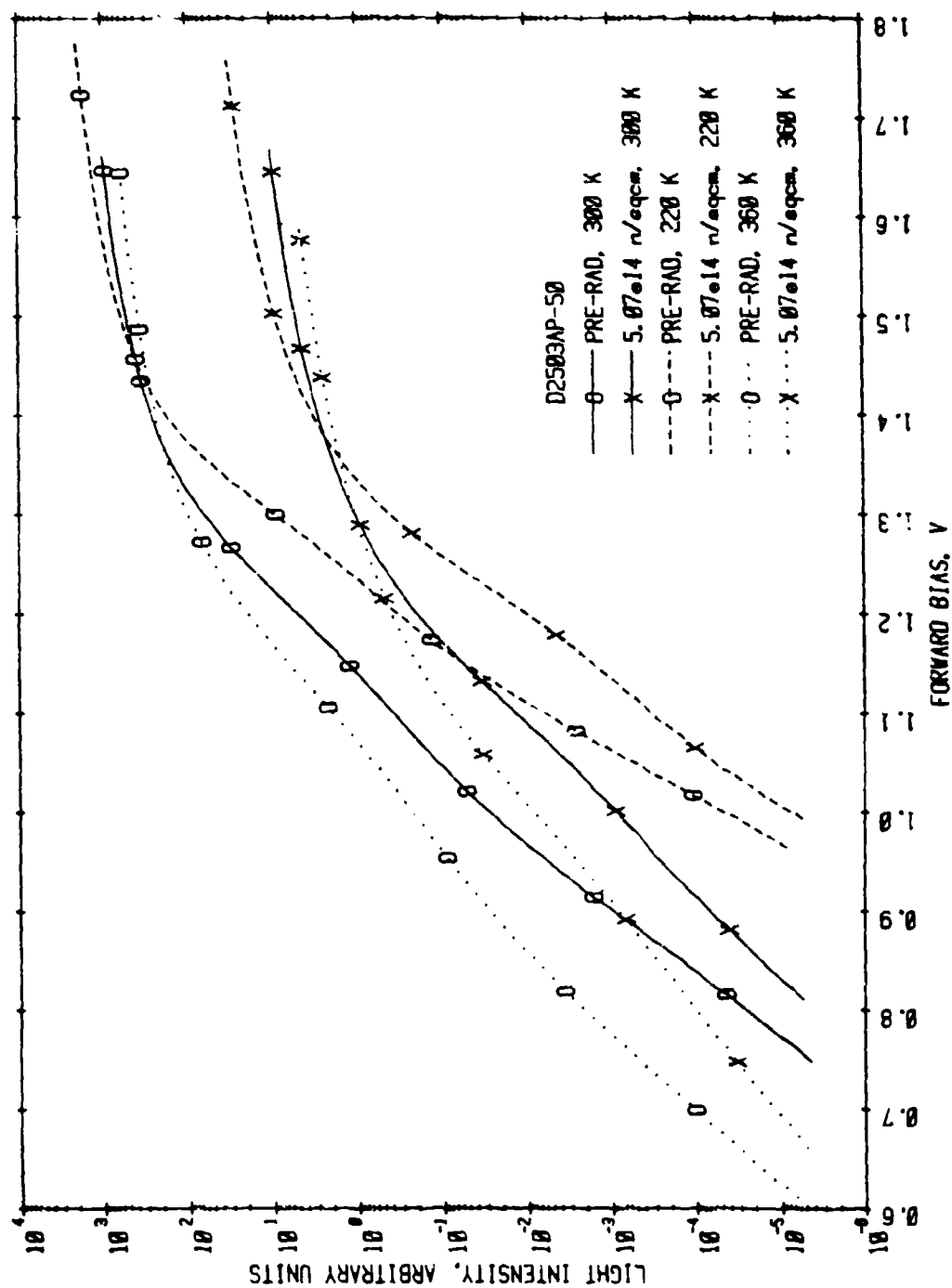


Figure 33. Neutron-induced reduction in total light output as a function of voltage and temperature for a bare Plessey Coas LFD. Relative degradation of light output is essentially independent of temperature.

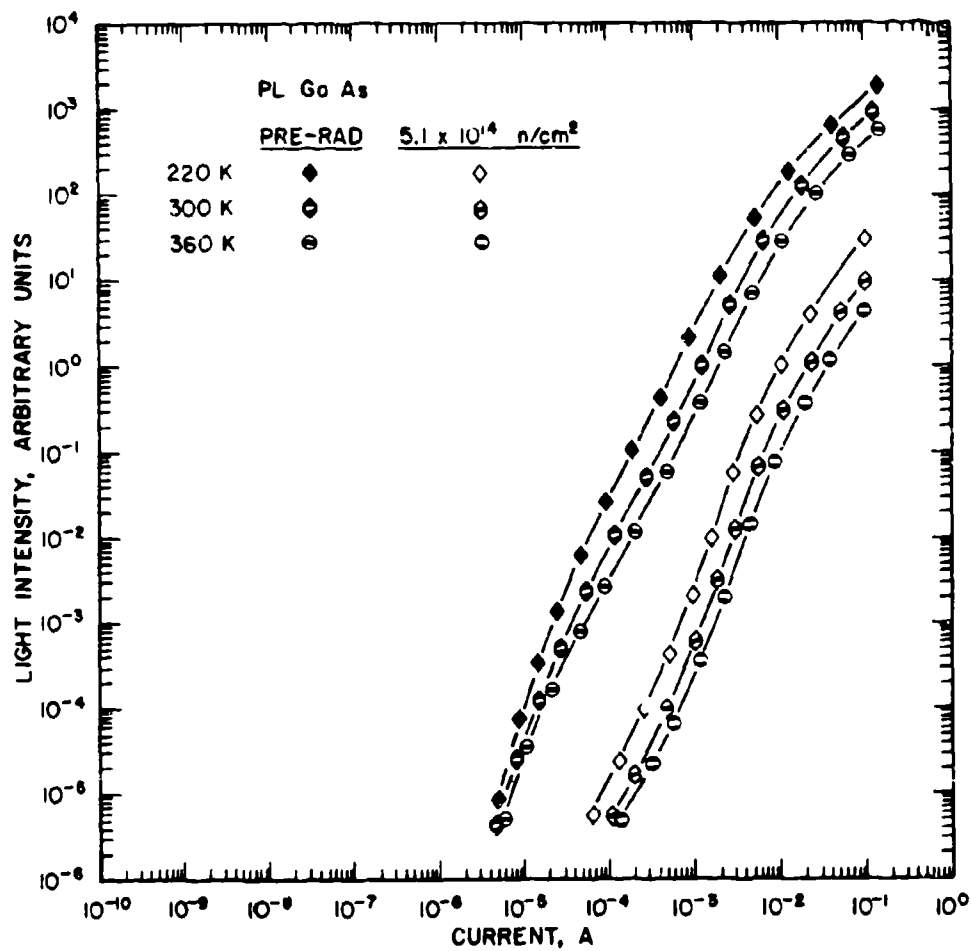


Figure 34. Neutron-induced degradation of the light intensity-current characteristic at three temperatures for a bare Plessey GaAs LED (D2503AP). Note that neutron induced reduction of light output is independent of temperature.

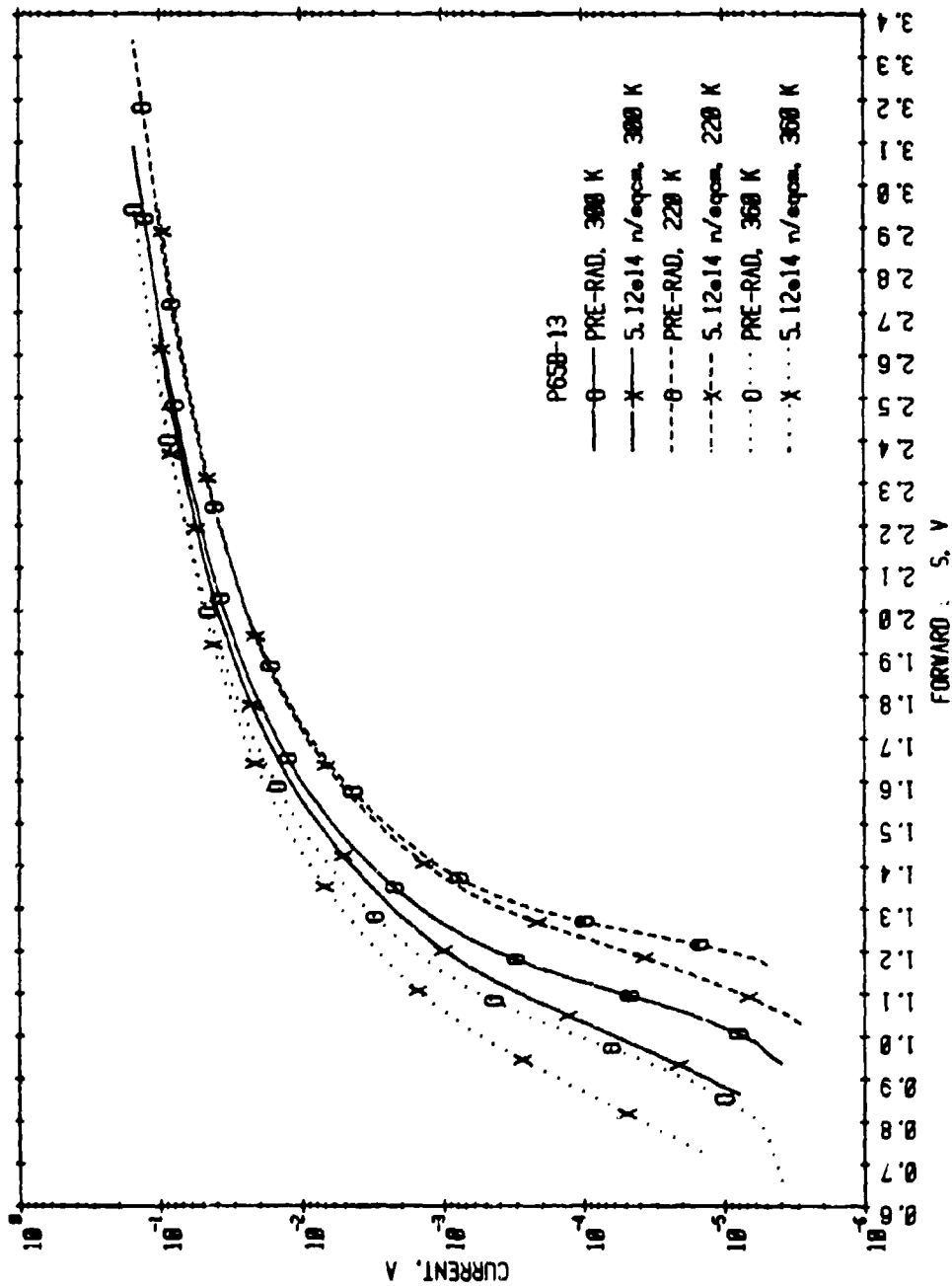


Figure 35. Neutron-induced increases in LED current as a function of voltage and temperature for a bare Plessey GaAlAs LED. The excess current observed at low voltages is somewhat greater at higher temperatures.

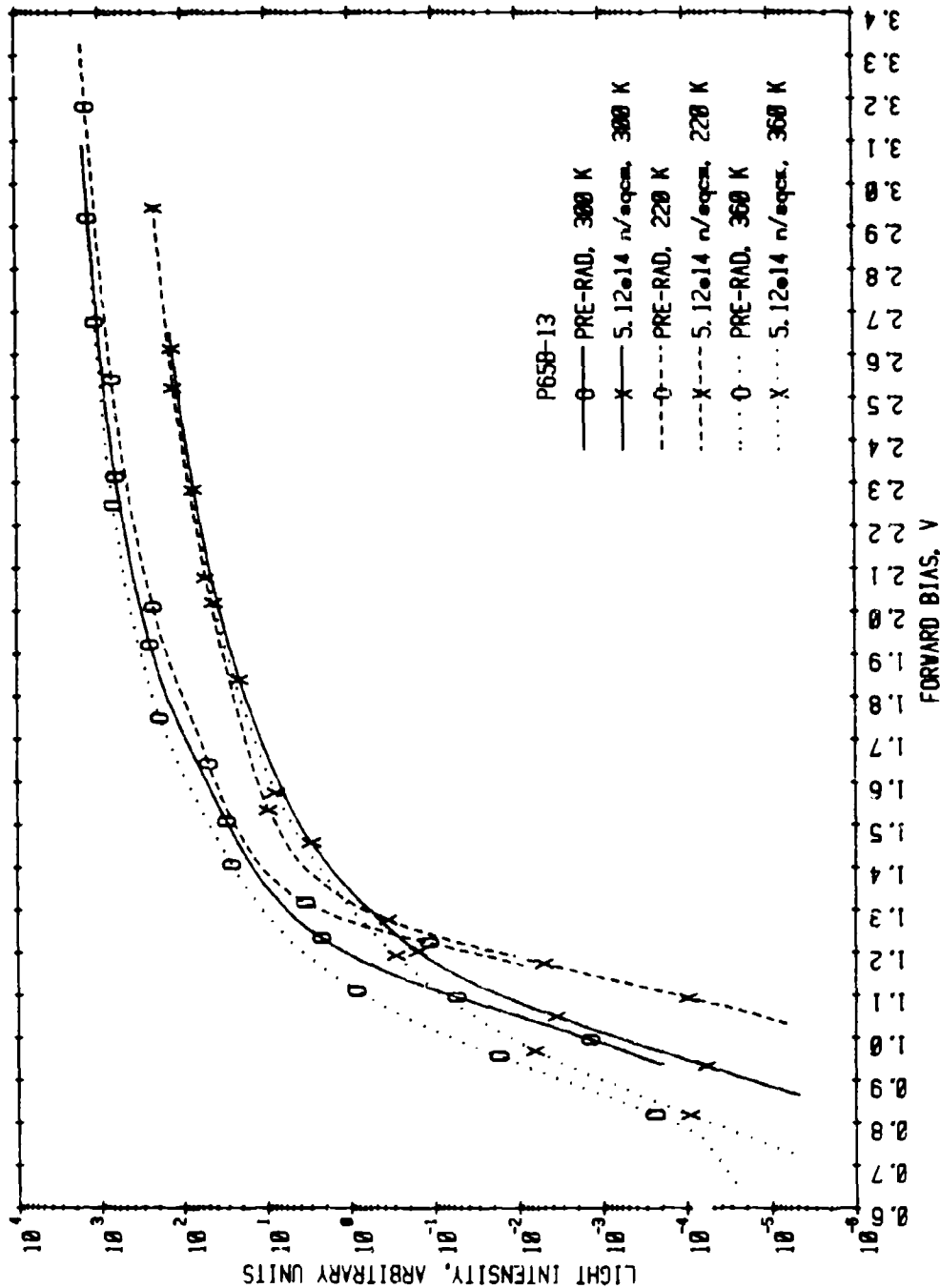


Figure 36. Neutron-induced degradation of total light output from a bare Plessey GaAlAs LED as a function of voltage and temperature. The decrease in output is greater at higher temperatures.

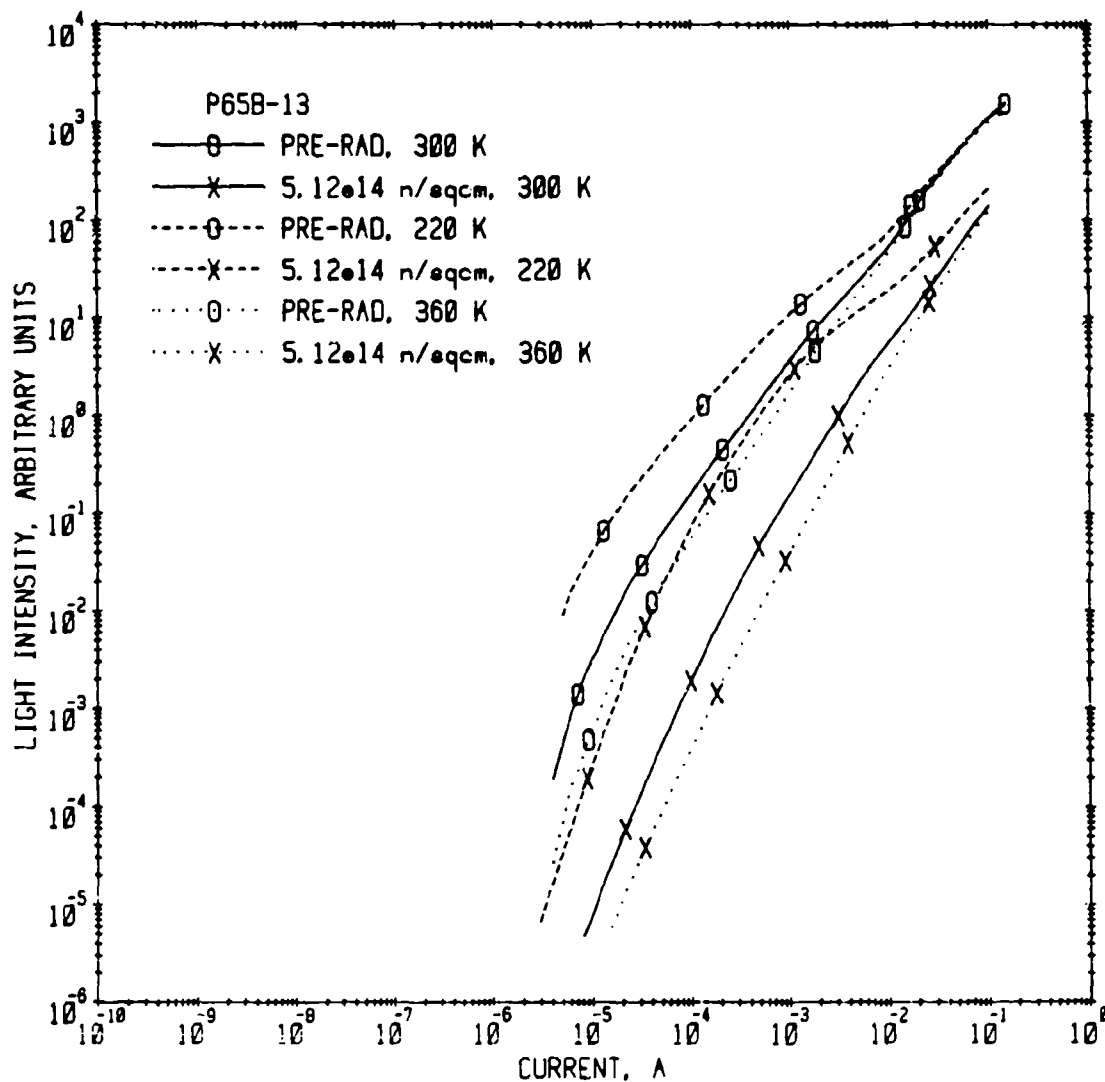
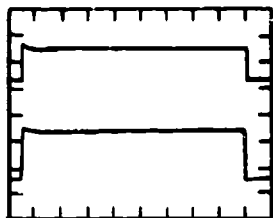


Figure 37. Reduction in light output as a function of current at three different temperatures for a bare Plessey GaAlAs LED irradiated to a fluence of 5.1×10^{14} n/cm². Degradation is somewhat greater at higher temperatures.

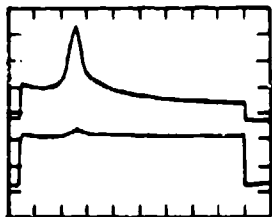
and gamma ray pulses present in the early data. In addition to Plessey LEDs the following LEDs were also irradiated: (1) The TIL26, an amphoterically Si doped GaAs LED fabricated by TI which is very sensitive to irradiation, (2) an LED with similar sensitivity manufactured at Bell Labs which is also amphoterically Si doped but in this case, GaAlAs, and (3) the TIXL-35, a TI Zn diffused GaAs LED which has a dome shape to minimize self absorption, and which exhibits very good radiation hardness.

Examples of the earlier measurements are shown in Figs. 38 and 39 for the Plessey bare GaAs LED, D2503AP-50, and LEDs from other suppliers, respectively. The reproductions of the three scope photographs in Fig. 38 illustrate the detected light pulse and LED current prior to, during, and several minutes after the neutron pulse. The upper trace is the signal transmitted via fiber to the APD in the instrument building, while the lower signal is the LED current. Note that in the center diagram after LED turn-on but before the neutron pulse, the light signal is the same magnitude as in the upper figure. The neutron pulse reaches a peak approximately 200 μ s after LED turn-on. At the end of the light pulse the signal has decreased relative to the pre-shot level by 3 to 4mV due to the neutron damage. This signal is equal to that taken several minutes later, shown in the bottom figure, indicating that there is no slow recovery of the damage. This latter result, that is the absence of slow transient annealing is characteristic of all the LEDs examined.

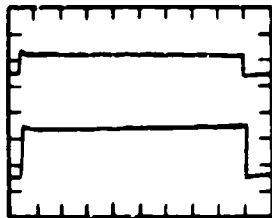
As indicated in the experimental procedure section, the positive pulses observed at about the same time as the neutron burst, as shown in the center drawing of Fig. 38, were due to extraneous effects such as electrical noise and gamma rays arriving directly at the APD. There was some evidence of fiber luminescence in these early measurements and also in the later data. However,



a) Prior to the neutron pulse



b) Neutron pulse



c) Several minutes after the pulse

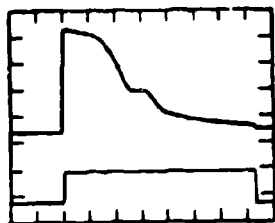
Figure 38. Neutron pulse exposure of a bare Plessey GaAs LED (D2503AP-50). Pulse fluence is $1.2 \times 10^{14} \text{ h/cm}^2$. This LED had already been subjected to neutron irradiation. The peak in the center picture is an artifact due to both electrical noise and gamma ray exposure of the detector. Upper trace is the light signal transmitted via fiber to an avalanche photodiode. Lower signal is the LED current pulse (150mA) viewed across 25 Ω . For all three pictures, vertical deflection for the light signal is 5mV/division and 2V/division for the current. Sweep time is 100 μs per division.

it was very weak as one would expect since most of the fiber near the reactor was shielded with lead. Further evidence of spurious electrical noise is shown by the peak on the LED current trace in the central diagram. Note that the vertical sensitivity for this trace is 2 V/cm in contrast with that for the light signal of 5 mV/cm. The neutron fluence delivered in the pulse was $1.2 \times 10^{13} \text{ n/cm}^2$ which resulted in about a 50% decrease in light output for the Plessey GaAs LED.

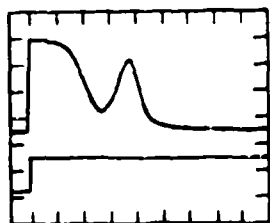
Figure 39a graphically demonstrates the radiation sensitivity of the TIL-26 when exposed to a neutron pulse for which $\phi = 5 \times 10^{12} \text{ n/cm}^2$. Note that the light output near the end of the current pulse is nearly zero in contrast with the pre-shot signal of approximately 40 mV. Similar data is shown in Fig. 39b for the Bell Labs GaAs LED which is also quite sensitive. This is not the case, however, for the relatively radiation hard TIXL-35 GaAs LED shown in Fig. 39c. Note that a pulse fluence of $4.4 \times 10^{13} \text{ n/cm}^2$ is required to produce a 60% reduction in output, a fluence value nearly ten times that for the TIL26.

Additional results of pulsed neutron measurements are shown in Fig. 40 for the bare Plessey GaAs LED P65B-13 and one of the recent pigtailed GaAs devices from the 3rd group in Table I. In both cases the decrease in output after the pulse is relatively small. As one might expect there is a positive signal due to luminescence in the fiber pigtail.

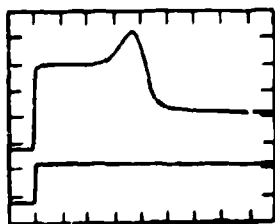
All of the pulsed neutron results have two features in common. First, there are no transient effects occurring within the LED during and immediately after the neutron pulse. The LEDs operate in normal fashion through the pulse and there is no increase in output immediately after the pulse which would be characteristic of transient damage recovery. Second, measurements several minutes after the pulse indicate that there is also no slow component of recovery.



- a) TIL-26 exposed to neutron pulse of $5 \times 10^{12} \text{ n/cm}^2$. Vertical deflection is 10mV/div. on upper trace and 2V/div. on lower trace. LED current = 100mA.

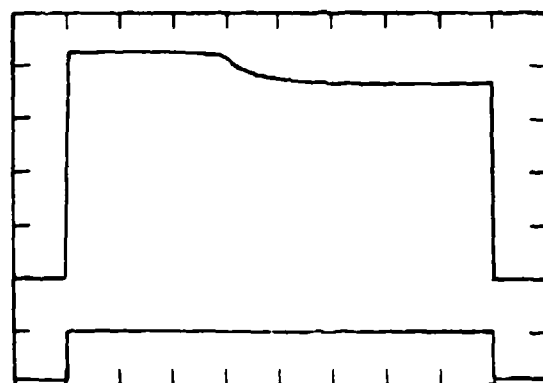


- b) Bell Labs GaAs:Si LED exposed to $4.3 \times 10^{13} \text{ n/cm}^2$. Vertical deflection is 5mV/div. on upper trace and 2V/div. on lower trace. LED current = 50mA.



- c) TIXL-35 GaAs: Zn with a neutron burst of $4.4 \times 10^{13} \text{ n/cm}^2$. Vertical deflection is 5mV/div. on upper trace and 5V/div. on lower trace. LED current = 150mA.

Figure 39. Neutron pulse exposure of three different LEDs: TIL26 is a highly sensitive amphoterically Si doped GaAs device; the GaAlAs LED in the center is also amphoterically Si doped and very sensitive. In the bottom picture, the TIXL-35 is a Zn diffused, dome shaped GaAs emitter whose hardness is relatively good. The peaks in the pictures are artifacts due to electrical noise and gamma rays. The upper trace is the light signal while the lower trace is the LED current. Sweep time for all three pictures is 50us per division.



a) Plessey bare GaAlAs LED
exposed to $\phi = 6.5 \times 10^{12} \text{ n/cm}^2$.



b) Plessey pigtailed GaAlAs LED
exposed to $\phi = 5.1 \times 10^{13} \text{ n/cm}^2$.

Figure 40. Neutron pulse exposure of two Plessey LEDs: a bare GaAlAs LED (P65B) and a pigtailed GaAlAs device (C45) from the most recent group. Special care was taken in these later measurements to eliminate the extraneous effects of noise and gamma ray interaction with the detector. Therefore, the peak in the lower picture is due to fiber luminescence as one would expect since the pigtail was also exposed. The upper trace is the light signal (10mV/division) and the lower trace is the LED current through a 25 Ω resistor (1V/division). Sweep time is 50 μ s/division.

5. Permanent Gamma Ray Damage in LEDs

The effects of Co-60 gamma ray irradiations to doses of 1×10^6 rads on the light output-current characteristics of various LEDs are shown in Fig. 41. These data demonstrate that a Megarad has no effect on the output of either the bare Plessey GaAs or GaAlAs LEDs. The decrease in output for the recent pigtailed GaAlAs LED is then associated with gamma-induced permanent attenuation in the fiber pigtail which is approximately 1m long. As will be shown, 1 Megarad is enough to affect 1m of the Corning fiber.

6. Permanent Gamma Ray Attenuation in Fibers

As indicated earlier, the changes in permanent attenuation caused by a single Co-60 exposure of 1×10^6 rads were determined by in situ measurements within the Co-60 Gamma Irradiation Facility (GIF). For the earlier 1025 fiber, transmission through the fiber was reduced by 14.2% for GaAs and 13.3% for GaAlAs due to a dose of 1 Megarad. For the length of fiber employed these values correspond to an induced attenuation of .15 dB/m (GaAs) and .13 dB/m (GaAlAs). These results are somewhat lower than previous work^{7,8,9} on Corning OVPO water-containing fibers, but agree within an order of magnitude. Data taken on the later SDF fiber agrees more closely with earlier studies.^{7,8,9} Our results indicate that the induced attenuation due to 10^6 rads was 0.43 dB/m at 820nm and 0.37 dB/m at 900 nm in the SDF fiber.

7. Transient Attenuation in Corning Fibers

As indicated earlier, two fibers were examined in this study. Although both fibers were from Corning, they have different characteristics. The earlier fiber was a step index 1025 silica core fiber with an N.A. = 0.16 and a core diameter of 90 μ m. More recently, a step index SDF (short distance fiber) (BP356) fiber with core diameter = 100 μ m and N.A. = 0.30 has been studied.

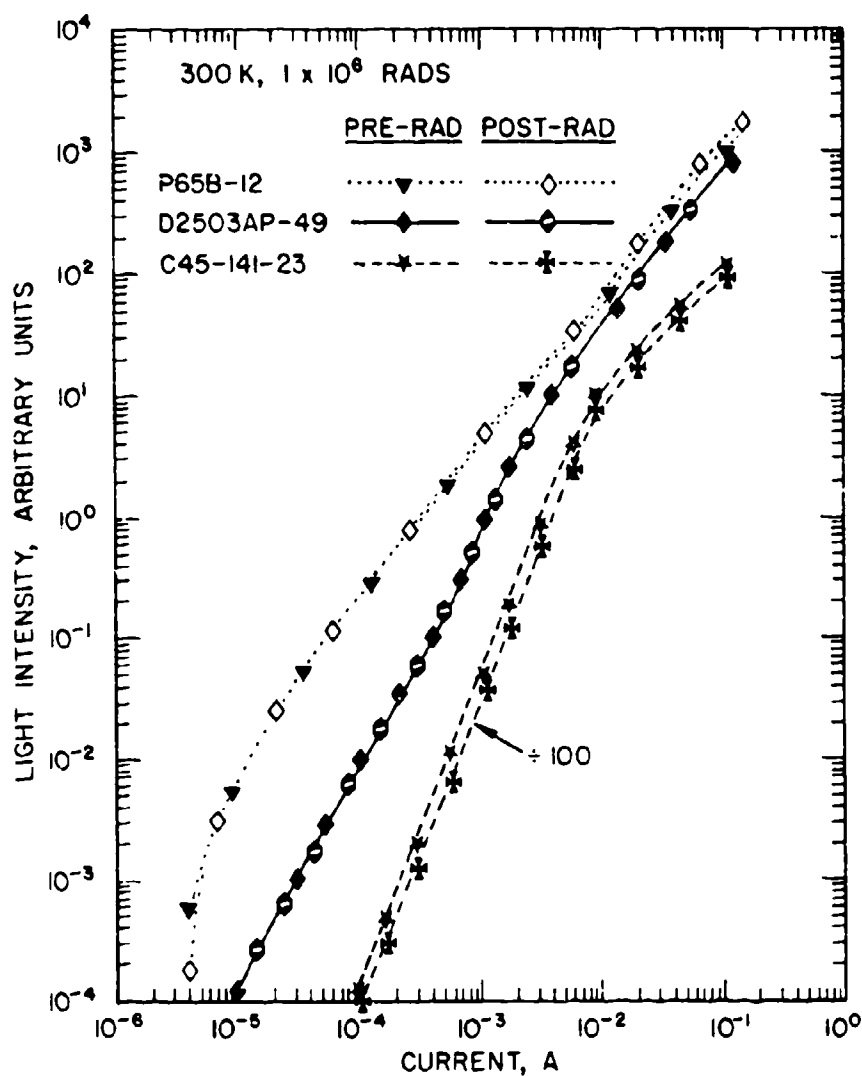


Figure 11. The effect of 1×10^6 rads Co-60 gamma rays on three different Plessey LEDs: a bare GaAs device (P65B), a bare GaAs LED (D2503AP), and a pigtailed GaAs LED (C45) from the most recent group. Data for the pigtailed device have been divided by 100 for purposes of clarity. For the bare LEDs, this irradiation does not affect the light intensity as a function of current. In the case of the pigtailed LED, the small decrease in output is due to induced attenuation in the fiber pigtail.

This latter fiber is the same as that used for the pigtailed on the most recent set of LEDs received from Plessey. As will be shown in more detail below, our results suggest that the peak transient attenuation, α_p , is about the same in the two fibers, but the attenuation recovery kinetics differ significantly between the two fibers.

In order to span a relatively large range in dose, the 1025 step index fiber was exposed to 50ns X-ray pulses on both REBA and HERMES. Peak transient attenuation, α_p , values derived from these measurements are shown in Fig. 42 as a function of the dose rate, $\dot{\gamma}$. Since the fiber pigtailed on the recent LEDs are typically 1m long, these data and those in subsequent figures can be read directly as the attenuation one can expect in the LED pigtail. Four types of data are shown: a separate piece of test fiber using first a GaAs source and then a GaAlAs source, and entire pigtailed GaAs and GaAlAs LEDs. The data for the GaAs source at 900nm lie along one line both for the test fiber and the pigtailed LED. The same is true for the GaAlAs at about 820nm except there is greater attenuation at the shorter wavelength. This is to be expected since transient attenuation in glass fibers is usually greater at shorter wavelengths.^{7,8,9} The slope of the lines indicates a linear relationship between α_p and $\dot{\gamma}$ which is in agreement with previous work at dose rates in this range.^{7,9} The coincidence of pigtailed LED and test fiber data implies that neither the lens nor the LED chip itself are affecting the transient attenuation results. Lastly, the magnitude of α_p is in agreement with previous studies^{7,9} of similar fibers.

The normalized recovery of the transient attenuation is shown in Fig. 43 for the 1025 step index fiber. These data indicate that the recovery is independent of wavelength and dose rate as found in previous work.^{7,9} In addition, although

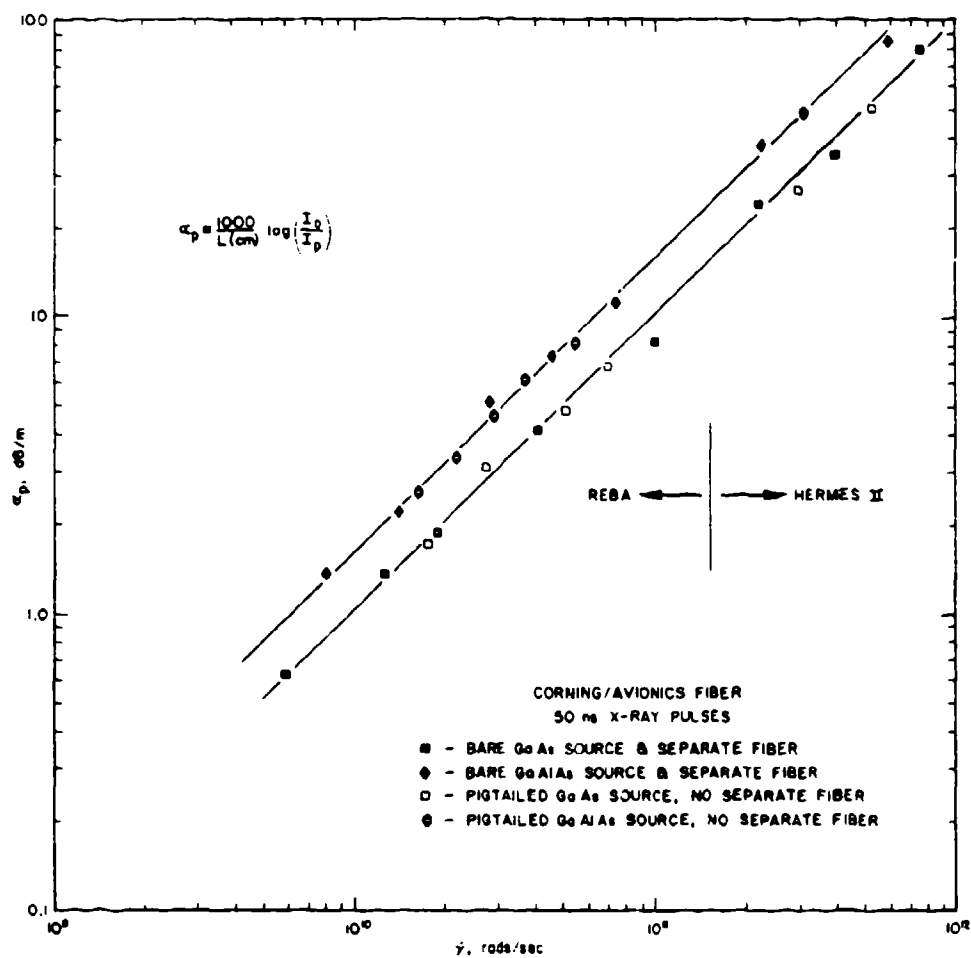


Figure 42. Peak transient attenuation induced in a Corning 1025 step index fiber by 50 ns wide X-ray pulses. These data were taken on both REBA and HERMES at room temperature. In the case of the bare GaAs and GaAlAs LED sources, the LEDs themselves were not exposed to X-rays. For pigtailed devices, the entire LED including pigtail was exposed.

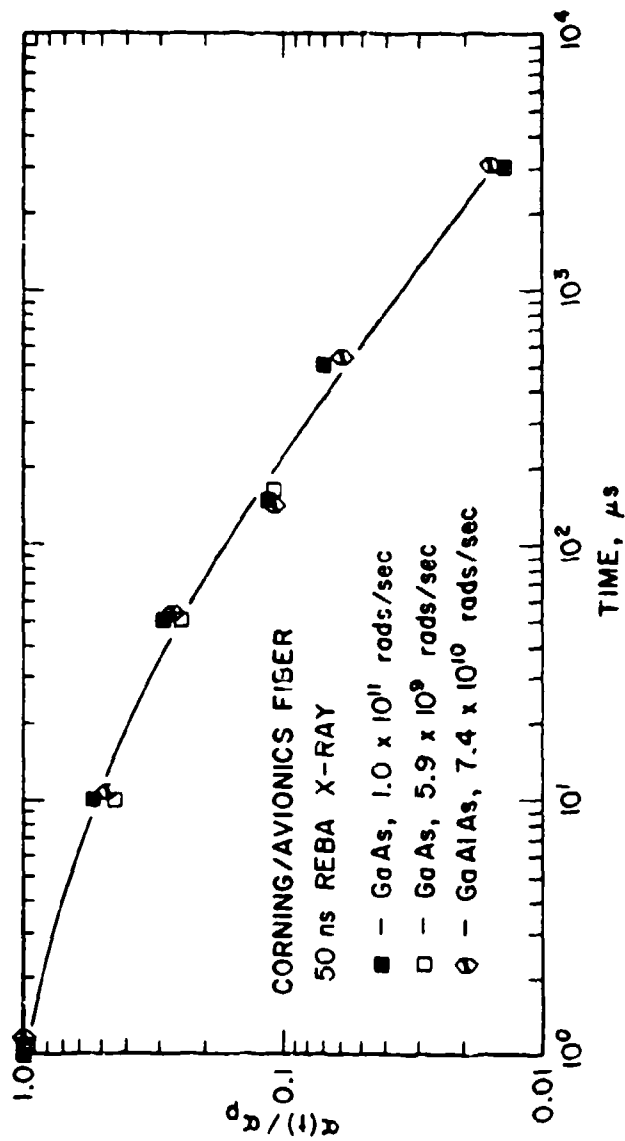


Figure 47. Normalized attenuation in a Corning 1025 step index fiber following X-ray exposure. The data indicate that the recovery is independent of wavelength over the range 820 nm-900 nm and dose over the range 0.3 Krad to 5.0 Krad.

not shown, the HERMES-II data to $\dot{\gamma} = 1 \times 10^{12}$ rads/sec also coincide with the results in Fig. 43. These measurements were taken at room temperature which is important to note because earlier work,^{7,9} and the data taken on the SDF fiber, to be described next, have shown that recovery of Corning fibers is temperature dependent.

Turning attention to the more recent Corning SDF step index fiber, BP356, Figs. 44-48 present the transient attenuation results for this fiber. Relative to the earlier fiber, the range of $\dot{\gamma}$ is less with the emphasis now on the temperature dependence of the attenuation. Shown in Fig. 44 are α_p data as a function of dose rate and temperature. For the range of dose rates, the increase in α_p with $\dot{\gamma}$ is linear at the measured temperature. Note that α_p increases much more rapidly at lower temperatures. Also included in Fig. 44 is a room temperature curve of the attenuation present 1ms after the X-ray pulse. This curve demonstrates that significant recovery has occurred in 1ms. The 25°C curve for α_p indicates that the peak transient attenuation in this fiber is approximately the same as that shown in Fig. 42 for the earlier step index fiber.

The peak transient attenuation data is shown plotted versus temperature in Fig. 45 with dose rate as a parameter. Once again, note the increase in α_p as the fiber temperature is decreased. The inverse dependence on temperature is stronger at larger dose rates.

Recovery of the X-ray induced transient attenuation at different temperatures is shown in Fig. 46 for a dose rate of 3.7×10^{10} rads/sec. As one would expect, the recovery is much slower at lower temperatures. Note that at -45°C the attenuation is still 1dB/m at 1 sec after the X-ray pulse. The recovery curves for the other dose rates have the same appearance as the family of curves in Fig. 46.

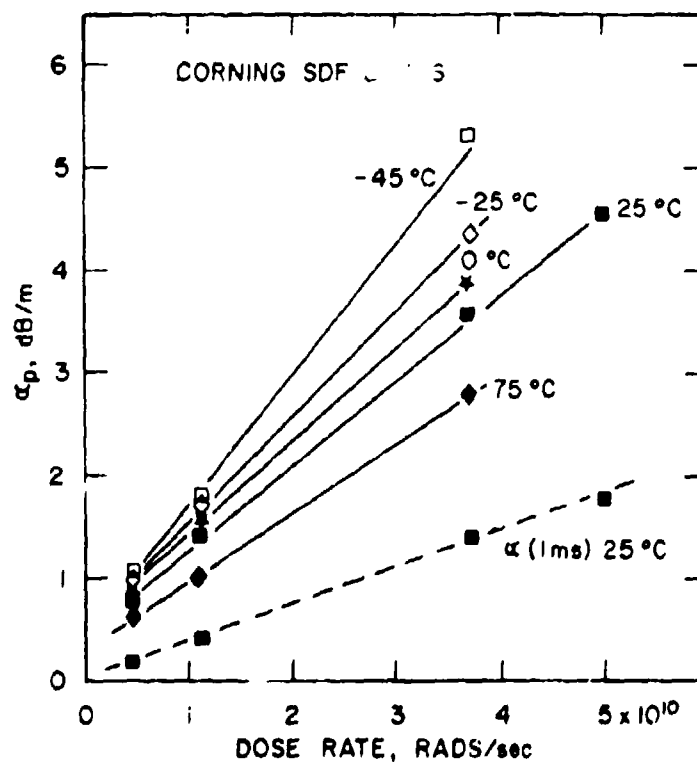


Figure 44. Peak transient attenuation in the Corning SDF step index fiber due to X-ray exposure on RZM. Over the dose range indicated, α_p is linear with dose at the temperatures shown with α_p increasing more rapidly at lower temperatures. The dashed curve for α at 1 ms indicates that linear behavior also occurs at later times.

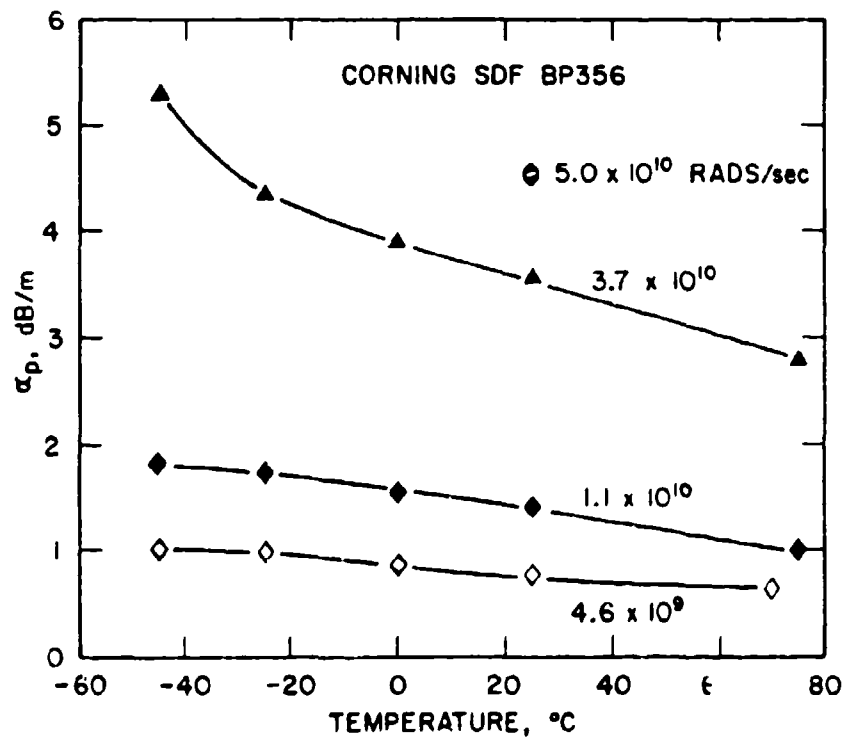


Figure 45. Peak transient attenuation as a function of temperature and dose rate induced in a Corning SDF fiber by 50ns REBA X-ray pulses. Note the more rapid increase with decreasing temperature at higher dose rates.

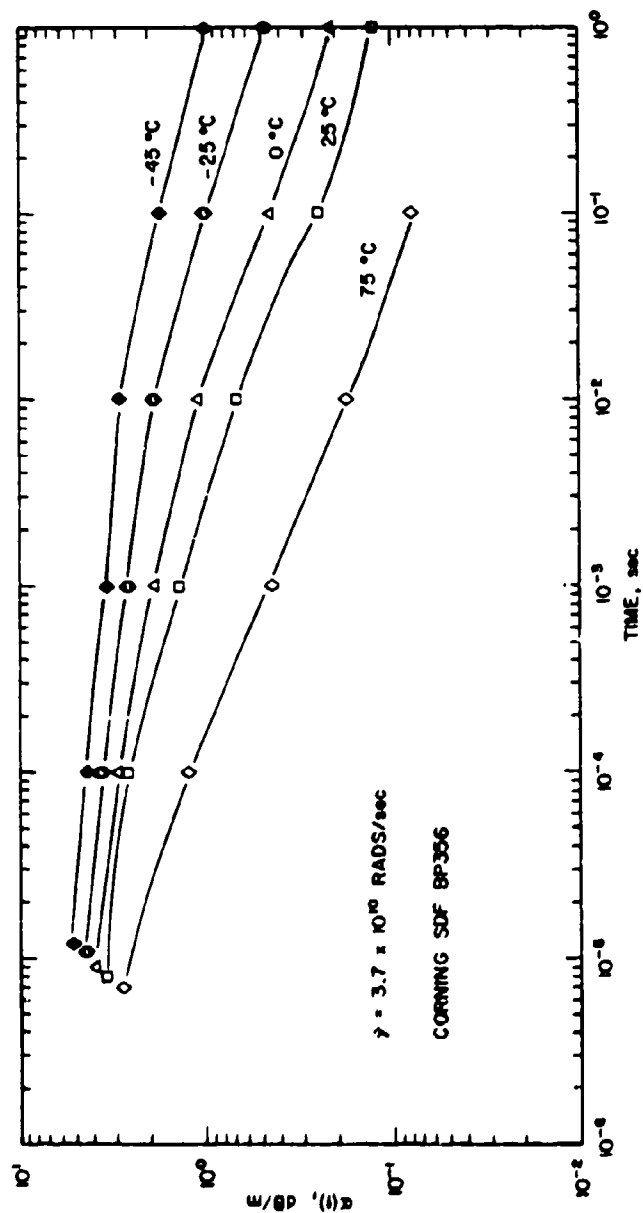


Figure 46. REBA X-ray induced transient attenuation in a Corning SDF step index fiber as a function of time and temperature. As expected for thermally activated annealing, the recovery is slower at lower temperatures. These curves have similar shapes at lower dose rates.

In order to discover whether or not the recovery rates depend on dose rate or temperature, one must examine the data in normalized form as in Figs. 47 and 48. In spite of the normalization to α_p , the curves in Fig. 47 have retained approximately the same separation as in Fig. 46. Thus, there is a temperature dependence of the attenuation recovery kinetics. This is in agreement with previous studies of doped Corning fibers.^{7,8,9} In contrast, certain fibers such as some pure silica core fibers, exhibit a temperature-independent recovery over a significant temperature range.^{7,9} A comparison of the room temperature curve in Fig. 47 with the data in Fig. 43 reveals that the recovery in the SDF fiber is much slower than in the 1025 fiber. For example, in 0.2ms $\alpha(t)/\alpha_p$ for the 1025 fiber has decreased to 0.1 while 45ms are required for $\alpha(t)/\alpha_p$ in the SDF fiber to reach the same value.

The results in Fig. 48 demonstrate that unlike the 1025 fiber, there appears to be a small dose rate dependence of the recovery in the SDF fiber at all the measured temperatures but the highest temperature of 75°C. Because the dose rate effect is relatively small, and because a dose rate dependence is rather unusual for fiber recovery, this effect is not considered to be real. In fact, at 25°C, $\alpha(t)/\alpha_p$ for 5.0×10^{10} rads/sec is smaller than that for smaller dose rates.

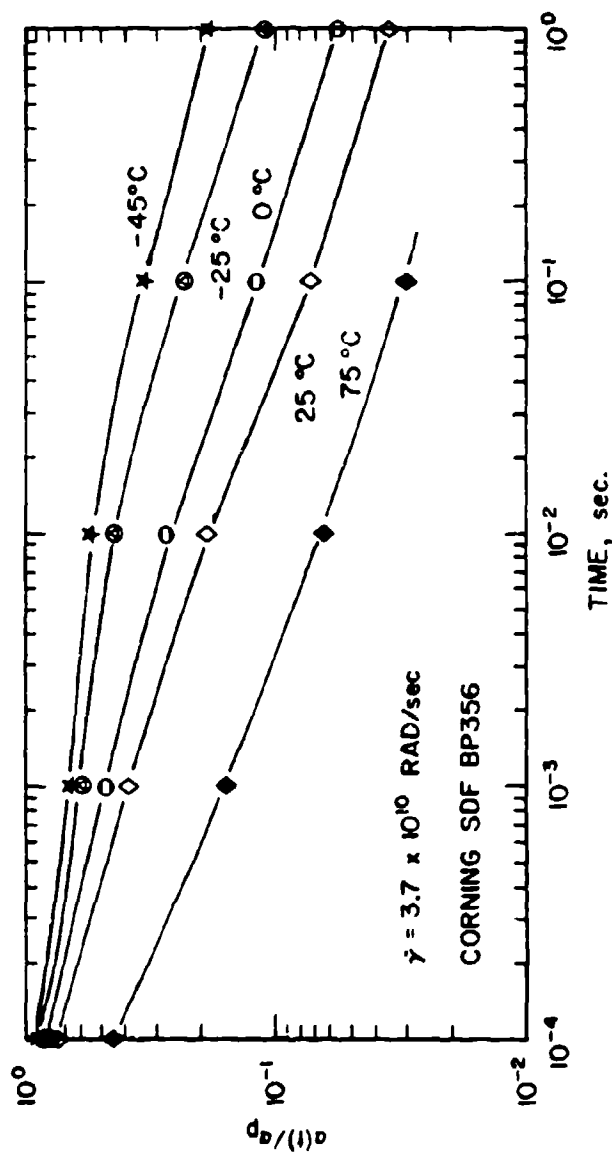


Figure 47. Normalized transient attenuation in a Corning SDF fiber as a function of time and temperature for a dose rate of 3.7×10^{10} rads/sec from REHA. Note that the normalization has not removed the temperature dependence of the recovery.

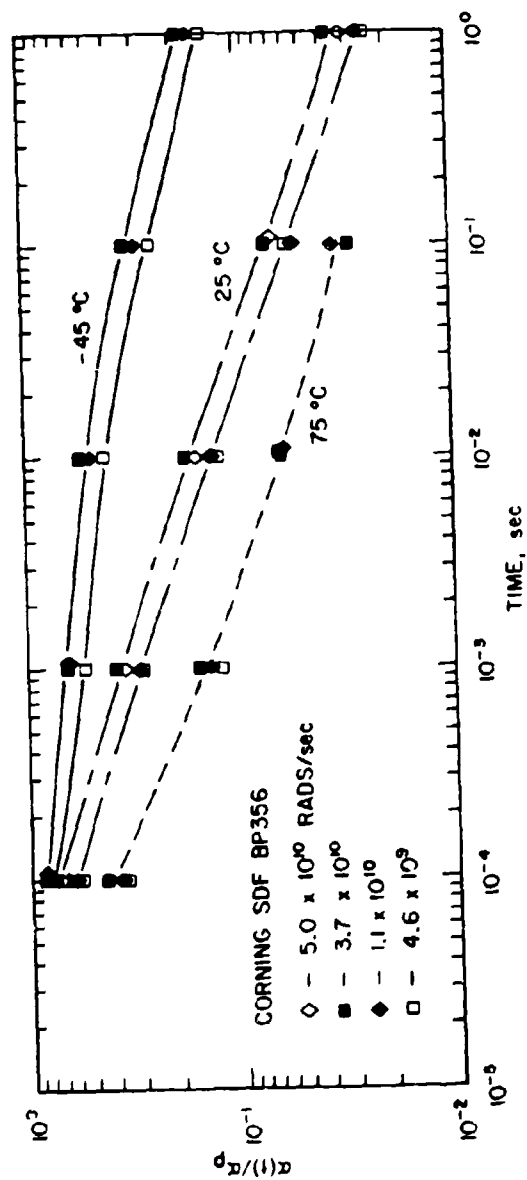


Figure 48. Normalized transient attenuation in a Corning SDF step index fiber as a function of time, temperature and dose rate. While there is some suggestion of a dose rate dependence of the recovery, this does not appear to be real. In this regard, note that $\alpha(t)/\alpha_p$ for 5.0×10^{10} rads/sec at 25°C is smaller than that for 3.7×10^9 rads/sec.

SECTION V

DISCUSSION

Since the primary radiation effects we have observed are permanent neutron damage in the LED chip itself and transient attenuation in the fiber pigtail, we will restrict our discussion primarily to these two phenomena.

1. Neutron Damage in the LEDs

We have seen in the previous section that the neutron induced degradation of the LEDs is made up of two major components: (1) the neutron induced excess current which leads to less light output for constant current operation, and (2) the competitive non-radiative recombination of excess carriers at neutron-induced centers in the neutral region of the LED. Since the neutron added current can be accommodated at constant voltage, the second mode of degradation is responsible for reduced output at constant voltage. The neutron induced excess current can be minimized under practical operating conditions by employing a small junction area LED so that the current density is very large. The second mode of degradation can be minimized by heavily doping the light producing region. This is known to increase the speed of the LED through a reduction in minority carrier lifetime. If done properly, this process does not result in a significant reduction in light output power. The final set of 12 GaAlAs LEDs received from Plessey have increased doping in order to decrease the rise time of the LEDs. Through additional comparisons among various LEDs, it will be shown in this section that the Plessey GaAlAs LEDs embody both techniques of reducing degradation, and are, thus, the most radiation hardened, high light output LEDs studied by this author.¹

The neutron induced degradation of constant voltage light output is shown in Fig. 49 as a function of neutron fluence for two of the Plessey high radiance LEDs and three of the planar TI devices. Comparing the two GaAs LEDs, the TI device starts

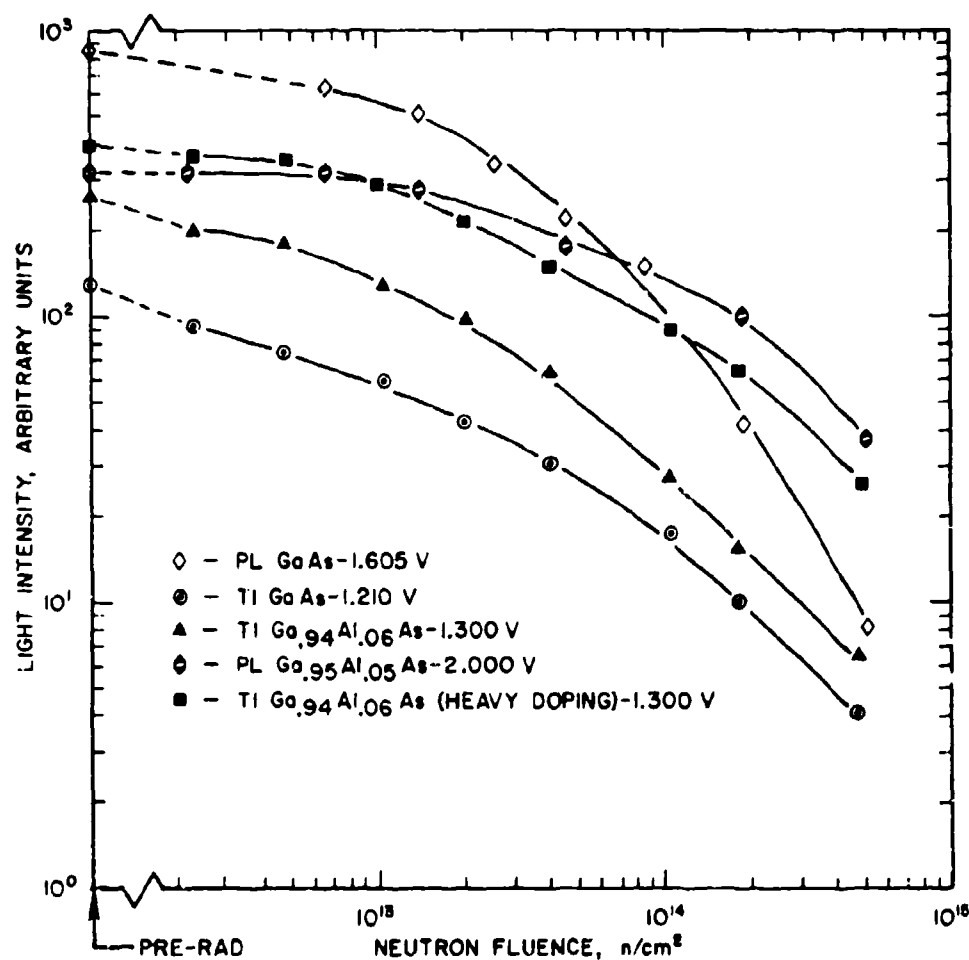


Figure 49. A comparison of room temperature constant voltage light output degradation curves for various LEDs. Included are the bare Plessey GaAs (D2503AF) and GaAlAs (P65B) and three planar TI devices. Note that the Plessey GaAlAs and the heavily doped TI GaAlAs LEDs have about the same degradation rate. Also, the Plessey GaAs LED degrades more rapidly at constant voltage than any of the other LEDs.

out at a much lower initial value but because its degradation rate is much less than the Plessey LED for the voltages shown, the output of the two LEDs are similar after $5 \times 10^{14} \text{ n/cm}^2$. The TI GaAlAs LED degrades at a rate similar to that for the TI GaAs device and greater than the rate for the Plessey GaAlAs LED which has the least sensitivity at constant voltage. Note, however, that for the more heavily doped planar GaAlAs LED, the degradation rate is less than the other TI GaAlAs device and about equal to that for the Plessey GaAlAs LED. This decrease in radiation sensitivity with increased doping is a demonstration of the technique referred to above which results in increased speed and a reduced pre-irradiation minority carrier lifetime. Because of material induced variations in the preirradiation lifetime, these constant voltage degradation rates can vary from sample to sample. However, as we have seen in previous figures, the Plessey GaAlAs LEDs are always less sensitive to irradiation than GaAs devices or TI GaAlAs LEDs with similar Al content. The fact that the Plessey GaAs LED has the greatest degradation rate at constant voltage serves to emphasize the importance of neutron-induced excess current for constant current operation. This follows from the fact that the Plessey GaAs LED has approximately the same radiation sensitivity as the TI GaAs LED when operated at constant current (Figure 27).

The role of neutron added current is more graphically illustrated in Figure 50 for GaAs LEDs and in Fig. 51 for GaAlAs devices. The light output, plotted as efficiency in Fig. 50, is shown at equal current levels for the TI and Plessey GaAs LEDs. Note that the high radiance Plessey device degrades at the same rate at 10mA as the TI devices do at 10mA and 50mA. However, for larger currents where the neutron induced excess current is minimal in the high current density Plessey LEDs, the high radiance devices degrade at a slower rate. Similar effects

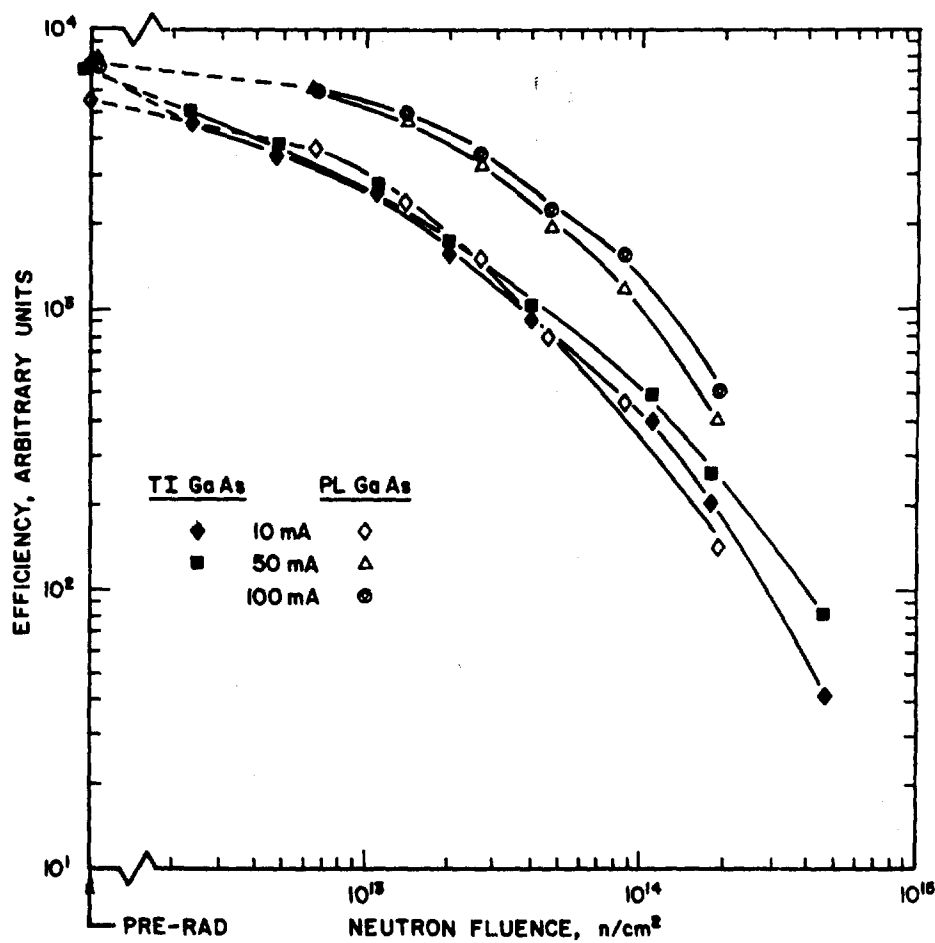


Figure 50. Room temperature constant current light output degradation curves for a bare Plessey GaAs LED (D2503AP) and a planar TI GaAs LED (SLH-1-2). In this figure light output divided by LED current, defined as the efficiency, has been plotted versus fluence. Note that as the current is increased the Plessey LEDs enter a range where there is negligible neutron-induced excess current resulting in a slower degradation.

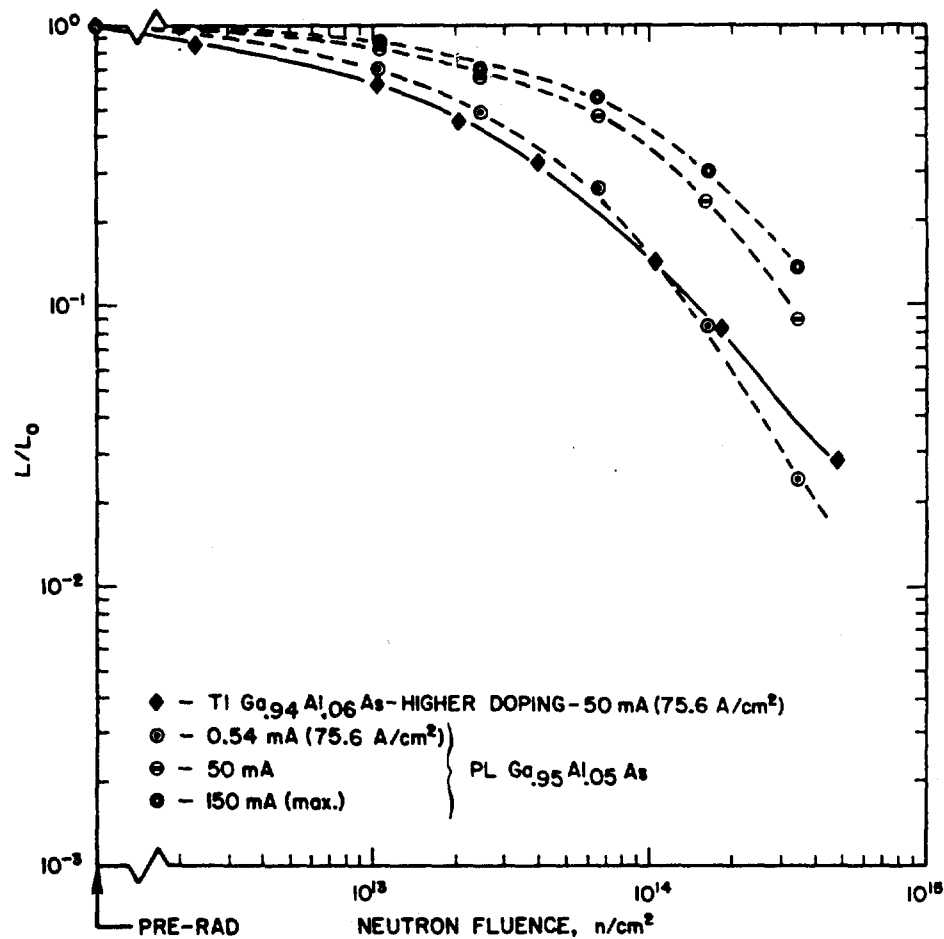


Figure 51. Normalized room temperature light output degradation curves for a bare Plessey high radiance GaAlAs LED (P65B) and a planar TI GaAlAs LED (SLH-5-5). Note that at the same current density the two devices have similar degradation rates but that at higher currents the Plessey LED degrades at a lower rate because of the lack of neutron-induced excess current.

are illustrated in Fig. 51 which shows light output normalized to the pre-irradiation output versus neutron fluence for Plessey and TI GaAs LEDs at different currents. If the Plessey LED is operated at the same current density, 75.6 A/cm², as the TI device the degradation rate is about the same in the two LEDs. However, if J is increased by a factor of about 100, the current density is in the range where there is no neutron induced excess current, and the degradation rate, as shown in Fig. 51, is much less. There is an additional, but small decrease in sensitivity as the current is raised further from 50mA to 150mA. Thus, the neutron added current can be a significant component of radiation induced degradation of constant current light output. The Plessey high radiance LEDs which normally operate at very high current densities are much less susceptible to this component of radiation damage, and are, therefore, very attractive light sources for fiber optics applications in radiation environments.

Further comparisons of normalized constant current light output degradation are shown in Fig. 52 for a variety of LEDs as a function of neutron fluence over the range 1×10^{11} n/cm² to 1×10^{15} n/cm². Note the wide variation in radiation sensitivity which serves to emphasize the importance of selecting the proper LED for nuclear environment applications. The most sensitive LED shown is the amphoterically Si doped GaAs TIL 26 whose output is down by more than three orders of magnitude at 1×10^{14} n/cm². The next most sensitive LEDs are two GaAs devices, HP-4120 and TIL-35, neither of which is amphoterically Si doped. Clustered together at somewhat greater fractional output are three LEDs: an RCA ternary InGaAs long wavelength (1060nm) emitter, the heavily doped TI GaAs LED shown earlier in Fig. 49, and the bare Plessey high radiance GaAs device, D2503AP. Recall that D2503AP and the heavily doped TI GaAs LED were shown to have about the same sensitivity at constant current. This followed from the decreased sensitivity in D2503AP due

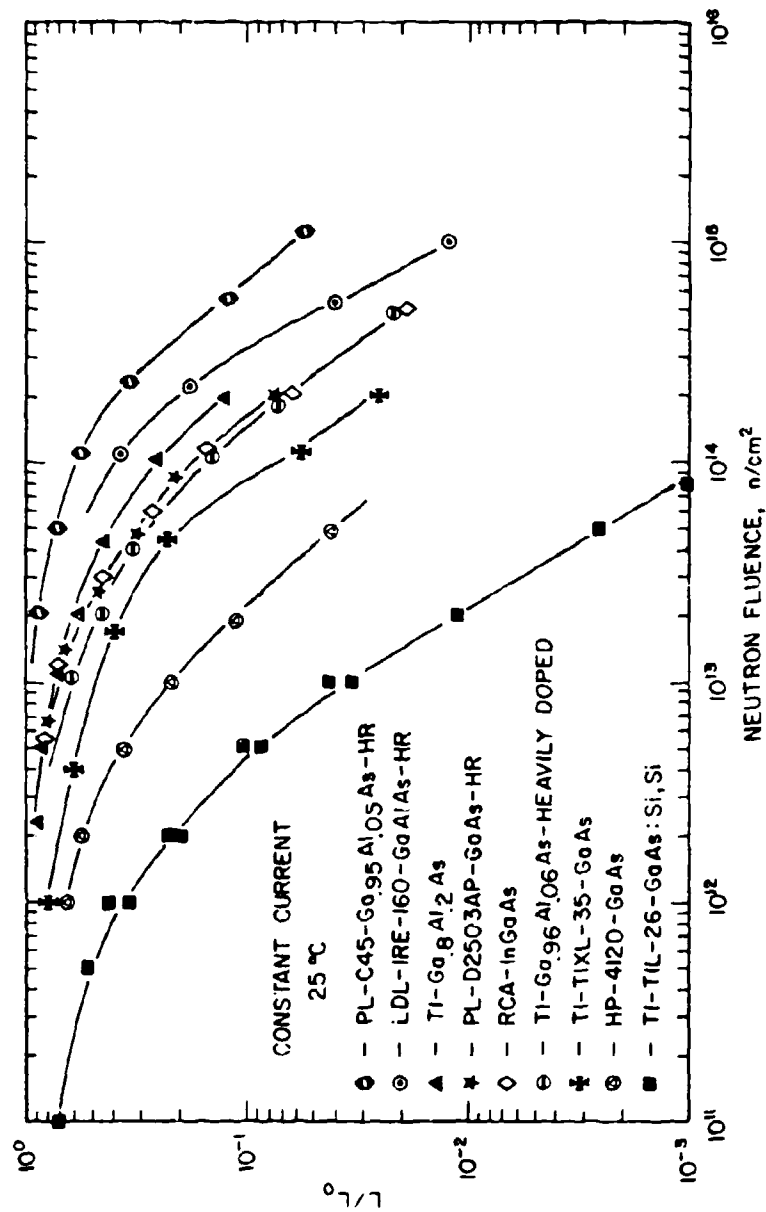


Figure 52. A comparison of normalized room temperature constant current light output degradation curves for a variety of LEDs. The most sensitive LED is the amphoterically Si doped GaAs TIL26, while the least sensitive LEDs are the most recent group of pigtailed, high radiance Plessey GaAlAs devices (C45). The HR designation means the device is a high radiance LED.

to a lack of excess current and in the TI device because of heavy doping, two effects which compensate each other in the comparison of the two LEDs. Next above this cluster of three LEDs is a TI GaAlAs device containing 20% Al. While this LED has good radiation hardness, its pre-irradiation power output is quite low. The second least sensitive LED is a high radiance (HR) GaAlAs device, the IRE-160, from Laser Diode Labs. As stated above, the most radiation-hard LEDs are the recent group of high radiance GaAlAs devices received from Plessey. It is important to note that these data are averages over nine of these LEDs rather than the hardest device from the group. That is, the average sensitivity of the C45 Plessey LEDs is lower than any of the LEDs shown in Fig. 52.

We have seen that high radiance LEDs, because of their small junction area, have very little excess current and are therefore relatively insensitive to neutrons for constant current operation. Note that of the six hardest LEDs shown in Fig. 52, three are high radiance (HR in Fig. 52) LEDs. Two of the others, the 20% Al TI LED and the RCA InGaAs LED, have very low pre-irradiation outputs so that their apparent hardness is deceiving because their output is low to begin with. The third planar LED, the heavily doped TI GaAlAs device, exhibits good hardness because of the heavy doping. As we have stated earlier, the Plessey C45 GaAlAs LEDs exhibit excellent hardness because they embody not only the heavy doping to produce increased speed and hardness, but also the lack of neutron-induced excess current.

As outlined in the Background section of this report, another basis for comparison of the radiation hardness of LEDs is to compute $\tau_0 K$ values. The smaller the pre-irradiation lifetime-damage constant product, the less sensitive the device is to irradiation. Care must be taken, however, to emphasize the particular operating

conditions under which the computed $\tau_0 K$ values are applicable. This precaution is demonstrated by the data in Figs. 53 and 54 for Plessey GaAs and GaAlAs LEDs, respectively. The data in these figures are plots of Eq. (13) which is appropriate for constant current operation when the total current is dominated by a diffusion mechanism. The fact that straight lines with slope = 1 can be drawn through the points indicates that Eq. (13) satisfactorily fits the data. Note, however, that as the current is increased, the plots move to the right indicating smaller $\tau_0 K$ values at larger currents. Although the change is not large in going from 50 to 100mA for the GaAs LED or from 50 to 150mA for the GaAlAs devices, it is important to restrict values of $\tau_0 K$ to corresponding current levels. With this in mind, we present in Table II values of $\tau_0 K$ computed from Figs. 53 and 54. For comparison, $\tau_0 K$ values are also given for the various planar TI LEDs with which we have compared the Plessey devices throughout this report. In addition, $\tau_0 K$ values are given for certain other LEDs we have studied in the past.¹ A comparison of the $\tau_0 K$'s in Table II leads to the same conclusion as that drawn from Fig. 52: the average data for the latest Plessey GaAlAs LEDs, C-45, gives the lowest $\tau_0 K$ value in Table II demonstrating that these devices have excellent radiation hardness.

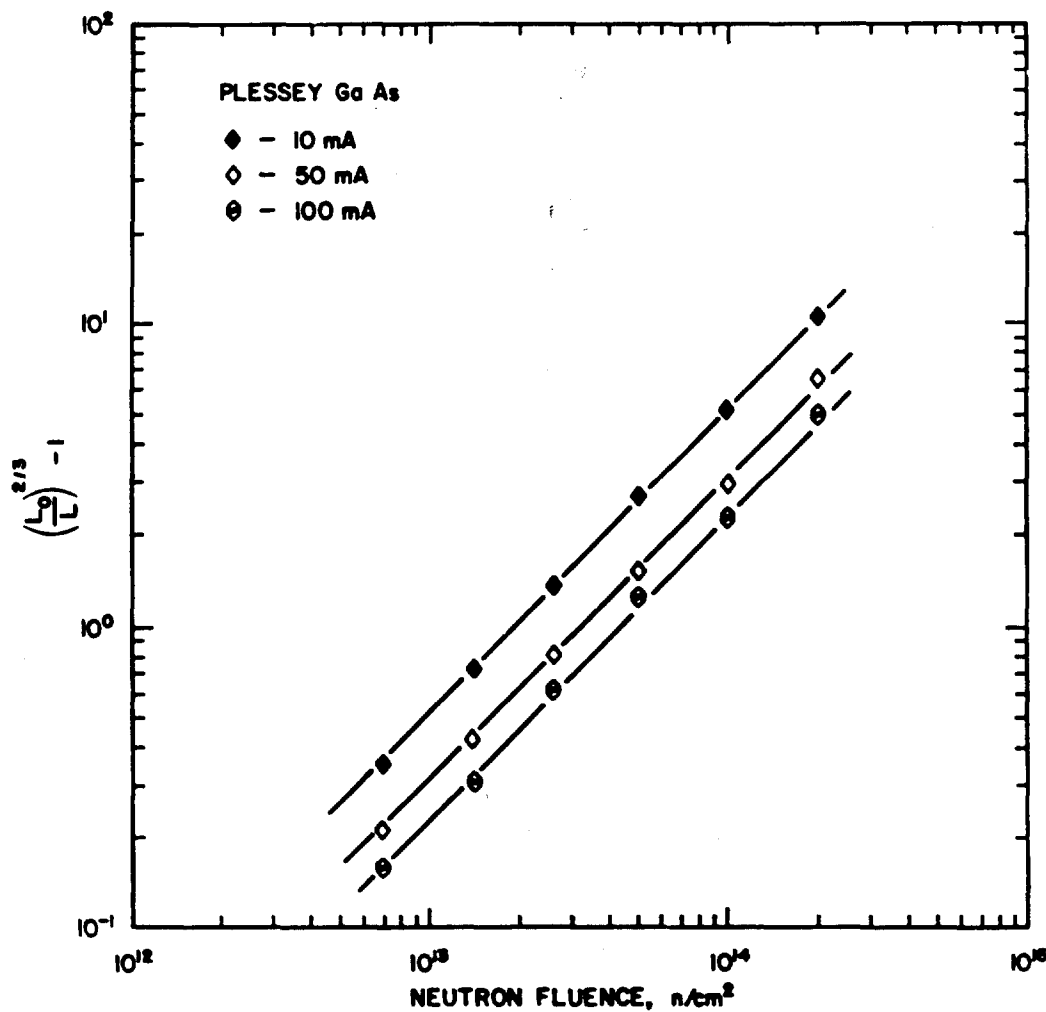


Figure 53. Analysis of constant current light output degradation from a Plessey high radiance GaAs LED (D2503AP) using Eq.(13). The quantity in parantheses is the ratio of the pre-irradiation light output to the post-irradiation light output. Note that the curves move to the right with increasing current resulting in a lower τ_0 K at higher currents.

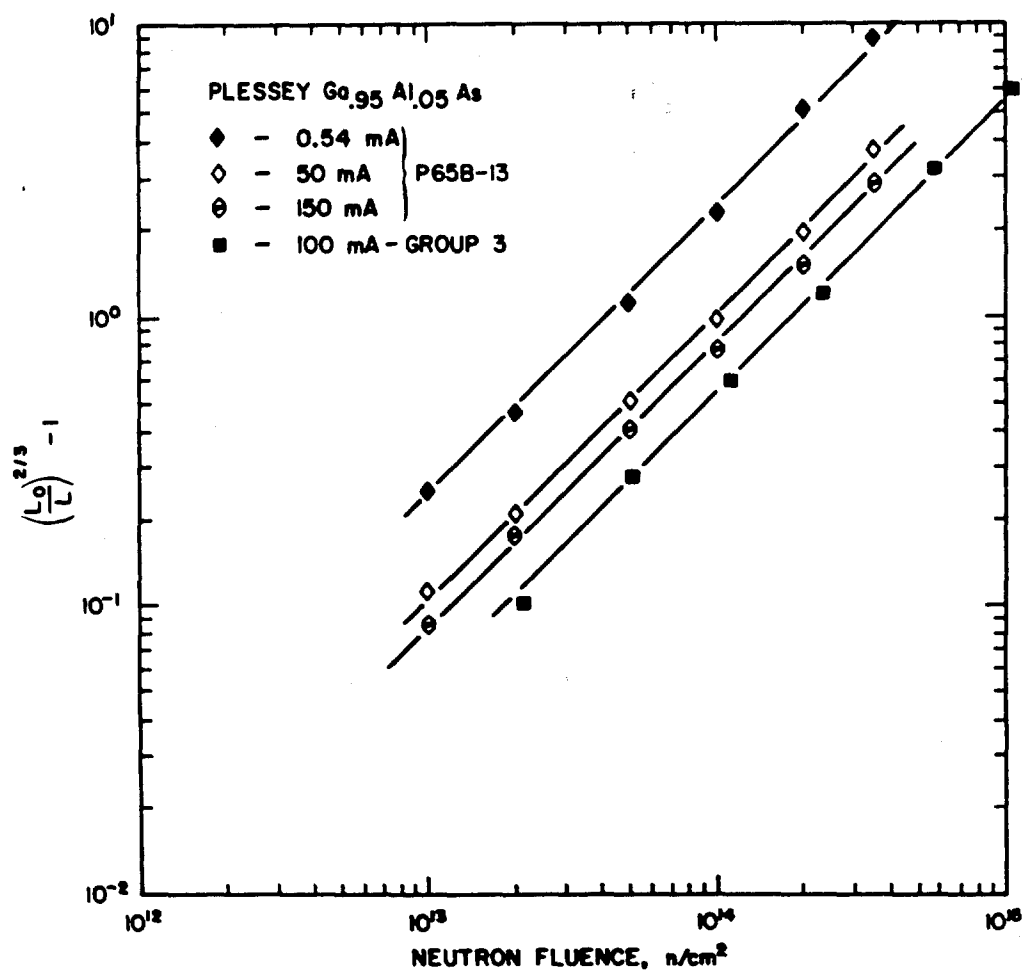


Figure 54. Analysis of constant current light output degradation from a Plessey bare, high radiance GaAlAs LED (P65B) and the average over nine of the most recent group (C45), designated group 3 in the Figure, of pigtailed GaAlAs LEDs. These latter devices have the lowest value of $\tau_0 K$ (curve furthest to the right) determined for the LEDs examined in this study.

Table 2

Pre-irradiation minority carrier lifetime-damage constant products, $\tau_0 K$, for neutron irradiation of LEDs operating at constant current.

<u>LED Type</u>	<u>LED Current</u>	<u>$\tau_0 K$, cm²/n</u>
Plessey GaAs (D2503AP)	10mA	5.3×10^{-14}
Plessey GaAs (D2503AP)	100	2.3×10^{-14}
Plessey Ga _{0.95} Al _{0.05} As(P65B)	0.54	2.4×10^{-14}
Plessey Ga _{0.95} Al _{0.05} As(P65B)	150	8.1×10^{-15}
Plessey Ga _{0.95} Al _{0.05} As(C45-average)	100	5.4×10^{-15}
TI GaAlAs(0,6,12% Al)	50	1.9×10^{-13}
TI GaAlAs(6%Al, high doping)	50	6.7×10^{-14}
TI GaAlAs(20% Al)	50	3.3×10^{-14}
TIL 26 (GaAs:Si, Si)	50	9.1×10^{-13}
Bell Labs GaP LED	50	2.2×10^{-14}
RCA InGaAs Long Wavelength	1	1.0×10^{-14}

2. Transient Fiber Attenuation and Pigtailed LED Output

The transient attenuation measurements on the Corning fiber pigtail material have shown, as one might expect, that this is a rather severe effect in this fiber. However, since the fiber is only used as a pigtail, the lengths being considered are relatively short, probably less than a meter. Indeed, one can envision many applications where a pigtail of a few tenths of a meter is sufficient, for which the losses would be reduced by a factor of 2 or 3 compared to those we have observed for a one meter length. Nevertheless, one must take seriously the attenuation problem in meter lengths of this fiber, and, to this end, we wish to make further comparisons of the Corning material with other fibers.

Normalized transient attenuation curves are shown in Fig. 55 for the two Corning fibers investigated in this work and for two fibers with undoped silica cores. Note that the recovery of the Corning SDF fiber, the one used for pigtails on the most recent LEDs, is slower than for the other three, especially at short times. These results demonstrate that more rapidly recovering fibers are available.

The strong attenuation and its slow recovery in Corning fibers has been attributed to the Ge doping of the silica core. These effects are further accentuated by the addition of B to the core. Typical results for such fibers, including our SDF fiber, are shown in Fig. 56. Note that the absolute attenuation in the SDF fiber falls between that for a Ge core fiber and the more intense attenuation found for the Ge + B doped core.⁸ As indicated in Fig. 56, it has been demonstrated⁸ that addition of P to the core suppresses the transient attenuation. However, the presence of P enhances the induced permanent attenuation.⁸

The wide variation in the way fibers respond to ionizing radiation, typified by the results in Fig. 56, indicates that the particular fiber optic system and the radiation environment it will experience must be well defined before a fiber

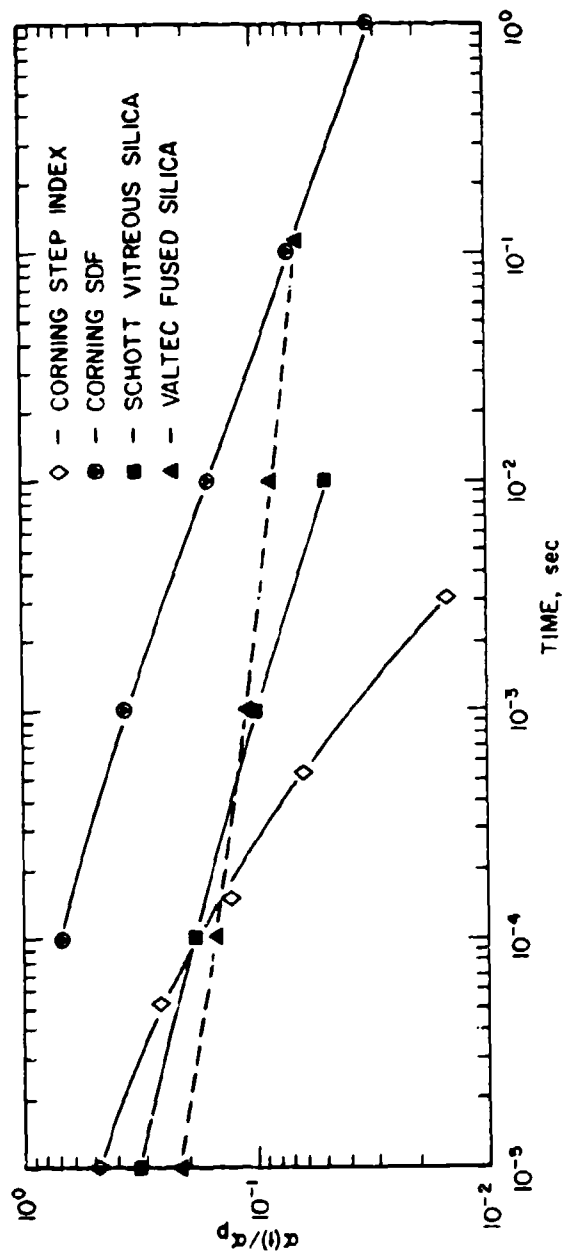


Figure 55. Room temperature transient attenuation at time, t , normalized to the peak transient attenuation, α_p , for four different fibers including the two Corning fibers examined in this study. Note that the Corning SDF material, the fiber used as a pigtail on the most recent LEDs, recovers slowly compared with the others. [from C. D. Skoog, Sandia Tech. Report SAND76-8056 (Nov. 1976)].

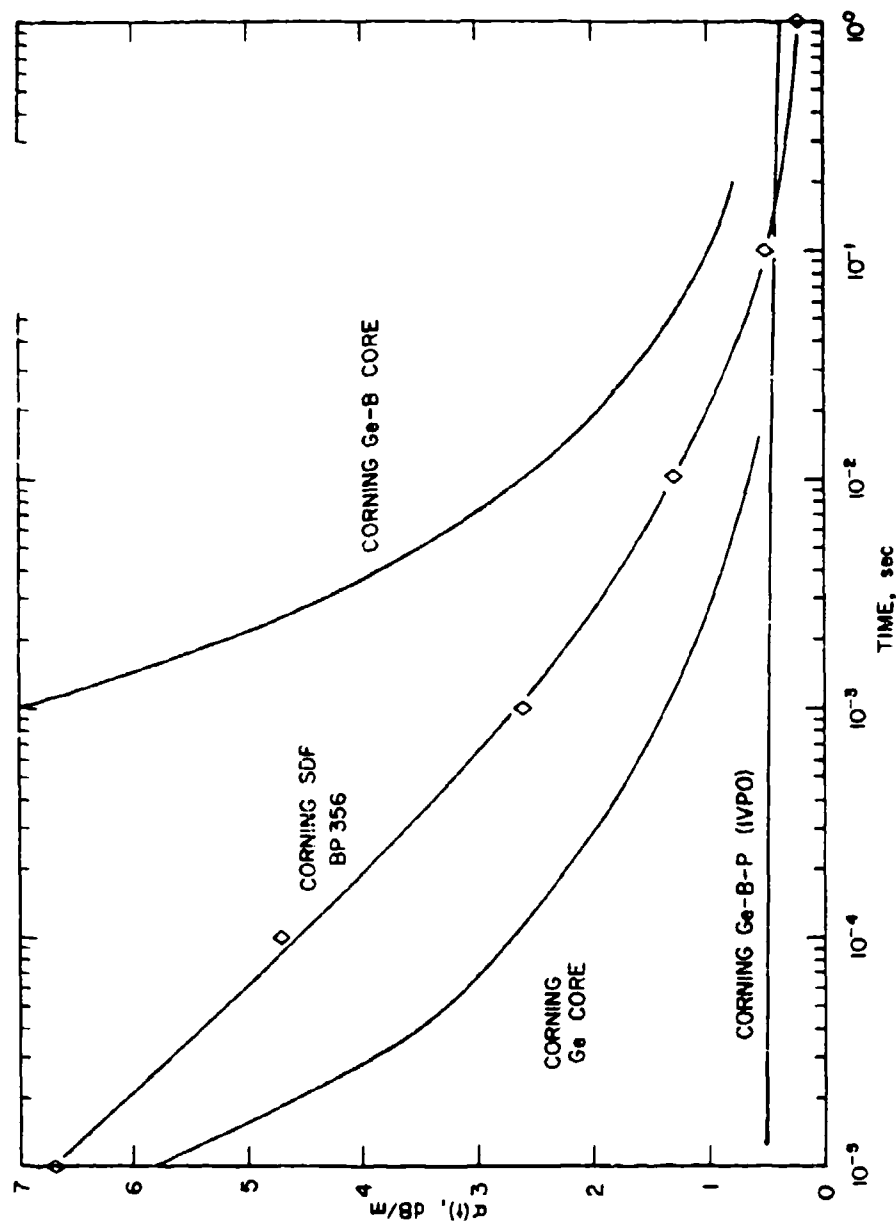


Figure 56. Room temperature transient attenuation from four Corning fibers including the SDF fiber studied herein. Data for the other fibers are for a dose of 3700 rads. Figure 44 has been used to scale up our data for the SDF fiber to an equivalent dose for presentation in this figure. The IVPO designation for the Ge-B-P doped core refers to the fabrication method. [from E. J. Friebele, Optical Engineering, 18, no. 6, 552 (1979)].

can be selected. For example, if system downtime must be a minimum, then a P doped fiber may be well suited. However, for an application in which the system can have a long downtime but which must tolerate high total dose, P doping would be a disadvantage. An additional example concerns polymer clad silica (PCS) fibers which have been found to generally have good radiation tolerance. One of the best of these is an ITT fiber, designated T323, which recovers to a loss of 0.12dB/m within 10 μ sec after a burst of 3700 rads,⁸ the dose used for the data in Fig. 56. Unlike the P doped fibers, the ITT fiber returns to nearly intrinsic attenuation within 5 sec rather than retaining significant permanent attenuation.⁸ While this fiber is consequently very attractive, it may not be appropriate for certain applications. Because of the polymer cladding the performance of these fibers is often poor at very low temperatures. Also, it may be difficult to use as a pigtail because the polymer cladding may cause difficulty in integrating and attaching the fiber to the LED, especially if a hermetic seal is required. Fortunately, as we have stated above, considerations of radiation induced attenuation are not as critical in the case of pigtails because of the short fiber lengths involved. One must also bear in mind, however, that the pigtail whether high loss or low loss, must be compatible with coupling or fusing to a possibly longer length of fiber which may have to be selected to satisfy stringent conditions.

We conclude this section by presenting a series of figures which depict actual expected average power output from the final group of Plessey LEDs under various conditions. The data in Figs. 57-60 were computed in the following manner. Along with the LEDs, Plessey supplied measured power emitted from the pigtail for each LED at -55°C, 25°C and 71°C at an LED current of 150mA. The following average power outputs were computed for the nine LEDs taken through the series

of neutron irradiations: 1073 μW at -55°C , 712 μW at 25°C , and 541 μW at 71°C . These values were then plotted versus temperature so that average values could be determined at -45°C , 25°C , and 75°C , the temperatures at which fiber attenuation data were taken. Reduced power outputs corresponding to specific neutron fluences were then calculated using the normalized light output degradation curve in Fig. 52. The same curve could be used to calculate post-irradiation power outputs at different temperatures since we have observed (see Figs. 32-37) that the degradation rate is essentially independent of temperature. Next we linearly superimpose the effects of transient attenuation with those of neutron reduced light output. This is valid because our results indicate that neutron irradiation does not affect the fiber pigtail and conversely, ionization does not affect the LED. The reduced power, $P(t,T)$, out of the fiber pigtail in the presence of transient attenuation is computed for a one meter long pigtail using the equations:

$$\alpha(t) = 10 \log \frac{P_{\text{ave}}(T)}{P(t,T)}, \text{ dB/m} \quad (17)$$

and
$$P(t,T) = P_{\text{ave}}(T)/10^{\alpha(t)/10}, \mu\text{W} \quad (18)$$

where $P_{\text{ave}}(T)$ is the average power out of the pigtail at a given temperature, T , with no transient attenuation ($\dot{\gamma} = 0$). These calculations result in the six sets of curves shown in Figs. 57-59 for three neutron fluence levels, $\phi = 0$, $1 \times 10^{14} \text{ n/cm}^2$, and $3 \times 10^{14} \text{ n/cm}^2$, and two values of dose rate; $\dot{\gamma} = 4.6 \times 10^9$ rads/sec and $\dot{\gamma} = 3.7 \times 10^{10}$ rads/sec. For the lower dose rate, the output power is essentially determined by the temperature and the neutron fluence. Even at 20 μs and -45°C the power is down by less than 20%. At one sec, the output is very close to complete recovery at all temperatures. However, for

$\dot{\gamma} = 3.7 \times 10^{10}$ rads/sec the transient attenuation has a strong effect on output. The power output curves at the three temperatures are quite different in shape and exhibit crossover points. These features result from the compensating effects of increasing light output with decreasing temperature and increasing attenuation at a given time with decreasing temperature. While the recovery is far from complete at 1 sec and -45°C , note that after this amount of time recovery is nearly complete at room temperature and above. The data in Fig. 59 demonstrate that for the largest ϕ and $\dot{\gamma}$, the power output can drop below $100 \mu\text{W}$ at early times at all temperatures.

The room temperature (25°C) data in Figs. 57-59 are displayed together in Fig. 60. The LED output varies from somewhat less than $100 \mu\text{W}$ at short times and the largest fluence to the pre-irradiation level of slightly over $700 \mu\text{W}$. Note that recovery is nearly complete after 1.0 sec. The data given in Figs. 57-60 illustrate that care must be taken in selecting the pigtail fiber and the LED so as to maximize power output for the specific conditions under which the fiber optic system will be used.

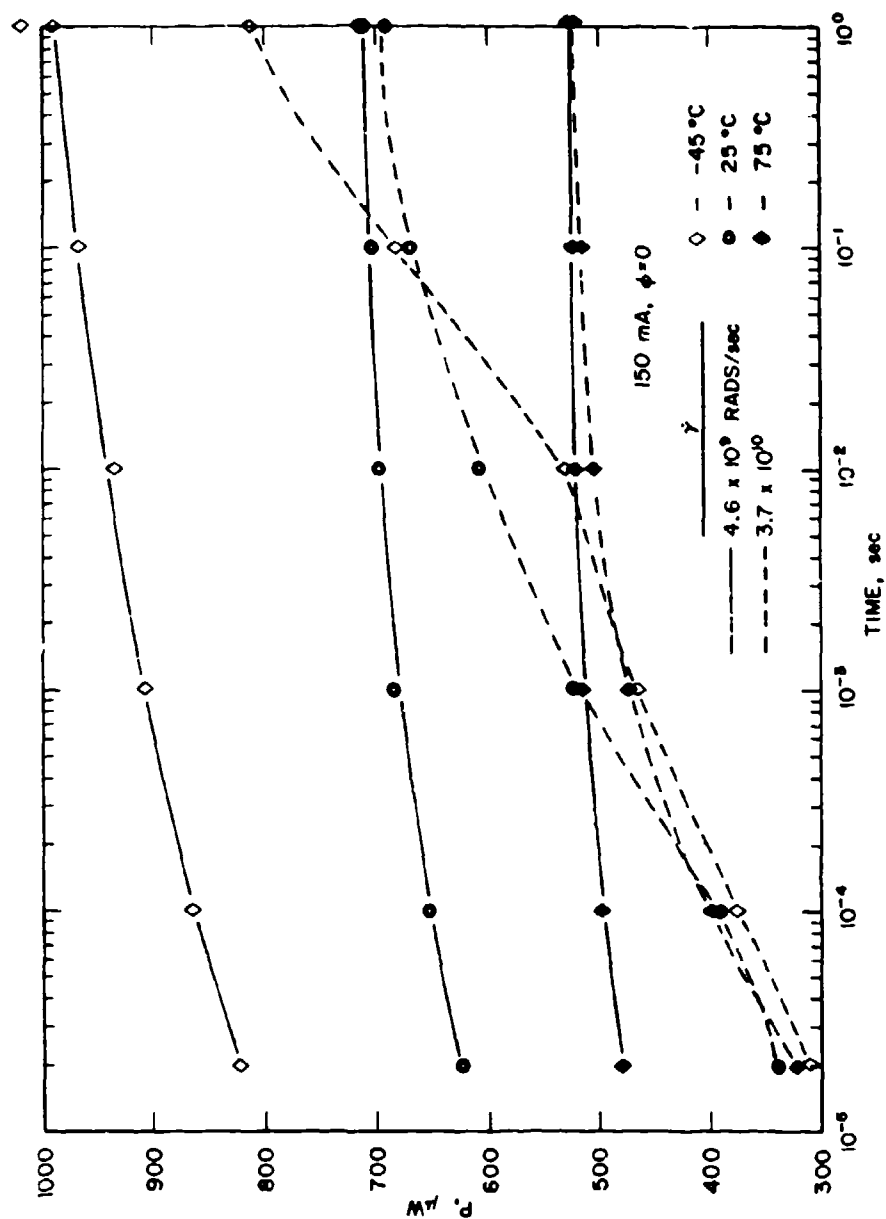


Figure 57. Actual expected average power output at a current of 150mA from the pigtail of the most recent set of LHS (045) as a function of temperature and time after two different γ value X-ray bursts. The neutron fluence is assumed to be 0 for this case.

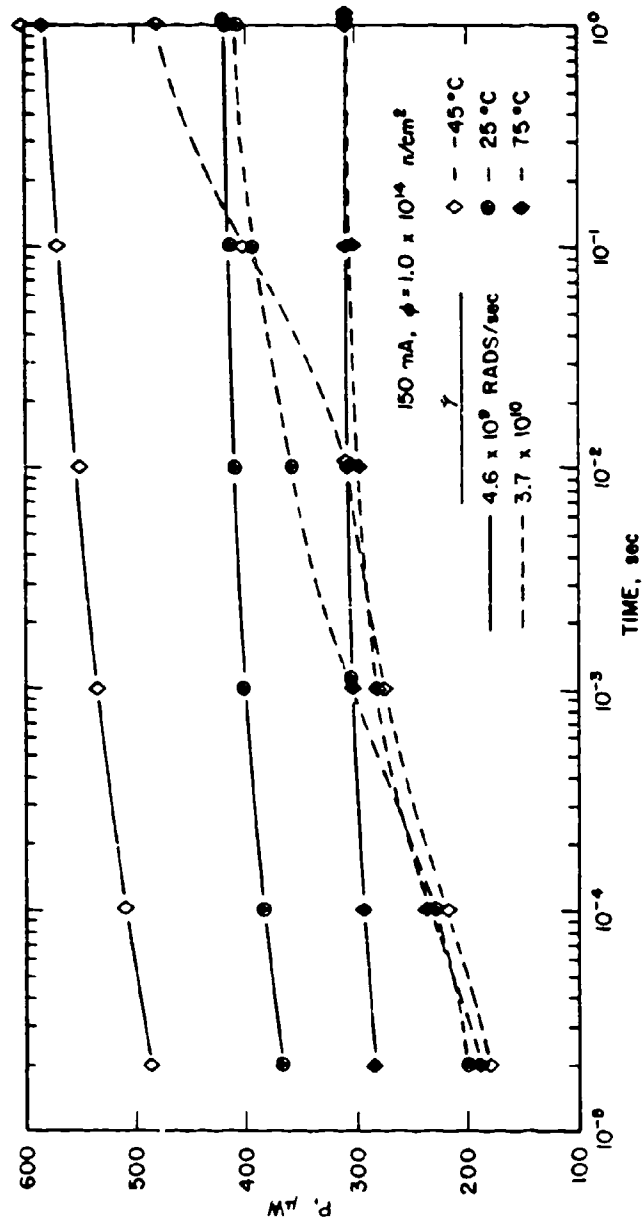


Figure 5A. Actual expected average power output at a current of 150mA from the pigtail of the most recent set of LEDs (C45) as a function of temperature and time after two different γ value X-ray bursts. The neutron fluence is assumed to be $1.0 \times 10^{14} \text{ n/cm}^2$ for this case.

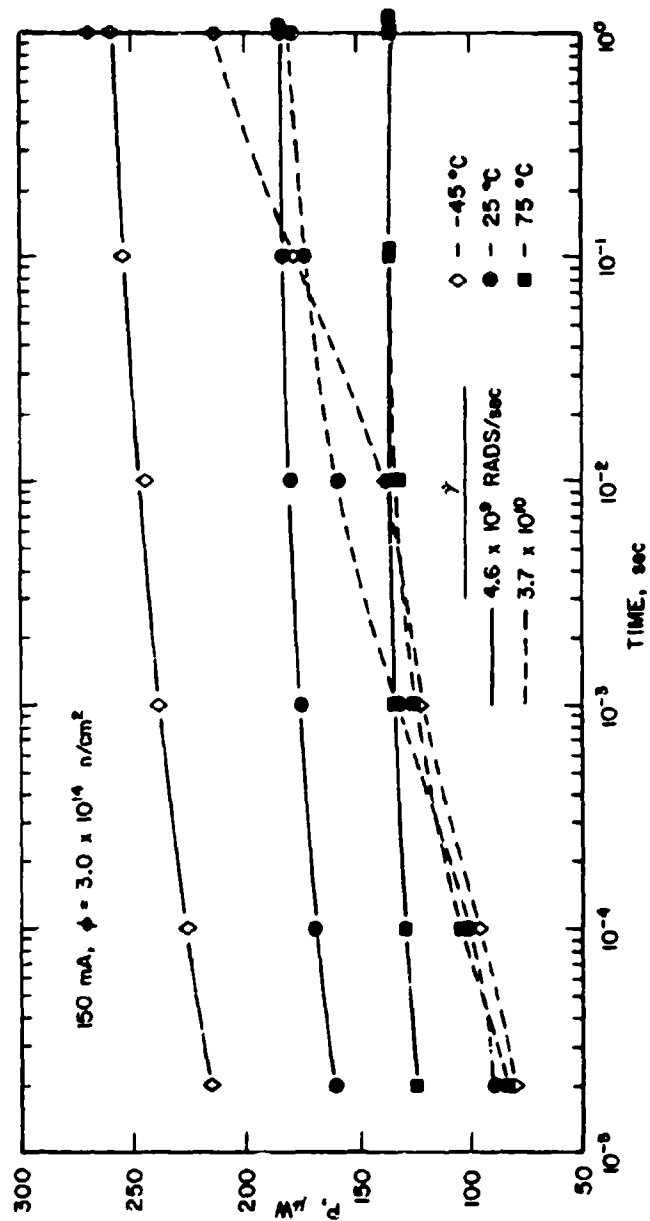


Figure 59. Actual expected average power output at a current of 150mA from the pigtail of the most recent set of LHDs (C45) as a function of temperature and time after two different γ value X-ray bursts. The neutron fluence is assumed to be 3.0×10^{14} n/cm² for this case.

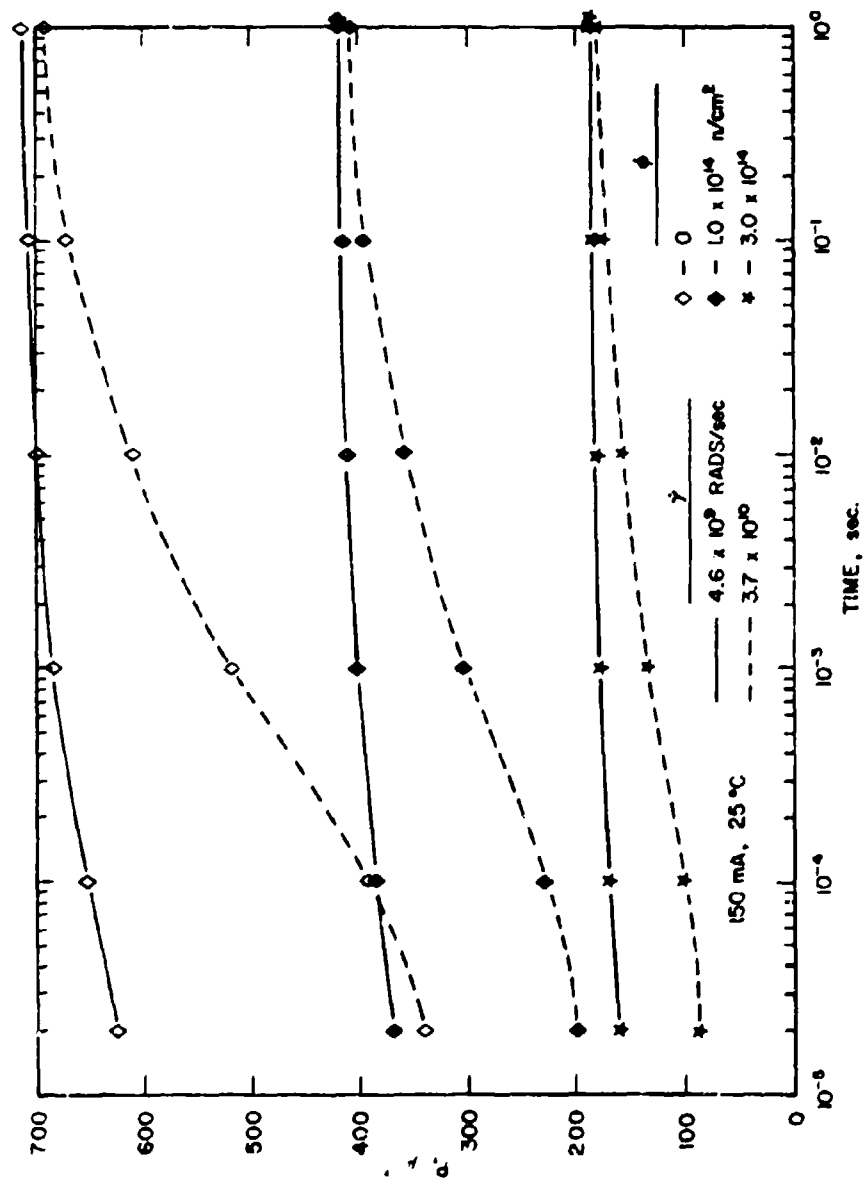


Figure 60. Room temperature data from Figs. 57-59. In this figure we show data for two values of γ and three fluence values. The average power output varies from slightly below 100mW to somewhat greater than 700mW.

SECTION VI

CONCLUSIONS AND RECOMMENDATIONS

In this section we summarize the important results of this study and propose recommendations based on these results. The following list comprises our major conclusions:

1. There are no uniquely transient effects within the LEDs due to pulsed neutron exposure at levels near $1 \times 10^{13} \text{n/cm}^2$ per pulse. The neutron pulse causes a permanent decrease in light output equivalent to that which results from a steady state irradiation.
2. Co-60 gamma irradiation of bare Plessey GaAs and GaAlAs LEDs to 10^6 rads did not result in any light output degradation as a function of voltage or current. A similar irradiation of pigtailed LEDs did cause a relatively small decrease in output due to permanent induced attenuation in the approximately 1 meter long fiber pigtail.
3. Pulsed X-ray exposure to levels of 5×10^3 rads ($\dot{\gamma} = 1 \times 10^{11} \text{rads/sec}$) of bare LEDs, pigtailed LEDs, and separate test pieces of the fibers used for pigtails has demonstrated that such irradiations affect only the fiber and not the LED or lens.
4. The Corning SDF (short distance fiber) BP356 fiber exhibits rather strong transient attenuation following X-ray exposure due to the dopants used in the fiber core. After an irradiation of 1.85×10^3 rads ($3.7 \times 10^{10} \text{rads/sec}$) the induced attenuation at 25°C is 1.4dB/m at a time of 1.0ms after the X-ray pulse. As the temperature is lowered, the attenuation becomes greater at a given time. Normalization of the attenuation to the

peak transient attenuation demonstrates that the recovery rate is temperature dependent and significantly slower at -45°C than at the maximum measurement temperature of $+75^{\circ}\text{C}$. Measurements of the SDF fiber and the earlier 1025 fiber suggest that there is no significant dependence of the recovery rate on wavelength or dose. However, as one might expect, the peak transient attenuation, α_p , is greater at the shorter wavelengths characteristic of GaAlAs (820-850nm) than at the emission wavelength of GaAs (900nm). In addition, α_p , and also $\alpha(t)$ at later times, vary linearly with dose over the dose range investigated. Extending this linear behavior at -45°C indicates that α_p would approximately equal 13.3 dB/m at -45°C and $\dot{\gamma} = 1 \times 10^{11}$ rads/sec. Using eqn (18), this further implies that the power emitted from a 1 meter long pigtail at the point in time where α_p occurs (roughly 10 μsec after the burst) would be only 4.7% of the emitted power prior to the X-ray pulse. At a time of 1ms after a 1×10^{11} rads/sec burst, $\alpha(1\text{ms}) = 8.9$ dB/m and the power would be 13% of the pre-irradiation power out of a 1 meter pigtail.

5. A Co-60 gamma irradiation of the two Corning fibers to a dose of 1×10^6 rads did result in additional permanent attenuation. Measured values were between 0.13 and 0.45 dB/m for a megarad. For potential applications employing long fiber lengths, the Co-60 induced attenuation increases would be a problem. However, for a typical pigtail length of about 1 m, the losses would correspond to approximately a 9% reduction in power output for an additional attenuation of 0.43 dB. Such losses should not pose any particular difficulty.

6. Perhaps the most important result found in this study is that the average hardness to neutron irradiation of nine of the most recent Plessey high radiance GaAlAs LEDs is greater than that of any other LEDs known to this author.¹ For constant high current operation, a neutron fluence of $4 \times 10^{14} \text{ n/cm}^2$ is required to reduce the output by a factor of 5. At an LED current of 150mA and a temperature of 25°C, this would correspond to a reduction in power out of the fiber pigtail from 712 μW prior to irradiation to 142 μW . We have attributed this exceptional tolerance to neutron irradiation to two effects: (1) the lack of neutron induced excess current at the very large current densities typical of these high radiance LEDs, and (2) the reduction in rise time and minority carrier lifetime caused by heavy doping. The number of neutron-induced non radiative recombination centers required to affect the short initial lifetime thus becomes quite large. With regard to wavelength selection of the fiber optic system, it is important to note that neither of these radiation hardening effects depend on material type. That is, a high speed, high radiance GaAs LED should have a similar radiation resistance. In the case of the bare Plessey GaAs LEDs (D2503AP) investigated herein, the greater susceptibility to neutron damage apparently results from the lower doping levels in these devices.

Because of the excellent resistance of the most recent set of Plessey pigtailed GaAlAs LEDs to permanent neutron damage, we strongly recommend them for all but the most stringent applications. Without knowing the detailed specifications of the radiation environment, which, in any case could probably not be discussed in an unclassified report, it is difficult to make specific recommendations. Fortunately, the definite superiority of these LEDs with regard to neutron hardness minimize the need for qualifying a recommendation. With regard to the Corning SDF fiber pigtail, the

situation is somewhat more tenuous. It is clear from the work herein and that of others, ^{7,8,9} that the transient attenuation in these fibers is strong and recovers relatively slowly with time. Therefore, for those applications which require low temperature operation with a minimum downtime, which we might define as $t < 1.0\text{ms}$, large dose ($\gamma > 10^6$ rads) or dose rate ($\dot{\gamma} > 10^{11}$ rads/sec), and long pigtail length (greater than 1.0 m), it would be appropriate to consider a fiber pigtail which is more immune to induced transient attenuation. However, it is not difficult to envision many applications in which the pigtail can be relatively short and can be coupled or fused with a fiber that has greater tolerance. We feel that the Corning SDF fiber is adequate for those applications where the pigtail length is reasonable, say less than about 1 m, the downtime can be equal to or greater than 1 ms, and γ is not extremely large. Once again, it is difficult for us to avoid being somewhat vague because we do not know the details of the contemplated applications. Rather, we will allow the power output figures (57-60) to speak for themselves. Hopefully, they will assist the system designer in making an informed decision about the applicability of these devices.

SECTION VII

REFERENCES

1. C. E. Barnes, Radiation Effects in Optoelectronic Devices, Sandia National Laboratories Technical Report SAND76-0726 (1977).
2. R. A. Polimadei, S. Share, A. S. Epstein, R. J. Lynch and D. Sullivan, Performance of Ga_{1-x}Al_xAs Light Emitting Diodes in Radiation Environments, IEEE Trans. Nucl. Sci. NS-21, no. 6, 96 (1974).
3. A. S. Epstein, S. Share, R. A. Polimadei, and A. H. Herzog, Effects of Neutron Irradiation on GaAs_{1-x}P_x Electroluminescent Diodes, Appl. Phys. Lett. 23, 472 (1973).
4. A. S. Epstein, S. Share, R. A. Polimadei, and A. H. Herzog, Gamma Irradiation and Annealing Effects in Nitrogen-Doped GaAs_{1-x}P_x Green and Yellow Light-Emitting Diodes, IEEE Trans. Nucl. Sci. NS-19, no. 6, 386 (1972).
5. A. S. Epstein, S. Share, R. A. Polimadei, and A. H. Herzog, Dopant and Alloying Effects in Gamma Irradiated GaAs Light Emitters, IEEE Trans Nucl. Sci. NS-23, 1654, (1976).
6. L. W. Aukerman, M. F. Millea, and M. McColl, Effects of Radiation Damage on the Behavior of GaAs p-n Junctions, IEEE Trans. Nucl. Sci. NS-13 no. 6, 174 (1976).
7. P. L. Mattern, L. M. Watkins, C. D. Skoog, and E. H. Barsis, Absorption Induced in Optical Waveguides by Pulsed Electrons as a Function of Temperature, Low Dose Rate Gamma and Beta Rays, and 14 MeV Neutrons, IEEE Trans. Nucl. Sci. NS-22 no. 6, 2468 (1975).
8. E. J. Friebele, Optical Fiber Waveguides in Radiation Environments, Optical Eng. 18, 552 (1979).
9. C. D. Skoog, A Summary of Radiation-Induced Transient Absorption and Recovery in Fiber Optic Waveguides, Sandia National Laboratories Technical Report SAND76-8056 (1976).